PB-216 216

THE INFLUENCE OF CAPILLARITY ON THE FLOW OF WATER AND AIR IN A POROUS MEDIUM

Donald Dean Adrian

Stanford University
Stanford, California

June 1964

DISTRIBUTED BY:

NTIS

National Technical Information Service
U. S. DEPARTMENT OF COMMERCE
5285 Port Royal Road, Springfield Va. 22151

WP00246

PB 216 216
June 1964
Technical Report No. 38

THE INFLUENCE OF CAPILLARITY ON THE FLOW OF AIR AND WATER IN A POROUS MEDIUM

Donald Dean Adrian

This research received support from
the Ford Foundation and through the
U.S. Public Health Service through
Grant WP-00246 and Fellowship WPPM-16,556(1)

Reproduced by
NATIONAL TECHNICAL
INFORMATION SERVICE
U S Department of Commerce
Springfield VA 22151

Department of CIVIL ENGINEERING
STANFORD UNIVERSITY

170

DEPARTMENT OF CIVIL ENGINEERING
Stanford University
Stanford, California

THE INFLUENCE OF CAPILLARITY ON THE FLOW OF WATER AND AIR IN A POROUS MEDIUM

By
Donald Dean Adrian
Ph.D.

Technical Report No. 38
June 1964

This research received support from the
Ford Foundation and from the U. S. Public Health Service
through Grant WP-00246 and Fellowship WPPM-16,565(1)

T

ACKNOWLEDGEMENTS

This report is a reproduction of the dissertation submitted by Mr. Donald Dean Adrian in partial fulfillment of the requirements for the degree of Doctor of Philosophy in the Department of Civil Engineering, Stanford University, Stanford, California.

Many of the topics discussed in this report were suggested by Professors J. B. Franzini and S. N. Davis who also provided valuable assistance in the analysis of these topics. George Tchobanoglous provided many valuable suggestions on the experimental portion of the investigation, helped construct the equipment, assisted in the experiments and drew the graphs. John Bruch assisted with the experiments and with the data reduction. Joe Duncan helped construct and assemble the equipment.

Financial assistance was provided by the Department of Civil Engineering, the Ford Foundation, and the Public Health Service through grant WP-00246 and fellowship WPPM-16,565(1).

ABSTRACT

In the usual analysis of the flow of water into a porous medium, such as infiltration into a soil, air resistance is neglected. Obviously, as water moves into the air-filled pores air must be driven out. In most cases the air flows with a negligible resistance compared to the resistance of water to flow. However, if the air escape route deeper into the medium is blocked by an impermeable barrier, the air will be trapped and its pressure will increase as the combined action of gravity and capillary forces try to force the air from the pores. This air pressure build-up will decrease the infiltration rate below the rate predicted from measurements of the permeability of the medium and its capillary characteristics.

Recent studies have shown that the movement of water into a horizontal porous medium can be described by the "diffusion equation"

$$\frac{\partial \theta}{\partial t} = \frac{\partial}{\partial x}\left[D \frac{\partial \theta}{\partial x} \right]$$

where θ is the moisture content on a volume basis, t is time, x is the horizontal coordinate and D is the "diffusivity." The"diffusivity" embodies the capillary characteristics and the permeability of the medium. For vertical flow a gravity term appears and the equation becomes more difficult to solve. An implicit assumption in the diffusion equation is that there is no air resistance. Due to the complexity of the equation it is difficult to predict the effect of an air pressure build-up on infiltration.

Instead, a simpler flow model was chosen. The saturation of the medium was assumed to be constant, and all of the capillary forces were

assumed to act at the air-water interface. When infiltration takes place into a medium having an impermeable bottom, it is possible to predict that the interface will eventually stop moving if the particle diameter is small enough because of the air pressure build-up ahead of the wetting front. For particles larger than about 0.03 cm diameter it was observed that air flowed through the wetted medium and escaped to the atmosphere, so the air pressure build-up was reduced. For mediums which can develop high capillary heads the air pressure build-up can be sufficiently great to cause a break to occur in the medium at the air-water interface. Experiments confirmed that a break could occur in the mediums although the location of the break was different than predicted by theory that was developed. This difference was caused by the escape of air at the beginning of the infiltration.

When similar columns were compared experimentally, one constructed so air could escape through the bottom of the column and the other having an impermeable bottom, significantly different infiltration rates were observed. The moisture contents in the columns were determined at different locations by use of gamma radiation attenuation equipment. This permitted continuous non-destructive determinations of the moisture content at frequent intervals. The radioactive source and the detector were mounted on a hoist in order to permit the moisture content to be determined at any elevation on the column.

TABLE OF CONTENTS

Chapter		Page
1	INTRODUCTION	1
2	EQUATIONS FOR UNSATURATED FLOW	5
3	EQUATIONS FOR SATURATED FLOW	13
	1. Discussion of Assumptions	13
	2. Infiltration Without Air Resistance and Without Capillary Forces	15
	3. Infiltration with Capillary Forces and Ponding	18
	4. Horizontal Flow in a Column with no Air Resistance	20
	5. Horizontal Flow into a Column with Resistance	21
	6. Horizontal Flow of Gases	24
	7. Vertical Flow Against Air Resistance	29
4	THEORY OF CAPILLARY EQUILIBRIUM	33
	1. Capillary Tube Analogy	33
	2. Hydraulic Radius Concept	34
	3. Surface Interface Concept	36
	4. Empirical Equations	44
5	EQUILIBRIUM AND STABILITY	47
	1. Theory	47
	1.1. Capillary forces neglected	47
	1.2. Capillary forces considered	51
	1.3. Special cases and examples	55
	2. Experimental Work	63
	2.1. Introduction	63
	2.2. Mediums used and general conduct of tests	63
	2.3. Tests on 10 cm columns	65
	2.4. Tests on 30 cm columns	67
	2.5. Discussion of tests on 10 cm and 30 cm columns	69
	2.6. Tests on longer columns	70
	2.7. Summary of experimental tests	72
6	INFILTRATION EXPERIMENTS	
	1. Experimental Equipment and Procedure	74
	1.1. Laboratory arrangement and temperature control	74
	1.2. Construction and tests of the plastic tube	75
	1.3. Description of the porous mediums	75
	1.4. Column packing procedure	79
	1.5. Measurements of infiltration and the wetting front	81

TABLE OF CONTENTS (cont.)

Chapter		Page
6	2. Equipment Tests	81
	2.1. Attenuation equation	81
	2.2. Moisture and density measuring equipment	82
	2.3. Verification of counting accuracy	84
	2.4. Attenuation and absorption coefficients of other materials	90
	3. Moisture Distribution During Infiltration	94
	4. Motion of the Wetting Front	98
	4.1. Observed and calculated positions of the wetting front	98
	4.2. Position of the wetting front compared with theory	104
	5. Infiltration Rates	113
	5.1. Numerical treatment of data	113
	5.2. Cumulative inflow and infiltration rates	115
	5.3. Comparison of theory and experiment	119
7	SUMMARY AND CONCLUSIONS	133
APPENDIX		136
	1. Movement of Air Through Saturated Mediums	136
	1.1. Solubility of air in water	136
	1.2. Steady-state diffusion of air through water	137
	2. Other Factors Influencing Capillary Phenomena	142
	3. Gamma Radiation Intensities	157
BIBLIOGRAPHY		158

LIST OF TABLES

5.1. Attenuation and Absorption Coefficients 90

A.1. Solubility of Air in Water at Various Temperatures under a Pressure of 1 Atmosphere 137

A.2. Direction of Vapor Transfer for Various Vapor Pressure and Temperature Gradients 149

A.3. Typical Gamma Radiation Counting Rates 157

LIST OF FIGURES

Figure		Page
2.1	Relative Permeability Curves for Unsaturated Flow	6
2.2	Elementary Volume for Establishing Continuity Equations . .	7
3.1	Infiltration into a Column with no Air Resistance	15
3.2	Displacement of one Immiscible Liquid by Another	21
3.3	Pressure Variation in Gas Flow	26
3.4	Comparison of Air and Water Flowrates Through Identical Porous Mediums	27
3.5	Infiltration Against Air Resistance	29
4.1	Doubly Curved Surface Under Uniform Tension	37
4.2	Plan View of Square-Packed Spheres	38
4.3	Cross Section Showing an Elevation View of Plane AA_1 . . .	39
4.4	Plan View of Triangularly-Packed Spheres	41
4.5	Enlarged View of Three Adjacent Spheres	41
4.6	Capillary Rise in Uniform Porous Media	46
5.1	Infiltration into a Closed Volume	48
5.2	Equilibrium Interface Position and Soil Stability	58
5.3	Equilibrium Interface Position and Soil Stability	61
5.4	Equilibrium Interface Position and Soil Stability	62
5.5	Photograph of Column Breakage	63
6.1	Experimental Tube Construction Details	76
6.2	Sieve Analysis of Roseville White Sand	77
6.3	Photograph of 0.0080 cm Diameter Glass Beads	78

LIST OF FIGURES (cont.)

Figure		Page
6.4	Sieve Analysis of Glass Beads	80
6.5	Schematic Drawing of the Moisture Measuring Equipment . .	83
6.6	Photograph of the Counting Equipment	85
6.7	Attenuation Coefficient for Aluminum	87
6.8	Absorption Coefficient for Lead	88
6.9	Absorption Coefficient for Water	89
6.10	Attenuation Coefficient for Plastic	91
6.11	Absorption Coefficient for Roseville Sand	92
6.12	Absorption Coefficient for Glass Beads	93
6.13	Moisture Content for Various Attenuations	95
6.14	Interpolation Diagram for Moisture Content	96
6.15	Moisture Distribution During Infiltration	97
6.16	Observed and Calculated Positions of the Wetting Front .	100
6.17	Observed and Calculated Positions of the Wetting Front .	101
6.18	Observed and Calculated Position of the Wetting Front . .	102
6.19	Wetting Front Location, Roseville White Sand	103
6.20	Interface Position During Infiltration	105
6.21	Comparison of Theory with Experiment	106
6.22	Comparison of Theory with Experiment with no Air Resistance	107
6.23	Wetting Front as a Function of Time	108
6.24	Roseville White Sand	109
6.25	Roseville White Sand	110
6.26	Air Escape During Infiltration	112
6.27	Sieve Analysis Geology Department Sand	114

LIST OF FIGURES (cont.)

Figure		Page
6.28	Cumulative Inflow and Infiltration Rate, no Air Resistance	116
6.29	Inflow and Infiltration Rate	117
6.30	Inflow and Infiltration, Graded Beads	118
6.31	Inflow and Infiltration, Roseville Sand	120
6.32	Inflow and Infiltration, Roseville Sand	121
6.33	Infiltration Rate Glass Beads	122
6.34	Interface Position at Various Times	124
6.35	Dimensionless Infiltration Curves	125
6.36	Downward Infiltration Without Air Resistance	126
6.37	Downward Infiltration Without Air Resistance	127
6.38	Downward Infiltration Without Air Resistance	128
6.39	Roseville White Sand	130
6.40	Downward Infiltration Without Air Resistance	131
6.41	Downward Infiltration Without Air Resistance	132
A.1	Water, Pressure and Air Concentration Distributions in a Porous Medium	139
A.2	Vapor Pressure as a Function of Temperature	146

CHAPTER 1

INTRODUCTION

The underground movement of water has been of interest to man since early in history. During most of this period the nature of water movement remained a mystery, although there were developments in the construction of wells and collection works as early as 800 B.C. Todd (1959) points out that Vitruvius understood the role played by recharge on the presence of springs at the base of mountains, although his ideas were largely unknown or ignored for many centuries. The writings of Mariotte, published in 1686, contain data from the river Seine at Paris which show that runoff is less than precipitation, thus supporting the theory of infiltration. Undoubtedly, the most important contribution to the quantitative study of ground-water movement was made by Henry Darcy, a French engineer, who in 1856 published a report which contained a relation describing the flow of water through sand beds. This relation has since become known as Darcy's law. Dupuit and others applied Darcy's law to a variety of flow problems and developed boundary value problems to describe flow towards a well and seepage through earth dams. Many more flow problems have since been solved, so there are now a number of mathematically elegant solutions to a variety of steady flow problems [El Nimr (1962)] and some unsteady flow problems [De Weist (1960)].

The effects of capillary action at the air-water interface of the flow are ignored in the boundary value problems associated with the movement of water through soils. The mathematical problems become much more complex if capillary forces are included. The flow is also assumed to completely saturate the soil. Wyckoff and Botset (1936) conducted research on the simultaneous flow of air and water in porous mediums. Additional work was carried out by persons interested in petroleum engineering applications of the results and by soil scientists. In the simultaneous flow of air and water in a porous medium, capillary forces are present at each air-water interface in the interior of the flow field and at the boundaries. The effects of capillary forces within the flow field have been investigated by Scott and Corey (1961) and others. Electronic computers have stimulated an interest in numerical solutions to unsteady unsaturated flow [Wang (1963), Ashcroft, et al., (1962) and Hanks and Bowers (1962)]. The application of unsaturated flow theory to infiltration [Philip (1957)] has brought a wealth of information to the hydrologist. However, the work with unsaturated flow which has been applied to hydrology to date has been based on the assumption that the air in the soil offered no resistance to flow.

The assumption that there is only a negligible resistance to infiltration due to air flow has resulted in a lack of attention being paid to the presence of air in the soil in cases when it may have a significant effect on infiltration. Two factors encourage the neglect of air resistance during infiltration: (1) it is felt that the air's resistance to flow is negligible in comparison to water's resistance

to flow; (2) including the effects of air resistance makes the equations describing the flow more difficult to solve. A recent publication [Wilson (1963)] discusses some of the complexities which are introduced into infiltration problems when the flow of air ahead of the wetting front is considered.

Air resistance may also arise if the air is not free to escape as it is displaced by infiltrating water. The air pressure could become very large if the wetting front advanced until the entrapped air occupied only a fraction of its original volume. As a result, a significant difference between the infiltration rates could be expected when comparing two soils which were identical in all respects except that one had provision for all air ahead of the wetting front to escape and the other allowed none of the air to escape. Both situations may arise in nature. The first could occur when infiltration takes place into soil which contains cracks and open root channels. The second could occur if a permeable soil was underlain by an impermeable layer and there were no continuous vertical or lateral passages which would permit the air to escape. Nearly all the laboratory work on infiltration has been carried out with equipment which was carefully designed to offer as little resistance to the escape of air as possible. Also, most of the work which has considered capillary forces and their effect on infiltration has been carried out in horizontal columns of soil to avoid the difficulties which gravity effects might bring about in the mathematical formulation of the problem. The combined action of gravity and

capillary forces can result in significantly higher pressures in the air which is displaced by the infiltrating water and which is not free to escape. This is particularly true where the permeable layer extends over a large vertical distance. As a result, there is no adequate treatment of the combined effect on infiltration rates of capillary forces, gravity and the air which is displaced by the infiltrating water. The present work is an attempt to remedy this situation.

CHAPTER 2

EQUATIONS FOR UNSATURATED FLOW

It is now well accepted that Darcy's law will adequately describe the flow of a Newtonian fluid through porous media. Darcy's law may be written

$$V = - k \frac{\rho}{\mu} g \frac{\partial h}{\partial s} \tag{2.1}$$

where each term has the following significance:

V = discharge per unit area through which flow takes place, $[V] = LT^{-1}$

k = intrinsic permeability of the porous medium, $[k] = L^2$

ρ = mass density of the fluid, $[\rho] = ML^{-3}$

μ = dynamic viscosity of the fluid, $[\mu] = ML^{-1}T^{-1}$

g = the acceleration of gravity, $[g] = LT^{-2}$

h = hydraulic head of the flowing fluid at some point in the porous medium: it is the height to which a column of liquid would rise in a piezometer placed at this point in the porous medium, $[h] = L$

s = a coordinate in the direction of V, $[s] = L$.

For many applications in which only a single fluid is flowing, it has become common practice to modify the form of Darcy's law by combining terms into the form

$$V = - K \frac{\partial h}{\partial s} \tag{2.2}$$

where it is seen that

$$K = k \frac{\rho}{\mu} g \tag{2.3}$$

K is called the "permeability" and has the dimension LT^{-1}.

This relation between the hydraulic gradient $\frac{\partial h}{\partial s}$, the permeability, and the discharge per unit area together with the appropriate boundary conditions has made it possible to solve a number of important flow problems in the fields of geology, civil engineering, agricultural engineering, and petroleum engineering.

The form of Darcy's law given by Eqs. (2.1) and (2.2) has been found to be restricted to saturated flow. Wyckoff and Botset (1936) studied the combined flow of a liquid and a gas through sand and discovered that K is a function of the percent saturation of the sand. Figure 2.1 is typical of their results in which relative permeability

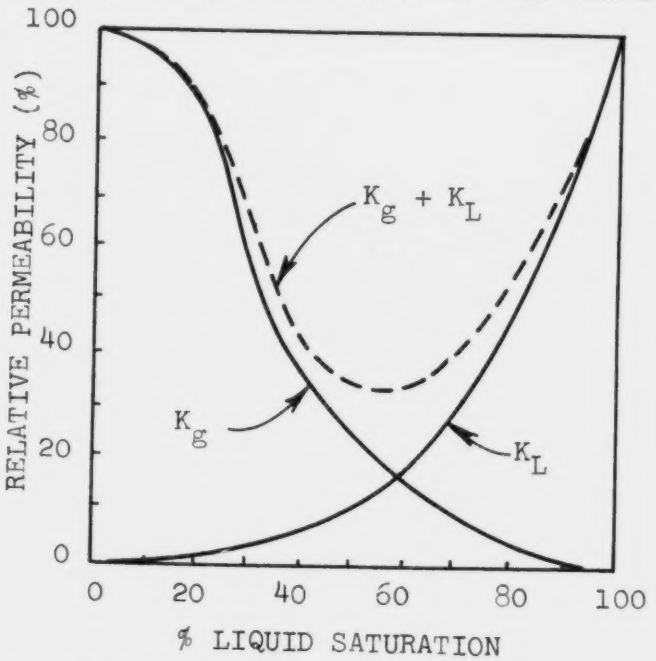

Figure 2.1. Relative Permeability Curves for Unsaturated Flow.

is defined as the ratio of the permeability at a given saturation to the permeability at 100% saturation. For flow of a liquid and a gas, the dashed line of Figure 2.1 indicates that the sum of the liquid and gas relative permeabilities is less than or equal to the maximum relative permeability of either the liquid or the gas.

The unsaturated flow may be analyzed in more detail to describe mathematically the influence of the various parameters on the flow. The equation for the conservation of mass is of fundamental importance in most flow problems. Consider an element of porous medium having sides dx, dy, dz and porosity n. Let u, v, and w be the approach velocities given by Darcy's law in the X, Y, and Z directions, respectively. For the cube in Figure 2.2, the mass fluxes through sides

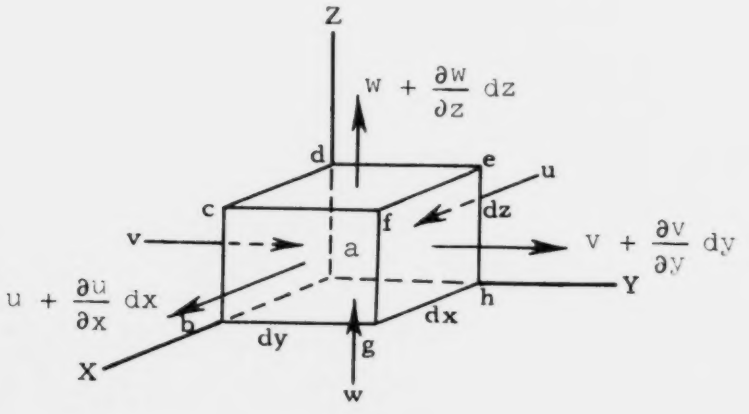

Figure 2.2. Elementary Volume for Establishing Continuity Equations.

abcd, adeh, and abgh are ρv, ρu, and ρw, respectively, while through sides efgh, bcfg, and cdef the mass fluxes are $\rho v + \frac{\partial(\rho v)}{\partial y} dy$, $\rho u + \frac{\partial(\rho u)}{\partial x} dx$, and $\rho w + \frac{\partial(\rho w)}{\partial z} dz$, respectively. For the elementary volume dxdydz, the mass flux into the volume minus the mass flux out of the volume is the increase in the mass stored in the volume or $n\frac{\partial(\rho\theta')}{\partial t} dxdydz$, where θ' is the fractional saturation of the voids. Thus,

$$\rho v dxdz - (\rho v + \frac{\partial(\rho v)}{\partial y} dy)dxdz + \rho u dydz - (\rho u + \frac{\partial(\rho u)}{\partial x} dx)dydz$$

$$+ \rho w dxdy - (\rho w + \frac{\partial(\rho w)}{\partial z} dz)dxdy = n \frac{\partial(\rho\theta')}{\partial t} dxdydz \qquad (2.4)$$

On canceling the common terms, this becomes

$$- \frac{\partial(\rho v)}{\partial y} - \frac{\partial(\rho u)}{\partial x} - \frac{\partial(\rho w)}{\partial z} = n \frac{\partial(\rho\theta')}{\partial t} \qquad (2.5)$$

and if the fluid is incompressible so ρ may be considered a constant, the equation of continuity becomes

$$\frac{\partial u}{\partial x} + \frac{\partial v}{\partial y} + \frac{\partial w}{\partial z} = - n \frac{\partial\theta'}{\partial t} \qquad (2.6)$$

The volume of fluid per unit volume of soil is $\theta = n\theta'$, so the equation takes the form

$$\frac{\partial u}{\partial x} + \frac{\partial v}{\partial y} + \frac{\partial w}{\partial z} = - \frac{\partial\theta}{\partial t} \qquad (2.7)$$

and if the flow is steady so there is the same mass of outflow as inflow, the equation of continuity [Lamb (1932)] becomes

$$\frac{\partial u}{\partial x} + \frac{\partial v}{\partial y} + \frac{\partial w}{\partial z} = 0 \qquad (2.8)$$

If it is assumed that Darcy's law applies to unsaturated flow and that K or k may be expressed as a function of θ, i.e.,

$$V = - K(\theta) \frac{\partial h}{\partial s} \qquad (2.9)$$

then it can be substituted into the equation of continuity to obtain a differential flow equation. First, however, it is useful to define a potential $\Phi = gh$, in which case Darcy's law for saturated flow becomes

$$V = - k \frac{\rho}{\mu} \frac{\partial \varphi}{\partial s} \qquad (2.10)$$

For unsaturated flow, capillary forces which are not present in saturated flow come into prominence, so the potential is assumed to be made up of two components: a gravity component given by gz, where the Z-axis is vertical, and a capillary component given by gh_c, where h_c is the capillary head. The capillary head is a function of the moisture content in such a way that $h_c = 0$ when $\theta = n$. Darcy's law with these features incorporated when applied to unsaturated flow takes the form

$$V = - k(\theta) \frac{\rho g}{\mu} \frac{\partial (z + h_c)}{\partial s} = - k(\theta) \frac{\rho g}{\mu} \left(\frac{\partial z}{\partial s} + \frac{\partial h_c}{\partial s}\right) \qquad (2.11)$$

For the special case of flow in the horizontal direction through a soil contained in a tube which is constructed so that the water is applied at atmospheric pressure and the air is free to escape, the equation becomes

$$V_x = - k(\theta) \frac{\rho g}{\mu} \frac{\partial h_c}{\partial x} \tag{2.12}$$

Combining Eqs. (2.11) and (2.6) yields

$$\frac{\rho g}{\mu} \frac{\partial}{\partial x} [k(\theta)\{\frac{\partial z}{\partial x} + \frac{\partial h_c}{\partial x}\}] + \frac{\rho g}{\mu} \frac{\partial}{\partial y} [k(\theta)\{\frac{\partial z}{\partial y} + \frac{\partial h_c}{\partial y}\}] + \frac{\rho g}{\mu} \frac{\partial}{\partial z} [k(\theta)\{\frac{\partial z}{\partial z} + \frac{\partial h_c}{\partial z}\}] = \frac{\partial \theta}{\partial t} \tag{2.13}$$

The above equation is not easily dealt with in the general case where $\theta = \theta(x,y,z,t)$. For unidirectional flow, however, two of the three terms on the left drop out. As a result, most of the work which has been done with unsaturated flow has dealt with one-dimensional flow. Moreover, horizontal flow is easier to handle than vertical flow as $\frac{\partial z}{\partial x}$ and $\frac{\partial z}{\partial y} = 0$ if the flow is horizontal. Thus, for horizontal flow, Eq. (2.13) becomes

$$\frac{\partial}{\partial x} [k(\theta) \frac{\partial h_c}{\partial x}] = \frac{\mu}{\rho g} \frac{\partial \theta}{\partial t} \tag{2.14}$$

By the chain rule of differentiation, this equation becomes

$$\frac{\partial}{\partial x} [k(\theta) \frac{\partial h_c}{\partial \theta} \frac{\partial \theta}{\partial x}] = \frac{\mu}{\rho g} \frac{\partial \theta}{\partial t} \tag{2.15}$$

It is convenient to define a term called the diffusivity as

$$D(\theta) = \frac{\rho g}{\mu} k(\theta) \frac{\partial h_c}{\partial \theta} \tag{2.16}$$

so that Eq. (2.16) becomes

$$\frac{\partial \theta}{\partial t} = \frac{\partial}{\partial x} [D(\theta) \frac{\partial \theta}{\partial x}] \tag{2.17}$$

This result was obtained by Klute (1952) and has since become the basic flow equation used in a number of investigations of unsaturated flow. The diffusivity has been experimentally evaluated from inflow data for horizontal columns [Bruce (1956)]. At the present time, however, there is no treatment of horizontal unsaturated flow with air resistance. A limited success in solving Eq. (2.17) numerically has been achieved, but difficulties with hysteresis complicate the problem unless a single wetting or drying cycle is followed.

The equation applicable to vertical unsaturated flow is readily determined from Eq. (2.15) to be

$$\frac{\partial \theta}{\partial t} = \frac{\rho g}{\mu} \frac{\partial}{\partial z} \left[k(\theta) \left\{ \frac{\partial z}{\partial z} + \frac{\partial h_c}{\partial z} \right\} \right] \tag{2.18}$$

The term $\frac{\partial z}{\partial z} = \pm 1$, depending on the orientation of the coordinate axes relative to the direction of flow. With the Z-axis positive upwards, the equation for downward flow is

$$\frac{\partial \theta}{\partial t} = \frac{\partial}{\partial z} \left[D(\theta) \frac{\partial \theta}{\partial z} \right] - \frac{\rho g}{\mu} \frac{\partial k}{\partial z} \tag{2.19}$$

and the equation for upward flow is

$$\frac{\partial \theta}{\partial t} = \frac{\partial}{\partial z} \left[D(\theta) \frac{\partial \theta}{\partial z} \right] + \frac{\rho g}{\mu} \frac{\partial k}{\partial z} \tag{2.20}$$

These two equations are not in a useful form to be solved or even to have the characteristics of the solution examined. The dependence of the diffusivity on θ has been examined and can be experimentally

determined. In order to separate out the terms which have to be determined experimentally, it is useful to treat $\frac{\partial k(\theta)}{\partial z}$ by the chain rule to obtain

$$\frac{\partial k}{\partial z} = \frac{\partial k}{\partial \theta} \frac{\partial \theta}{\partial z} \tag{2.21}$$

and then define

$$R(\theta) = \frac{\rho g}{\mu} \frac{\partial k}{\partial \theta} \tag{2.22}$$

$R(\theta)$ may be called the "randomicity" function, as it expresses the effect of the pore size distribution of the medium. It can be evaluated from experimental measurements such as those obtained by Brooks and Corey (1964) or Bruce (1956). The equations describing downward flow and upward flow become

$$\frac{\partial \theta}{\partial t} = \frac{\partial}{\partial z} \left[D(\theta) \frac{\partial \theta}{\partial z} \right] - R(\theta) \frac{\partial \theta}{\partial z} \tag{2.23}$$

and

$$\frac{\partial \theta}{\partial t} = \frac{\partial}{\partial z} \left[D(\theta) \frac{\partial \theta}{\partial z} \right] + R(\theta) \frac{\partial \theta}{\partial z} \tag{2.24}$$

These partial differential equations together with the appropriate boundary conditions and the experimentally determined functions $D(\theta)$ and $R(\theta)$ are sufficient to permit the numerical solution of upward and downward flow. Hysteresis would make it necessary to solve the equations on either a wetting or drying cycle.

CHAPTER 3

EQUATIONS FOR SATURATED FLOW

3.1 Discussion of Assumptions

The partial differential equations which were derived in Chapter 2 adequately describe the flow of water in porous mediums. A serious drawback to their use is the extreme difficulty which is encountered in solving them. Experimentally obtainable data are necessary for the diffusivity function $D(\theta)$ and the randomicity function $R(\theta)$. Even after these data are available, it is necessary to resort to digital computers to cope with the resulting lengthy numerical solutions. As a consequence, it is difficult to estimate the changes brought about by altering various flow parameters. The parameter to which attention will be directed in this work is the effect of air displaced by the wetting front on infiltration. One of the implicit assumptions which were made in deriving the unsaturated flow equations was that the air offered a negligible resistance to flow. Experimental work carried out by Nielsen, Biggar and Davidson (1962) raised questions on the validity of the unsaturated flow equations for horizontal flow when water at reduced pressure was applied to horizontal soil columns and the air was free to escape, so there is justification for reformulating the flow equations in more tractable form if attention can be focused on the changes brought about by air resistance.

To focus attention more closely on the effects of air resistance on infiltration, some simplifying assumptions will be made. If the saturation of the medium were constant, the hydraulic conductivity would be constant. The medium could reach a state of complete saturation and thus have a constant hydraulic conductivity, or it might attain a constant percentage of saturation everywhere in the flow field and thus have a constant hydraulic conductivity whose value would be less than the saturated hydraulic conductivity. Another assumption that would simplify the flow picture would be to assume there was a sharp wetting front so there would be a definite air-water interface, ahead of which the medium would be at whatever moisture content existed prior to the beginning of infiltration and behind which the medium would be completely saturated, or nearly so. With these assumptions the capillary forces which would assist infiltration could be considered to act at the interface.

There are mediums which have capillary characteristics which make them behave in a manner reasonably consistent with the above assumptions. The degree to which a medium becomes saturated when placed in contact with water is determined mainly by its pore size distribution. If the pores vary widely in size, some will fill and transport water more easily than others. With the many interconnections which exist between the various pores, some will be bypassed for a short distance, then will become blocked by water and entrap air. As a result, the medium may vary in the degree of saturation with distance from the water source. Also, the air-water interface will not be as well defined as

it would be if the pore sizes were all the same. When the pore sizes are all nearly the same, there should be much less tendency for some sections of pores to be bypassed for short distances resulting in the entrapment of air. Thus mediums with a uniform pore size distribution should have a well-defined air-water interface and should saturate reasonably uniformly. Uniform pore size distributions are obtained by using a medium made up of particles having a constant size and shape, such as glass beads. Additional data on the effect of pore size distribution on the saturation of porous mediums are contained in a recent publication by Brooks and Corey (1964).

3.2 Infiltration Without Air Resistance and Without Capillary Forces

If downward infiltration into a homogeneous and isotropic porous medium is considered, assuming the infiltrating water completely fills the pores, it is possible to obtain an explicit expression for the location of the wetting front as a function of time. The most elementary case to consider is that in which there is no air resistance and where capillary forces are neglected, as illustrated in Figure 3.1.

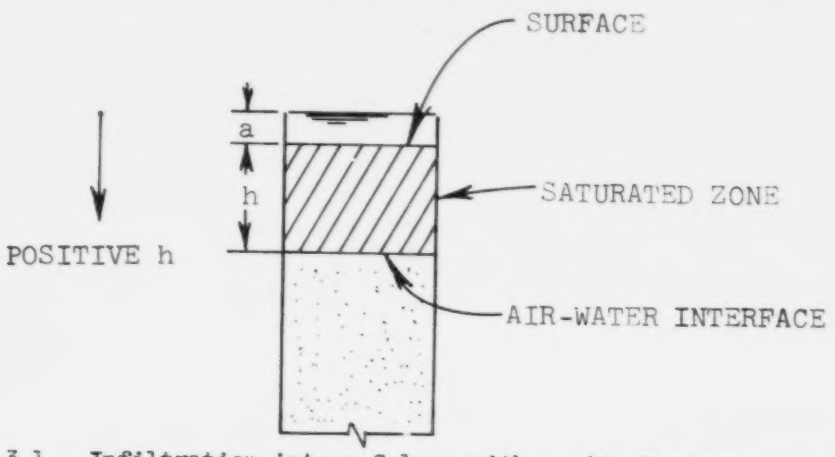

Figure 3.1. Infiltration into a Column with no Air Resistance.

In developing the differential equation of flow, it is assumed that water is applied uniformly to the surface of the column of soil. The depth a of water on the surface is kept constant. After some time the water has infiltrated to a depth h measured from the top of the column as reference level. The velocity of the wetting front $\frac{dh}{dt}$ is related to the flux through the surface by $V = n \frac{dh}{dt}$, where V is the approach velocity given by Darcy's law $V = K(dh_\ell/dz)$, where K is the permeability of the medium to water and dh_ℓ/dz is the head loss gradient which is the negative of the hydraulic energy gradient. In this case the head loss gradient is $\frac{h+a}{h}$. Combining these equations yields

$$\frac{dh}{dt} = \frac{K}{n} \frac{h+a}{h} \tag{3.1}$$

which becomes after separating variables

$$(1 - \frac{a}{h+a})dh = \frac{K}{n} dt$$

The boundary conditions may be expressed as

$$h = h_1 \quad \text{when} \quad t = t_1 \tag{3.2a}$$

$$h = h_2 \quad \text{when} \quad t = t_2 \tag{3.2b}$$

Integrating between these limits yields

$$(h_2-h_1) - a \ln(\frac{h_2 + a}{h_1 + a}) = \frac{K}{n} (t_2-t_1) \tag{3.3}$$

which may be made dimensionless by dividing the entire equation by some expression which has the dimensions of length. A dimension which is convenient for laboratory work is the column length ℓ. Equation (3.3) becomes

$$\left(\frac{h_2}{\ell} - \frac{h_1}{\ell}\right) - \frac{a}{\ell}\, \ell n \left(\frac{\left(\frac{h_2}{\ell} + \frac{a}{\ell}\right)}{\left(\frac{h_1}{\ell} + \frac{a}{\ell}\right)} \right) = \frac{Kt_2}{n\ell} - \frac{Kt_1}{n\ell} \qquad (3.4)$$

By the usual convention for dimensionless variables let $\frac{h_2}{\ell} = h_2^*$, $\frac{h_1}{\ell} = h_1^*$, $\frac{a}{\ell} = a^*$, $\frac{Kt_2}{n\ell} = t_2^*$ and $\frac{Kt_1}{n\ell} = t_1^*$. It is convenient to consider the case where $h_1^* = 0$ when $t_1^* = 0$ and then replace h_2^* by h^* and t_2^* by t^*. Equation (3.4) for this case becomes

$$h^* + a^* \ell n\left(\frac{a^*}{a^* + h^*}\right) = t^* \qquad (3.5)$$

If no water is ponded on the surface but is supplied at the infiltration rate, the distance a will be zero and Eq. (3.5) has to be examined to determine whether it is still applicable. The term $a^* \ell n\left(\frac{a^*}{a^* + h^*}\right)$ may be considered the quotient of two functions $f(a^*) = \ell n\left(\frac{a^*}{a^* + h^*}\right)$ and $g(a^*) = \frac{1}{a^*}$. Thus the limit

$$\lim_{a^* \to 0} a^* \ell n\left(\frac{a^*}{a^* + h^*}\right) = \lim_{a^* \to 0} \frac{f(a^*)}{g(a^*)} = \frac{-\infty}{\infty} \qquad (3.6)$$

is an undetermined form. Application of L'Hospitals' rule [Taylor (1959)] results in the examination of the limit given by $\lim_{a^* \to 0} \frac{f'(a^*)}{g'(a^*)}$, which is

$$\lim_{a^* \to 0} \frac{a^* + h^*}{a^*} \left(\frac{a^* + h^* - a^*}{(a^* + h^*)^2} \right) \Bigg/ \frac{-1}{(a^*)^2} = \lim_{a^* \to 0} \frac{-a^* h^*}{a^* + h^*} = 0 \qquad (3.7)$$

Hence, Eq. (3.5) is applicable even in the absence of ponding and the solution for no ponding is

$$h = \frac{K}{n} t \qquad (3.8)$$

or, in dimensionless form,

$$h^* = t^* \qquad (3.9)$$

The advantage of the dimensionless forms of the infiltration equations is that families of solutions can be obtained for various values of a^* and these curves are easily compared to experimental data determined from many different soils.

The infiltration rate is given by the approach velocity V from Darcy's equation. Thus for the general case Eq. (3.5) may be rewritten

$$h + a \, \ell n\left(\frac{a}{a+h}\right) = \frac{Kt}{n} \qquad (3.10)$$

which permits the calculation of the time required for the wetting front to reach any given value of h. Finally, infiltration rate may be determined as a function of time by combining Eq. (3.1) with Eq. (3.10).

3.3 Infiltration with Capillary Forces and Ponding

Reference to Figure 3.1 is helpful in developing the equations for vertical flow when capillary forces are acting at the interface.

The head loss gradient is $h+a+h_c/h$, so that Darcy's equation combined with the equation of continuity becomes

$$\frac{dh}{dt} = \frac{K}{n} \frac{h+a+h_c}{h} \tag{3.11}$$

Separation of the variables and establishment of the limits of integration results in

$$\int_{h_1}^{h_2} \left\{1 - \frac{a+h_c}{h+a+h_c}\right\} dh = \frac{K}{n} \int_{t_1}^{t_2} dt \tag{3.12}$$

which integrates to

$$(h_2-h_1) + (h_c+a)\ \ell n \left(\frac{h_1+a+h_c}{h_2+a+h_c}\right) = \frac{K}{n} (t_2-t_1) \tag{3.13}$$

If $h_2 = h$ when $t_2 = t$ and $h_1 = 0$ when $t_1 = 0$, the above equation reduces to

$$h + (h_c+a)\ \ell n \left(\frac{a+h_c}{h+a+h_c}\right) = \frac{Kt}{n} \tag{3.14}$$

This equation may be written in dimensionless form if it is nondimensionalized on the column length. The only new dimensionless term will be $h_c^* = h_c/\ell$. The other terms are the same as in Sec. 3.2. In dimensionless form Eq. (3.14) becomes

$$h^* + (h_c^* + a^*)\ \ell n \left(\frac{a^* + h_c^*}{h^* + a^* + h_c^*}\right) = t^* \tag{3.15}$$

In principle, Eqs. (3.11) and (3.14) may be combined to give the infiltration rate as a function of time. However, Eq. (3.14) cannot

be solved directly for h as an explicit function of time, but the time required for any given h value to be reached may be computed. Then by using this value of h in Eq. (3.11), the infiltration rate at this particular time is readily computed. These values may be presented graphically to show infiltration rate as a function of time.

The equations in Sec. 3.3 are more general then those of Sec. 3.2. By setting $h_c = 0$, Eq. (3.10) is obtained as a special case of Eq. (3.14).

3.4 Horizontal Flow in a Column with no Air Resistance

Horizontal flow into a column has been studied frequently under the assumption that only capillary forces act and that there is no air resistance. For horizontal flow with the water applied at zero pressure, Eq. (3.11) may be written

$$V = K \frac{h_c}{x} \tag{3.16}$$

where the X-axis is horizontal. Combining this with the equation of continuity $V = n \frac{dx}{dt}$ results in

$$\frac{dx}{dt} = \frac{Kh_c}{nx} \tag{3.17}$$

which integrates to

$$\frac{x^2}{2}\Big]_{x_1}^{x_2} = \frac{Kh_c}{n}(t_2 - t_1) \quad \text{or} \quad \frac{x_2^2 - x_1^2}{2} = \frac{Kh_c}{n}(t_2 - t_1) \tag{3.18}$$

and by letting $x_2 = x$ when $t_2 = t$ and $x_1 = 0$ when $t_1 = 0$, the equation simplifies to

$$x^2 = \frac{2Kh_c}{n} t \tag{3.19}$$

or

$$x = \left(\frac{2Kh_c}{n}\right)^{\frac{1}{2}} \sqrt{t} \tag{3.20}$$

3.5 Horizontal Flow into a Column with Resistance

As a first step in considering horizontal flow with resistance consider two immiscible liquids in a horizontal porous medium. Let the capillary pressure at the interface be p_c and let the liquid being imbibed be supplied at atmospheric pressure and the liquid being displaced be discharged at atmospheric pressure. The capillary force at the interface will be the only driving force. The flow diagram and the pressure diagram is shown in Figure 3.2. The pressure diagram can

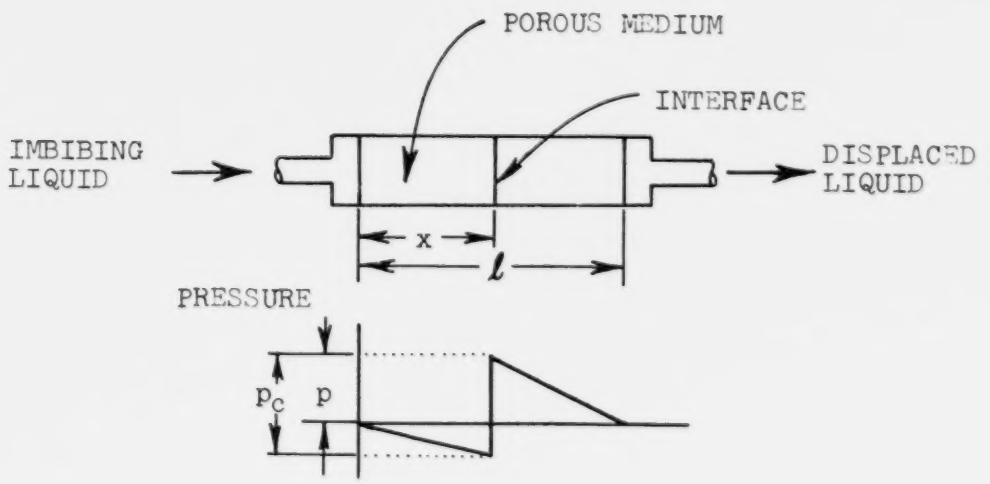

Figure 3.2. Displacement of One Immiscible Liquid by Another.

be qualitatively obtained by noting that the imbibing fluid is being pulled ahead by part of the capillary pressure force, while the displaced fluid is being pushed out by a portion of the capillary pressure force. The value of p is unknown and will vary with position and velocity. Darcy's equation combined with the equation of continuity for the imbibing fluid will be

$$n \frac{dx}{dt} = K_1 \frac{p_c - p}{\gamma_1 x} \tag{3.21}$$

and for the second fluid

$$n \frac{dx}{dt} = K_2 \frac{p/\gamma_2}{\ell - x} \tag{3.22}$$

Solving for p yields

$$p = \gamma_2 n \frac{dx}{dt} \frac{\ell - x}{K_2} \tag{3.23}$$

which can be combined with Eq. (3.21) to yield

$$n \frac{dx}{dt} = K_1 \frac{p_c - \frac{\gamma_2}{K_2} (\ell - x) n \frac{dx}{dt}}{\gamma_1 x} \tag{3.24}$$

or

$$\int_{x_1}^{x_2} \left\{ n\gamma_1 x + \frac{n\gamma_2 K_1}{K_2} (\ell - x) \right\} dx = K_1 p_c \int_{t_1}^{t_2} dt \tag{3.25}$$

which integrates to

$$\frac{n\gamma_1}{2} (x_2^2 - x_1^2) + \frac{n\gamma_2 K_1}{K_2} \ell (x_2 - x_1) - \frac{n\gamma_2 K_1}{2K_2} (x_2^2 - x_1^2) = K_1 p_c (t_2 - t_1) \tag{3.26}$$

This result may be rearranged as

$$\frac{x_2^2 - x_1^2}{2} = \frac{\gamma_2 K_1}{2\gamma_1 K_2}(x_2^2 - x_1^2) - \frac{\gamma_2 K_1}{\gamma_1 K_2}\ell(x_2 - x_1) + \frac{K_1 p_c (t_2 - t_1)}{n\gamma_1} \qquad (3.27)$$

The liquid which is being displaced has a negligible resistance to flow when K_2 becomes very large. Examination of Eq. (3.27) when $K_2 \to \infty$ yields

$$\frac{x_2^2 - x_1^2}{2} = \frac{K_1 p_c (t_2 - t_1)}{n\gamma_1} \qquad (3.28)$$

which is identical to Eq. (3.18), which was derived under the assumption that the second fluid had no resistance to flow. Equation (3.27) can be rearranged to solve for x_2 as a function of time by noting

$$0 = x_2^2 + x_2 \frac{\frac{\gamma_2 K_1 \ell}{\gamma_1 K_2}}{(\frac{1}{2} - \frac{\gamma_2 K_1}{4\gamma_1 K_2})} - \left[x_1^2 + x_1 \frac{\frac{\gamma_2 K_1 \ell}{\gamma_1 K_2}}{(\frac{1}{2} - \frac{\gamma_2 K_1}{4\gamma_1 K_2})} + \frac{K_1 p_c (t_2 - t_1)}{n\gamma_1 / (\frac{1}{2} - \frac{\gamma_2 K_1}{4\gamma_1 K_2})} \right] \qquad (3.29)$$

so that

$$x_2 = -\frac{\gamma_2 K_1 \ell}{\gamma_1 K_2 (\frac{1}{2} - \frac{\gamma_2 K_1}{4\gamma_1 K_2})} + \left(\left[\frac{\gamma_2 K_1 \ell}{\gamma_1 K_2 (\frac{1}{2} - \frac{\gamma_2 K_1}{4\gamma_1 K_2})} \right]^2 \right.$$

$$\left. + 4\left[x_1^2 + \frac{x_1 \gamma_2 K_1 \ell}{\gamma_1 K_2 (\frac{1}{2} - \frac{\gamma_2 K_1}{4\gamma_1 K_2})} + \frac{K_1 p_c (t_2 - t_1)}{n\gamma_1 (\frac{1}{2} - \frac{\gamma_2 K_1}{4\gamma_1 K_2})} \right] \right)^{\frac{1}{2}} \qquad (3.30)$$

In case $x_1 = 0$ when $t_1 = 0$ and $x_2 = x$ when $t_2 = t$, Eq. (3.30) becomes

$$x = - \frac{\gamma_2 K_1 \ell}{\gamma_1 K_2 (\frac{1}{2} - \frac{\gamma_2 K_1}{4\gamma_1 K_2})} + \left(\left[\frac{\gamma_2 K_1 \ell}{\gamma_1 K_2 (\frac{1}{2} - \frac{\gamma_2 K_1}{4\gamma_1 K_2})} \right]^2 + \frac{4 K_1 p_c t}{n\gamma_1 (\frac{1}{2} - \frac{\gamma_2}{4\gamma_1} \frac{K_1}{K_2})} \right)^{\frac{1}{2}} \quad (3.31)$$

3.6 Horizontal Flow of Gases

To determine the resistance of air flow in a porous medium, it will be necessary to examine the applicability of Darcy's law to the flow of a compressible fluid. Because of the compressibility of a gas, the equation of continuity must be written

$$\rho_1 V_1 = \rho_2 V_2 = \rho V \quad (3.32)$$

at any two sections 1 and 2 in a porous medium. The general vector form of Darcy's equation for the flow of any Newtonian fluid is [Hubbert (1940)]

$$\vec{V} = k \frac{\rho}{\mu} (\vec{g} - \frac{1}{\rho} \text{ grad } p) \quad (3.33)$$

For horizontal flow this becomes

$$V = - k \frac{\rho}{\mu} (\frac{1}{\rho} \frac{\partial p}{\partial x}) \quad (3.34)$$

and when applied to a compressible flow, the result is

$$\rho V = - k \frac{\rho}{\mu} \frac{\partial p}{\partial x} \quad (3.35)$$

where ρ and V are evaluated at the same location in the porous medium. The gas flow may be considered as an isothermal process, so the perfect gas equation

$$p = \rho RT \tag{3.36}$$

may be written

$$\frac{p}{\rho} = \text{constant} \tag{3.37}$$

or

$$\frac{p_o}{\rho_o} = \frac{p}{\rho} = \text{constant} \tag{3.38}$$

where p_o and ρ_o are the pressure and density at reference conditions. Equation (3.36) combined with Eq. (3.35) yields

$$\rho V = - \frac{k}{\mu} \frac{\rho_o}{p_o} p \frac{\partial p}{\partial x} \tag{3.39}$$

which becomes

$$\rho V = - \frac{k}{\mu} \frac{\rho_o}{p_o} \frac{1}{2} \frac{\partial p^2}{\partial x} \tag{3.40}$$

For a constant mass flow rate all terms of Eq. (3.40) are constant, so that $\frac{\partial p^2}{\partial x} = \text{constant}$. This result indicates that the gradient of the square of the pressure is constant for gas flow in contrast to the horizontal flow of a liquid in which the gradient of the pressure is constant. Figure 3.3 illustrates the pressure variation in gas flow over a distance ℓ of porous medium. From the diagram it is obvious that

$$\frac{\partial p^2}{\partial x} = \frac{p_2^2 - p_1^2}{\ell} = \frac{(p_2 + p_1)}{2} \frac{2(p_2 - p_1)}{\ell} = \frac{2\bar{p}(p_2 - p_1)}{\ell} \tag{3.41}$$

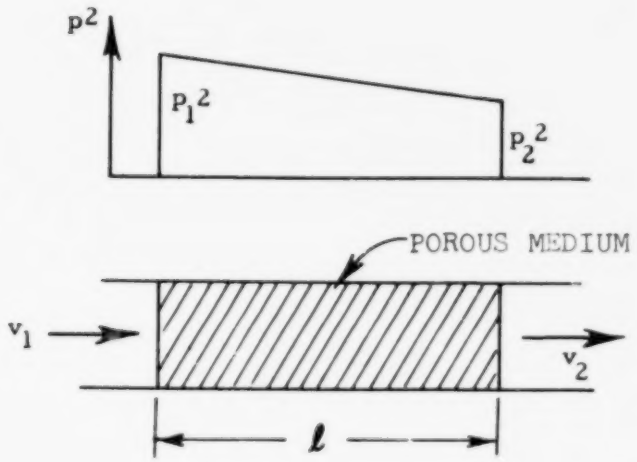

Figure 3.3. Pressure Variation in Gas Flow.

where $\bar{p}$ is the average of the inlet and outlet pressures between two sections a distance ℓ apart. Equations (3.40) and (3.41) yield

$$\rho V = - \frac{k}{\mu} \frac{\rho_o}{p_o} \bar{p} \frac{p_2 - p_1}{\ell}$$

which may be written

$$\rho V = \frac{k}{\mu} \frac{\rho_o}{p_o} \bar{p} \frac{p_1 - p_2}{\ell} \tag{3.42}$$

If the gas is discharged at atmospheric pressure and atmospheric pressure is used as the reference condition, then

$$V_o = \frac{k}{\mu} \frac{\bar{p}}{p_o} \frac{p_1 - p_2}{\ell} \tag{3.43}$$

where V_o is the exit velocity into the atmosphere.

To compare the difference in volume discharge rates between air and water, consider the two horizontal columns shown in Figure 3.4.

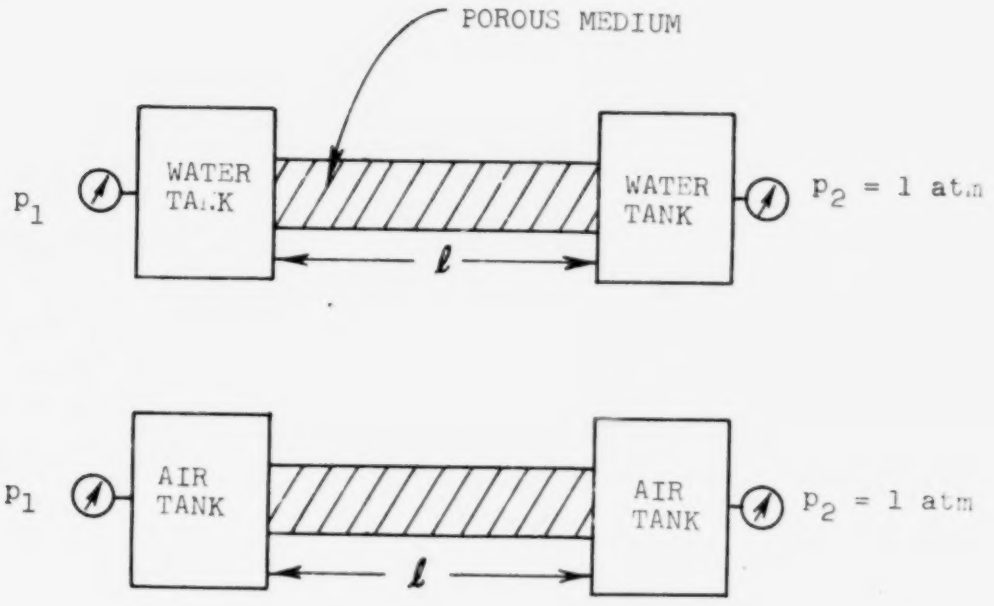

Figure 3.4. Comparison of Air and Water Flowrates Through Identical Porous Mediums.

Let the pressure on the inlet side at the center line be atmospheric pressure. Then consider the ratio of the exit velocities of air and water measured under atmospheric pressure conditions. The ratio will be

$$\frac{V_{air}}{V_{water}} = \frac{\frac{k}{\mu_{air}} \frac{\bar{p}}{p_o} \frac{p_1 - p_2}{\ell}}{\frac{k}{\mu_{water}} \frac{p_1 - p_2}{\ell}} \tag{3.44}$$

which becomes

$$\frac{V_{air}}{V_{water}} = \frac{\mu_{water}}{\mu_{air}} \frac{p_1 + p_2}{2p_o} \tag{3.45}$$

or

$$\frac{V_{air}}{V_{water}} = \frac{\mu_{water}}{\mu_{air}} \frac{1}{2} \left(1 + \frac{p_1}{p_o}\right) \tag{3.46}$$

This indicates that for a pressure p_1 only slightly greater than atmospheric pressure the limit of the ratio

$$\frac{V_{air}}{V_{water}} = \frac{2.359 \cdot 10^{-5}}{3.737 \cdot 10^{-7}} = 63.2$$

where the viscosities of air and water at 60°F have been used. At higher values of p_1 the ratio will increase. This result justifies the neglect of air resistance in most infiltration problems.

In the previous derivation of Darcy's equation for gas flow, the intrinsic permeability was considered constant. Pioneering research by Klinkenberg (1941) proved that for pressures below about 20 atmospheres a gas does not behave as a Newtonian fluid when flowing through a porous medium having very small pore spaces. His studies indicate that there is slip between the gas and the solid particles of the medium, which results in higher intrinsic permeabilities being observed for gases than for liquids. This effect was most apparent in the least permeable samples which contained the finest pore spaces. For a mean pressure near atmospheric pressure the apparent intrinsic permeability

to air was usually less than 50% higher than the intrinsic permeability to liquids. This Klinkenberg slip phenomenon further decreases the resistance offered by air to flow.

3.7 Vertical Flow Against Air Resistance

The previous section demonstrated that in most situations the resistance of air to flow was negligible in comparison to the resistance of water to flow. This conclusion was predicated on the assumption that the air was free to escape from the soil. If the air is not free to escape, it will be compressed and its pressure will increase. A simple model illustrating this effect is shown in Figure 3.5 where there is

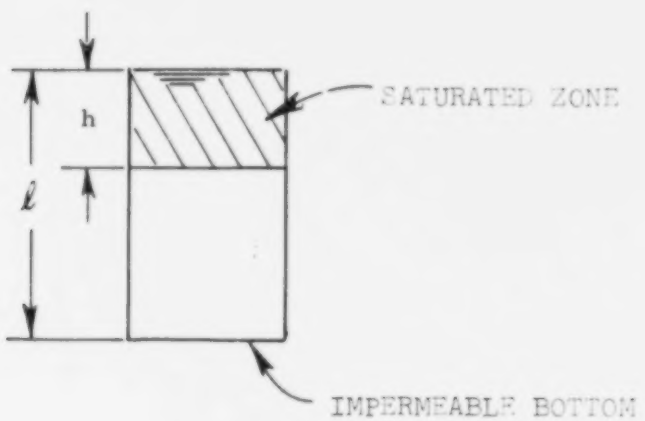

Figure 3.5. Infiltration Against Air Resistance.

infiltration into a vertical column which is sealed at the bottom. Consider the soil to be dry originally, so the volume of air contained

in the pore space would be $nA\ell$, where n is the porosity of the medium, A is the cross-sectional area of the column, and ℓ is its length. If water is ponded on the surface so that the air-water interface moves to a distance h below the surface, the volume occupied by the air will be $nA(\ell-h)$. The original pressure on the air was atmospheric pressure p_o and the pressure when the interface has dropped a distance h will be p_1. These pressures are related through the perfect gas law as

$$p_o\, nA\ell = p_1\, nA(\ell-h) \tag{3.47}$$

which becomes

$$p_1 = p_o \frac{\ell}{\ell-h} \tag{3.48}$$

To determine the head loss gradient used in Darcy's equation, it is useful to recall that p_o and p_1 are absolute pressures rather than gauge pressures. The head loss gradient is then

$$\frac{h_\ell}{h} = \frac{h + h_c - (\frac{p_1}{\gamma} - \frac{p_o}{\gamma})}{h} \tag{3.49}$$

which may be substituted into Darcy's equation to obtain

$$V = K \frac{h + h_c - (\frac{p_1}{\gamma} - \frac{p_o}{\gamma})}{h} \tag{3.50}$$

This result may be combined with the equation of continuity to obtain the differential equation for the flow

$$n\frac{dh}{dt} = K\frac{h + h_c - (p_1 - p_o)/\gamma}{h} \tag{3.51}$$

Substituting p_1 as a function of h from Eq. (3.48) into the above equation gives

$$n\frac{dh}{dt} = K\frac{h + h_c - (\frac{p_o \ell}{\ell - h} - p_o)/\gamma}{h} \tag{3.52}$$

After separating the variables, the differential equation becomes

$$\frac{\ell h - h^2}{\ell h - h^2 + h_c \ell - h_c h - \frac{p_o}{\gamma} h}\, dh = \frac{K}{n}\, dt \tag{3.53}$$

or

$$\int_{h_1}^{h_2}\left[1 - \frac{h(h_c + \frac{p_o}{\gamma})}{h^2 + h(h_c + \frac{p_o}{\gamma} - \ell) - h_c \ell} + \frac{h_c \ell}{h^2 + h(h_c + \frac{p_o}{\gamma} - \ell) - h_c \ell}\right] dh = \frac{K}{n}\int_{t_1}^{t_2} dt \tag{3.54}$$

This equation may be integrated to obtain

$$\frac{K(t_2 - t_1)}{n} = (h_2 - h_1) - \frac{h_c + \frac{p_o}{\gamma}}{2} \ln\left[\frac{h_2^2 + (h_c + \frac{p_o}{\gamma} - \ell)h_2 - h_c \ell}{h_1^2 + (h_c + \frac{p_o}{\gamma} - \ell)h_1 - h_c \ell}\right]$$

$$+ \frac{(h_c + \frac{p_o}{\gamma} - \ell)^2 + (h_c + \frac{p_o}{\gamma} - \ell)\ell + 2h_c \ell}{2[(h_c + \frac{p_o}{\gamma} - \ell)^2 + 4h_c \ell]^{\frac{1}{2}}}$$

$$\times \ln\left[\left\{\frac{2h_2 + (h_c + \frac{p_o}{\gamma} - \ell) - [(h_c + \frac{p_o}{\gamma} - \ell)^2 + 4h_c \ell]^{\frac{1}{2}}}{2h_2 + (h_c + \frac{p_o}{\gamma} - \ell) + [(h_c + \frac{p_o}{\gamma} - \ell)^2 + 4h_c \ell]^{\frac{1}{2}}}\right\}\left\{\frac{2h_1 + (h_c + \frac{p_o}{\gamma} - \ell) + [(h_c + \frac{p_o}{\gamma} - \ell)^2 + 4h_c \ell]^{\frac{1}{2}}}{2h_1 + (h_c + \frac{p_o}{\gamma} - \ell) - [(h_c + \frac{p_o}{\gamma} - \ell)^2 + 4h_c \ell]^{\frac{1}{2}}}\right\}\right] \tag{3.55}$$

The previous result can be simplified somewhat by selecting $h_2 = h$ when $t_2 = t$ and $h_1 = 0$ when $t_1 = 0$. For this case the result is

$$\frac{Kt}{n} = h - \frac{h_c + \frac{p_o}{\gamma}}{2} \ell n \left[\frac{h^2 + (h_c + \frac{p_o}{\gamma} - \ell)h - h_c \ell}{-h_c \ell} \right] + \frac{(h_c + \frac{p_o}{\gamma} - \ell)^2 + (h_c + \frac{p_o}{\gamma} - \ell)\ell + 2h_c \ell}{2[(h_c + \frac{p_o}{\gamma} - \ell)^2 + 4h_c \ell]^{\frac{1}{2}}}$$

$$\times \ell n \left[\left\{ \frac{2h + (h_c + \frac{p_o}{\gamma} - \ell) - [(h_c + \frac{p_o}{\gamma} - \ell)^2 + 4h_c \ell]^{\frac{1}{2}}}{2h - (h_c + \frac{p_o}{\gamma} - \ell) + [(h_c + \frac{p_o}{\gamma} - \ell)^2 + 4h_c \ell]^{\frac{1}{2}}} \right\} \left\{ \frac{(h_c + \frac{p_o}{\gamma} - \ell) + [(h_c + \frac{p_o}{\gamma} - \ell)^2 + 4h_c \ell]^{\frac{1}{2}}}{(h_c + \frac{p_o}{\gamma} - \ell) - [(h_c + \frac{p_o}{\gamma} - \ell)^2 + 4h_c \ell]^{\frac{1}{2}}} \right\} \right]$$

(3.56)

There is a maximum value that may be assigned to the upper limit of the integration as will be shown later in Chapter 4. To evaluate the infiltration rate as a function of time, a procedure similar to that followed in Sec. 3.3 may be followed. The time required for the wetting front to advance a distance h may be calculated from Eq. (3.56). Then the pressure ahead of the wetting front may be calculated for this value of h from Eq. (3.48). The next step is to use the above results in Eq. (3.50) to obtain the infiltration rate. A series of calculations following the above procedure permits enough data to be obtained to graph the infiltration rate as a function of time. The foregoing is of course based on the premise that there is no escape of air upward through the medium.

CHAPTER 4

THEORY OF CAPILLARY EQUILIBRIUM

It is a common observation that if a porous medium is in contact with a water table, there will be water which migrates upward into the soil. This wetted zone is often known as the "capillary fringe." The thickness of the capillary zone varies with the soil type, but with some idealizations it is possible to obtain analytic expressions for the height of capillary rise.

4.1 The Capillary Tube Analogy

The simplest model to use is the one which idealizes the porous medium as a collection of capillary tubes. From a balance of gravity forces and surface tension forces in a capillary tube it is easy to determine that the height of capillary rise h_c is given as

$$h_c = \frac{4T \cos \theta}{\gamma D} \tag{4.1}$$

where T is the surface tension with dimensions of M/T^2, γ is the specific weight of water, D is the diameter of the tube, and θ is the angle of contact between the water surface and the tube. The analogy is then made that the porous medium should have the same type of expression for the thickness of its capillary fringe. In the case of a porous medium, if D is replaced by the grain diameter of the medium, the height of capillary rise becomes

$$h_c = \frac{4T \cos \theta}{\gamma d} \tag{4.2}$$

This is not a satisfactory treatment, as the grain diameter is not as good a measure of the capillary characteristics of the medium as the pore diameter. However, it is difficult to determine the pore diameter, particularly for media whose particles vary considerably in size. Thus Eq. (4.2) ought to be multiplied by some factor that relates pore diameter to grain diameter.

4.2 Hydraulic Radius Concept

Another approach is to borrow from hydraulics the useful concept of the hydraulic radius to help describe the capillary rise in porous media. In hydraulics the hydraulic radius is defined as the ratio between the cross-sectional area of a conduit and the wetted perimeter of the conduit. Thus, the hydraulic radius of a circular pipe flowing full is

$$R_H = \frac{\pi D^2}{4\pi D} = \frac{D}{4} \tag{4.3}$$

For a circular pipe the height of capillary rise in terms of the hydraulic radius would be

$$h_c = \frac{T \cos \theta}{\gamma R_H} \tag{4.4}$$

The hydraulic radius of a porous medium may be expressed in terms of the properties of the medium by observing that $R_H = A\ell / P_w \ell$, where ℓ is an arbitrary length of medium and P_w is the wetted perimeter.

Then $A\ell$ is the volume of the voids and $P_w\ell$ is the surface area of the medium. Let V_T be the total volume of porous medium being considered, so the volume of voids will be nV_T. If there are N spheres of diameter d in V_T, the surface area of the spheres will be $N\pi d^2$, so the hydraulic radius becomes

$$R_H = \frac{nV_T}{N\pi d^2} \tag{4.5}$$

The volume of the voids is nV_T; the volume is also $V_T - N\pi d^3/6$. Thus $nV_T = V_T - N\pi d^3/6$, which may be solved for N to yield $N = [V_T(1-n)]/\pi d^3$, which may be substituted into Eq. (4.5) to give

$$R_H = \frac{d}{6}\frac{n}{1-n} \tag{4.6}$$

The term $d/6$ is the ratio of the volume of a sphere to its surface area and may be termed a shape-size factor. This factor is useful when other than spherical media are considered: the number 6 may be considered a shape factor and d a size factor. Thus, for other than spherical media

$$R_H = \frac{d}{S}\frac{n}{1-n} \tag{4.7}$$

where d may be determined by sieving and S is the shape factor. Values of S for various sands are given by Fair and Hatch (1933). Equation (4.4) then becomes

$$h_c = \frac{T\cos\theta}{\gamma}\frac{S}{d}\frac{1-n}{n} \tag{4.8}$$

in which the first term expresses the fluid properties, and the second term expresses the characteristics of the porous medium. From a comparison of Eqs. (4.2) and (4.8), the equivalent size of a capillary tube giving the same capillary rise as that in a porous medium is

$$D = \frac{4d}{S} \frac{n}{1-n} \tag{4.9}$$

This relation gives the ratio to be used in modeling if the medium and the capillary tube are constructed of the same material. If they are constructed of material with different wetting properties, then

$$D = \frac{4d}{S} \frac{n}{1-n} \frac{\cos \theta_c}{\cos \theta_m} \tag{4.10}$$

where θ_c is the angle of the contact of the liquid in the capillary tube, and θ_m is the angle of contact of the liquid in the porous medium.

4.3 Surface Interface Concept

Another approach to describe the height of capillary rise in porous media of uniform spheres is to examine the forces acting at the air-water interface. From an analysis of the forces acting on a doubly curved surface which is under tension, the pressure difference across the surface is

$$\Delta p = T\left(\frac{1}{R_1} + \frac{1}{R_2}\right) \tag{4.11}$$

where T is the tension expressed as a force per unit length and R_1 and R_2 are the principle radii of curvature. The surface is shown in Figure 4.1. This concept of a pressure difference being established

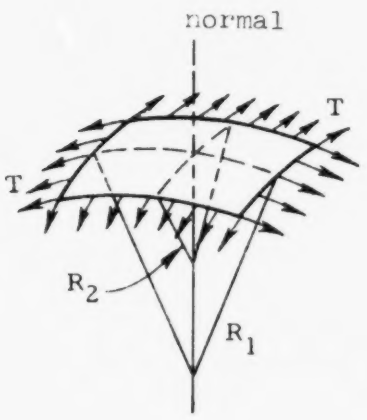

Figure 4.1. Doubly Curved Surface Under Uniform Tension.

by surface tension forces acting on curved interfaces may be applied to water in the interstices of porous media.

A few special packings of spherical media will be considered to illustrate the application of this concept. Consider first the packing of spheres shown in Figure 4.2. The air-water interface is considered to be in equilibrium. That is, the water has risen through the porous medium a height h_c and is now at static equilibrium. The nature of the packing below the level shown in the figure is not specified.

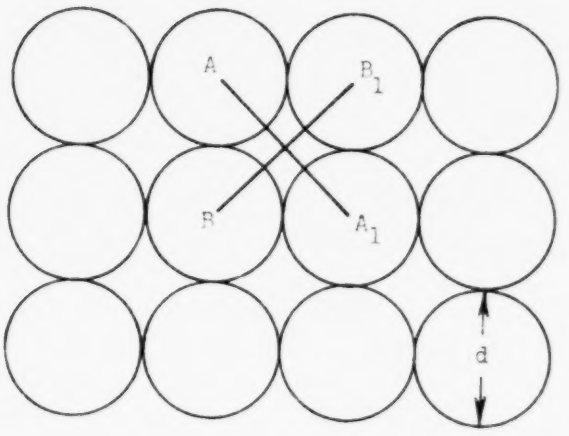

Figure 4.2. Plan View of Square-Packed Spheres.

Consider two vertical planes which cut the medium at AA_1 and BB_1, the planes being constructed so A, A_1, B, and B_1 are located at the center of four adjacent spheres. The planes meet orthogonally. The distance $AB = BA_1 = A_1B_1 = AB_1 = d$, so that $AA_1 = BB_1 = \sqrt{2}\, d$. Then the distance between the closest points of the spheres with centers at A and A_1 is $\sqrt{2}\, d - d$, which is also the distance between the closest points of the spheres with centers at B and B_1. These distances are shown in Figure 4.2. The air-water interface's position is not yet known. From Eq. (4.11) it is seen that the maximum pressure difference occurs when $\frac{1}{R_1} + \frac{1}{R_2}$ is a maximum. Due to the symmetry of the packing being considered $R_1 = R_2$, so

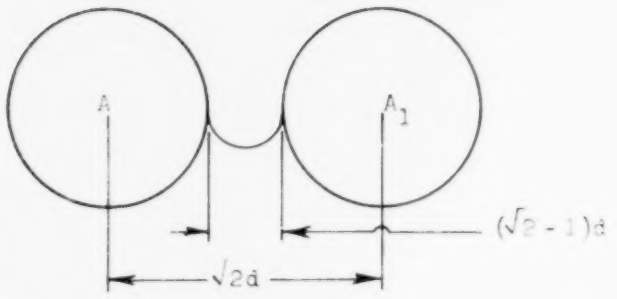

Figure 4.4. Cross-Section Showing an Elevation View of Plane AA_1.

the maximum values of $\frac{1}{R_1} + \frac{1}{R_2}$ will occur when R_1 is a minimum. This requires the interface to be attached to the spheres along the line running from A to A_1. Then $R_1 = R_2 = d(\sqrt{2}-1)/2$. The pressure difference across the interface then becomes

$$\Delta p = \frac{4T}{(\sqrt{2}-1)d} \tag{4.12}$$

which leads to the capillary rise becoming

$$h_c = \frac{4T}{(\sqrt{2}-1)d\gamma} \tag{4.13}$$

This model of the air-water interface in the porous medium leads to an interpretation for hysteresis in the capillary pressure in porous media. If the medium is originally saturated for some distance larger than h_c above a free water surface, and the water is then allowed to come to equilibrium with the atmosphere, the air-water interface has to pass through the position shown in Figure 4.3 and

the value of h_c should be given by Eq. (4.13). However, if the medium was originally dry and the water was moving upward under the influence of capillary forces, it would probably not reach the value of h_c. If the medium is packed in identical layers, the sequence of pressure differences across the interface as the interface moves from one layer through another to a third may be expressed qualitatively. The pressure differences across the interface will be called low if the pressure difference is less than given by Eq. (4.12), equal if the pressure difference is given by Eq. (4.12), and high if the pressure difference is larger than that predicted by Eq. (4.12). Then as the interface travels from one layer through another, to a third the pressure difference will be low while the interface is in contact with the lower half of the sphere, equal when the interface is in a position similar to the equilibrium position, then low again when the interface is in contact with the upper half of the spheres. Thus, the low pressure difference will eventually limit the height of capillary rise. That is, the capillary rise will be less than predicted by Eq. (4.13) if the medium is imbibing water.

Next, the surface tension forces acting at the interface with a different geometric packing will be considered. The packing under consideration is shown in Figure 4.4. This packing is much closer than the square-packing considered previously, so the height of capillary rise could be expected to be greater. An enlarged view of three adjacent spheres is shown in Figure 4.5. The centers of

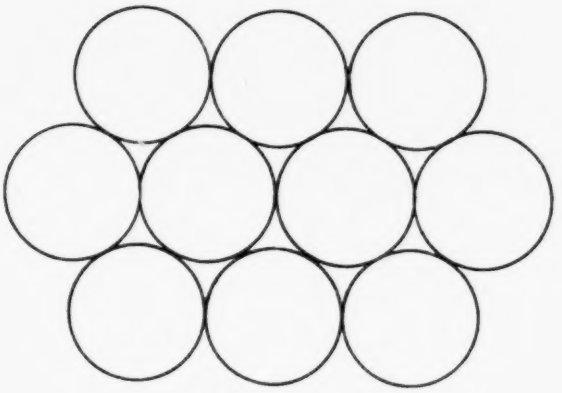

Figure 4.4. Plan View of Triangularly-Packed Spheres.

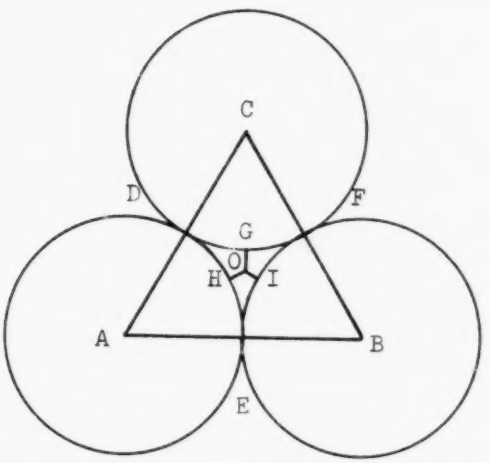

Figure 4.5. Enlarged View of Three Adjacent Spheres.

the spheres are at A, B, and C, and the point equidistant from their centers is the point O. An argument similar to that followed in the case of square-packed spheres can be used to establish attachment location of the interface to the spheres. If the interface is attached at points G, H, and I, the surface tension forces will be pulling vertically upward for a zero angle of attachment and thus the weight of water that could be supported by the interface would be a maximum. The evaluation of the pressure difference across the interface by means of Eq. (4.11) is more complex than in the previous case because the values of R_1 and R_2 are not immediately known as they are the principal radii of curvature. That is, they lie in planes intersecting at right angles. The lines OG, OH and OI meet at 120° angles, so it will be necessary to find the radius of curvature which lies in a plane perpendicular to one of these lines. Fortunately a theorem by Euler may be used to find the radius of curvature which lies in this plane. The theorem by Schwartz, Green and Rutledge (1960) states

$$\frac{1}{R} = \frac{1}{R_1} \cos^2 \theta + \frac{1}{R_2} \sin^2 \theta \qquad (4.14)$$

where R_1 and R_2 are the radii of curvature in two orthogonal planes, and R is the radius of curvature in a plane intersecting the plane of R_1 at the angle θ. Referring to Figure 4.5 again, R_1 may be taken as the radius OI and R may be taken as the radius OG which lies in a plane intersecting the plane of R_1 at an angle of 120°. The radius R_2 is unknown and lies in a plane perpendicular to OI.

The line OB intersects the line EB at an angle of 30° and the triangle OEB is a right triangle. Then the side OB is $2\sqrt{3}$ times as long as the side EB. In terms of the diameter of the spheres $OB = d\sqrt{3}$ so that OI becomes $d(\frac{1}{\sqrt{3}} - \frac{1}{2})$ when BI is subtracted from OB. The value of R_1 then becomes $R_1 = \frac{2-\sqrt{3}}{2\sqrt{3}}\, d$. This is also the value of R in the above equation due to the symmetry of OI and OG. R_2 may now be calculated from Eq. (4.14) as

$$R_2 = \frac{\sin^2 \theta}{\frac{1}{R} - \frac{1}{R_1}\cos^2 \theta}$$

which becomes

$$R_2 = \frac{\frac{3}{4}}{\frac{2\sqrt{3}}{(2-\sqrt{3})d}\left(1 - \frac{1}{4}\right)}$$

or

$$R_2 = \frac{2-\sqrt{3}}{2\sqrt{3}}\, d$$

Therefore, $R_1 = R_2 = \frac{2-\sqrt{3}}{2\sqrt{3}}\, d$ so that h_c is

$$h_c = \frac{\sqrt{3}}{(2-\sqrt{3})}\,\frac{T}{\gamma d} \qquad (4.15)$$

Again, the remarks which were made regarding the limitations of Eq. (4.13) are applicable to the above result. Hysteresis may restrict the capillary rise to some value less than that given by

Eq. (4.15) on an imbibition cycle, while the result may be closely approximated for a drying cycle. In random packing of spheres the packing is probably looser than a triangular packing and tighter than a square packing, so the values given for the height of capillary rise by Eqs. (4.13) and (4.15) may serve as estimates of the upper and lower bounds for the actual height of capillary rise for uniform spherical particles.

4.4 Empirical Equations

From a study of four sands under a variety of packings, the equation

$$h_c = \frac{0.56}{d_H} \left(\frac{1-n}{n}\right)^{2/3} \tag{4.16}$$

was developed by Mavis and Tsui (1939). In this equation h_c is given in centimeters, as is the harmonic mean grain diameter d_H n is the porosity of the medium. The harmonic mean of N discrete particles of diameter d_i is

$$d_H = \frac{N}{\sum_{i=1}^{N} \frac{1}{d_i}}$$

Another expression nearly identical to Eq. (4.8), except that it has been adjusted to apply to graded material, is the equation

$$h_c = 0.45 \frac{1-n}{n} \frac{1}{d_{10}} \tag{4.17}$$

which is cited in the Russian literature [Polubarinova-Kochina (1962)]. In this equation h_c is the capillary rise in centimeters and d_{10} is the effective diameter of the porous medium in centimeters. The effective diameter of a porous medium is defined as the sieve size such that 10% by weight of the porous medium will pass the sieve. The factor 0.45 may be obtained from Eq. (4.8) if the shape factor is 6, the angle of contact is 0°, and the physical properties of water at 15°C are used in Eq. (4.8).

The empirical equations have one obvious advantage over those derived previously in that they are applicable to graded material as well as to media of uniform size. Figure 4.6 shows a comparison of the expected heights of capillary rise predicted by the different equations for a variety of packings.

All of the equations for capillary rise are of the same form when applied to a medium of uniform size. The form is $h_c = c/d$, where c is a constant which differs for each equation. If the logarithm is taken of each equation, the form becomes

$$\log h_c = \log c - \log d$$

which can be represented as a straight line on log-log paper. The equations are shown plotted on a log-log scale in Figure 4.6 with the type of packing and the porosity as parameters.

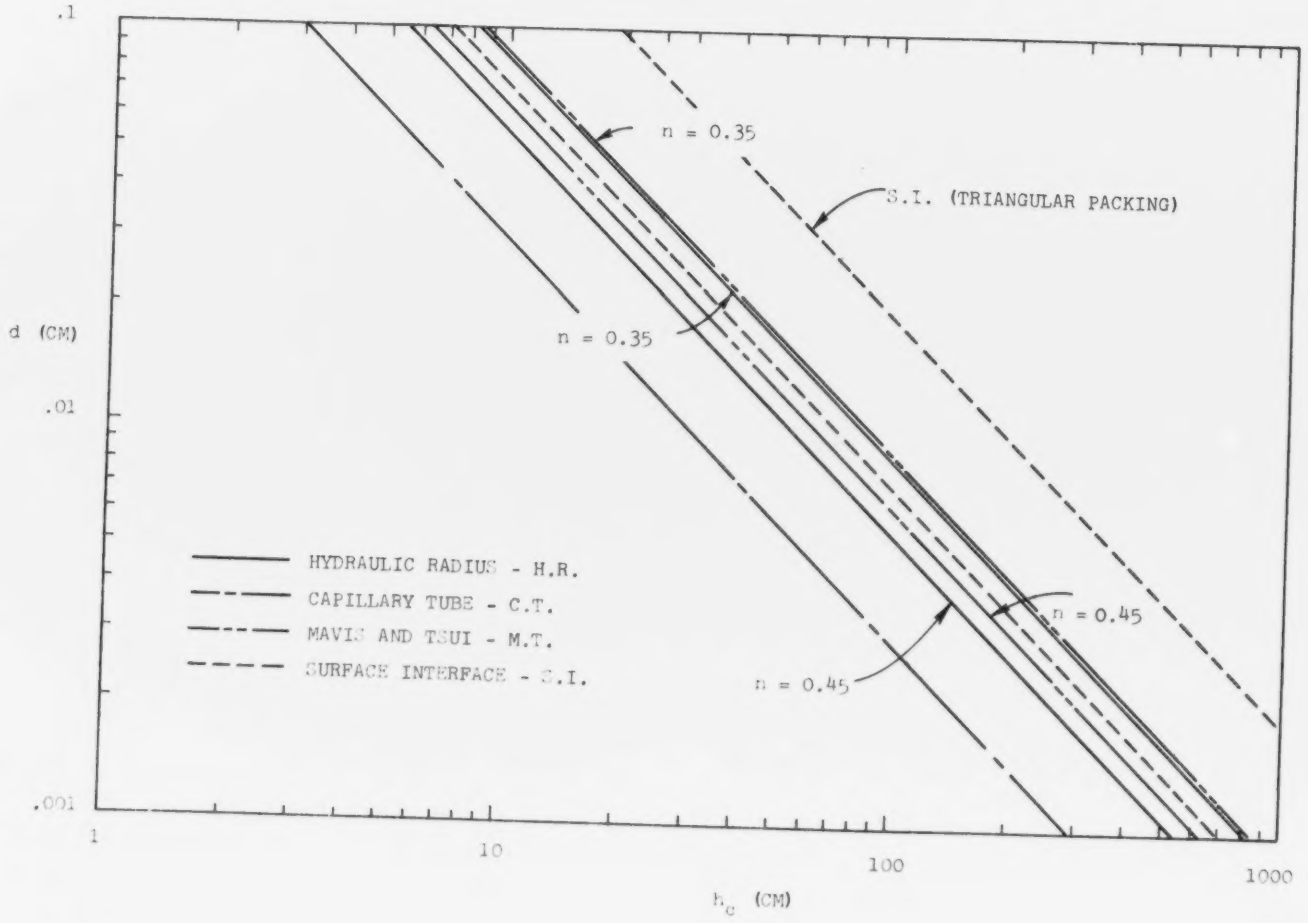

Figure 4.6. Capillary Rise in Uniform Porous Media.

CHAPTER 5

EQUILIBRIUM AND STABILITY

5.1 Theory

In the previous discussion it was assumed that infiltration took place without any resisting effect of the air which had occupied the soil pores before being displaced by the infiltrating water. There are cases in which this assumption is invalid: one such case being infiltration into a system made up of a permeable layer underlain by an impermeable layer. The air which is displaced from the pores by the infiltrating water cannot escape through the impermeable layer, so is trapped and compressed by the overlying water. It is assumed that the media extend infinitely in the horizontal direction and that the entire surface is subject to infiltration. A state of equilibrium may eventually be reached when the downward force due to the weight of the infiltrate water, atmospheric pressure and capillary forces is counterbalanced by the upward force due to the compressed entrapped air. Two situations will be considered, one in which capillary forces are neglected, and the other in which they are considered.

5.1.1 Capillary forces neglected

It will be helpful to refer to Figure 5.1 in this development. First we shall consider the situation where $a = 0$. Before the start of infiltration, the volume of air in the soil is $nA\ell$, where n is the porosity, A is the cross-sectional area, and ℓ is the distance

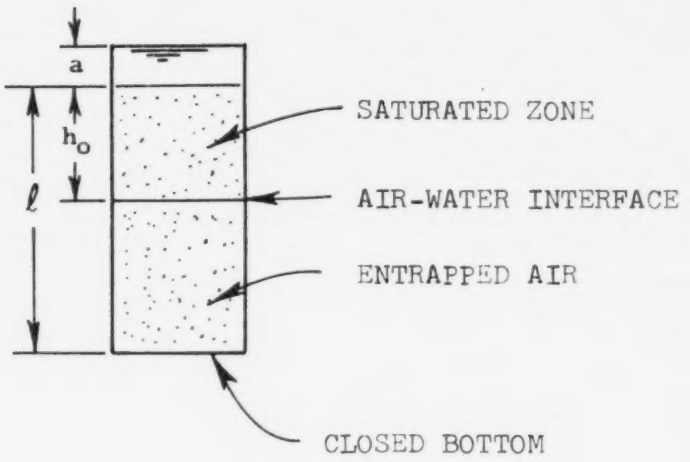

Figure 5.1. Infiltration into a Closed Volume.

from the surface to the impermeable layer. After infiltration has ceased, the volume of the air is $nA(\ell - h_o)$, where h_o is the distance from the surface of the soil to the air-water interface. It is assumed for simplicity that all of the air above the air-water interface has been displaced by the infiltrating water so that the soil is saturated above the interface.

The downward pressure on the interface at equilibrium is made up of atmospheric pressure p_o and the static pressure due to the weight of the infiltrate water γh_o, where p_o is the atmospheric pressure and γ is the specific weight of water. The upward pressure due to the compressed air is p_1. Equating these pressures yields

$$p_1 = p_o + \gamma h_o \tag{5.1}$$

The isothermal perfect gas relation $p_o V_o = p_1 V_1$ may be introduced to obtain an expression for h_o in terms of the soil and water properties. Thus,

$$p_o n A \ell = nA(p_o + \gamma h_o)(\ell - h_o)$$

which becomes, after simplifying,

$$p_o \ell = p_o \ell + \gamma h_o \ell - p_o h_o - \gamma h_o^2$$

which is further simplified to

$$h_o = \ell - \frac{p_o}{\gamma} \tag{5.2}$$

From this result it is concluded that no infiltration will take place unless the permeable soil layer is thicker than p_o/γ, which at sea level is 33.9 ft. If it is less than this, the equilibrium situation is such that the weight of water is insufficient to compress the air in the soil pores. This situation may be altered in two ways: first there may be ponding of water on the soil surface with the depth of water being a, second there may be capillary forces present which modify the above result.

If water is ponded on the surface to a depth a, the total downward pressure at the interface becomes $p_o + \gamma h_o + \gamma a$, while the upward pressure due to the compressed air is p_1. Equating these pressures yields

$$p_1 = p_o + \gamma h_o + \gamma a \tag{5.3}$$

Using the perfect gas law produces the result

$$p_o \ell = (p_o + \gamma h_o + \gamma a)(\ell - h_o)$$

which may be solved for h_o. Then

$$h_o = \frac{1}{2}\left\{-\left(a + \frac{p_o}{\gamma} - \ell\right) \pm \left[\left(a + \frac{p_o}{\gamma} - \ell\right)^2 + 4a\ell\right]^{\frac{1}{2}}\right\} \tag{5.4}$$

which must be examined carefully to determine the limits of infiltration, or even whether infiltration can take place. In case $a = 0$, Eq. (5.4) reduces to Eq. (5.2) if the negative radical is considered. This case will be treated first. The criteria that infiltration take place is that $h_o > 0$. That is,

$$-\left(a + \frac{p_o}{\gamma} - \ell\right) - \left[\left(a + \frac{p_o}{\gamma} - \ell\right)^2 + 4a\ell\right]^{\frac{1}{2}} > 0$$

or

$$\left(\ell - a - \frac{p_o}{\gamma}\right)^2 > \left(a + \frac{p_o}{\gamma} - \ell\right)^2 + 4a\ell$$

which becomes $0 > 4a\ell$, which is impossible. The other possibility is that

$$-\left(a + \frac{p_o}{\gamma} - \ell\right) + \left[\left(a + \frac{p_o}{\gamma} - \ell\right)^2 + 4a\ell\right]^{\frac{1}{2}} > 0$$

or

$$\left(a + \frac{p_o}{\gamma} - \ell\right)^2 + 4a\ell > \left(a + \frac{p_o}{\gamma} - \ell\right)^2$$

which reduces to $4a\ell > 0$, which is true in all cases other than when $a = 0$. Thus, if water is ponded to a depth a on a soil,

some infiltration will take place and the depth to the air-water interface will be

$$h_o = \frac{1}{2}\left\{(\ell - \frac{p_o}{\gamma} - a) + [(\ell - \frac{p_o}{\gamma} - a)^2 + 4a\ell]^{\frac{1}{2}}\right\} \qquad (5.5)$$

5.1.2 Capillary forces considered

When capillary forces are present at the air-water interface, they may be considered to pull downward on the water with a pressure given by γh_c, where h_c is the capillary head. The total downward pressure at the interface at equilibrium when $a = 0$ is then $\gamma h_o + p_o + \gamma h_c$, which is opposed by the upward pressure due to the entrapped air p_a. Equating these pressures yields

$$p_a = p_o + \gamma h_o + \gamma h_c \qquad (5.6)$$

Introduction of this expression into the perfect gas equation yields $p_o \ell = (p_o + \gamma h_o + \gamma h_c)(\ell - h_o)$, which may be solved for h_o to give

$$h_o = \frac{1}{2}\left\{-(h_c + \frac{p_o}{\gamma} - \ell) \pm [(h_c + \frac{p_o}{\gamma} - \ell)^2 + 4h_c\ell]^{\frac{1}{2}}\right\} \qquad (5.7)$$

In order for infiltration to take place if the negative radical is considered first, the requirement is that

$$-(h_c + \frac{p_o}{\gamma} - \ell) - [(h_c + \frac{p_o}{\gamma} - \ell)^2 + 4h_c\ell]^{\frac{1}{2}} > 0$$

or

$$(h_c + \frac{p_o}{\gamma} - \ell)^2 > (h_c + \frac{p_o}{\gamma} - \ell)^2 + 4h_c\ell$$

which becomes $0 > 4h_c\ell$. This is not possible. Considering the positive radical, the condition for infiltration to take place is that

$$-(h_c + \frac{p_o}{\gamma} - \ell) + [(h_c + \frac{p_o}{\gamma} - \ell)^2 + 4h_c\ell > 0$$

or

$$(h_c + \frac{p_o}{\gamma} - \ell)^2 + 4h_c\ell > (h_c + \frac{p_o}{\gamma} - \ell)^2$$

which becomes $4h_c\ell > 0$. Thus, infiltration will take place and the depth of infiltration will be given by

$$h_o = \frac{1}{2}\left\{(\ell - \frac{p_o}{\gamma} - h_c) + [(\ell - \frac{p_o}{\gamma} - h_c)^2 + 4h_c\ell]^{\frac{1}{2}}\right\} \qquad (5.8)$$

It is evident from the above equation that if $h_c = 0$. the equation for h_o reduces to Eq. (5.2), which was derived with capillary forces neglected. In addition, a comparison of Eqs. (5.8) and (5.5) shows that the effect of capillary forces on the equilibrium position of the air-water interface is the same as ponding water to a depth $a = h_c$ on the surface of the soil.

If water is ponded on the surface of the soil to a depth a and the capillary head is h_c , it may be verified in the same manner as was previously done that

$$h_o = \frac{1}{2}\left\{(\ell - \frac{p_o}{\gamma} - h_c - a) + [(\ell - \frac{p_o}{\gamma} - h_c - a)^2 + 4\ell(h_c + a)]^{\frac{1}{2}}\right\} \qquad (5.9)$$

An additional factor arises which must be considered before leaving this subject. Thus far it has been assumed that the entrapped air

compresses until equilibrium is reached. However, it may be possible that the air will compress until the upward pressure forces on the interface are enough to cause the soil to separate and be lifted upwards causing an air pocket to form. This would disrupt the action of the capillary forces in aiding infiltration and would very likely result in a different equilibrium position for the air-water interface than that given by Eqs. (5.2), (5.5), (5.8) or (5.9).

The question of soil stability is most easily understood if a cohesionless soil is considered, for in this case the weight of the overlying soil provides the mechanism to keep the soil grains in contact with each other. It is obvious that if capillary forces are absent, the weight of the infiltrating water will be insufficient to compress the displaced air enough to lift both the water and the soil. For this reason stability will be considered when capillary forces are present. Consider a soil in which water has infiltrated to a depth h_s below the surface. The weight of the soil above the wetting front is $\gamma_s h_s A(1-n)$, where γ_s is the specific weight of the soil particles. The weight of the infiltrating water is $\gamma_w h_s nA + \gamma_w a A$, where γ_w is the specific weight of water. The downward force of the atmosphere on the surface is $p_o A$. The opposing force on the interface due to the compressed entrapped air is $p_1 A$, where p_1 may be calculated from the perfect gas law as $p_1 = p_o \frac{\ell}{\ell - h_s}$. Thus, the opposing force due to the entrapped air is $p_o \frac{A\ell}{\ell - h_s}$. Equating the opposing forces for the situation where separation is impending,

$$p_o \frac{\ell}{\ell - h_s} = \gamma_s h_s (1-n) + \gamma_w h_s n + p_o - \gamma_w a$$

which may be simplified if the specific gravity of the soil S_s is substituted for the ratio γ_s/γ_w. After simplifying, the above equation becomes

$$h_s^2 - \frac{S_s \ell [1-n] + n\ell - a - (p_o/\gamma_w)}{S_s[1-n] + n} h_s - \frac{a\ell}{S_s[1-n] + n} = 0$$

which may be solved for h_s to obtain

$$h_s = \frac{1}{2}\left\{\frac{S_s \ell[1-n] + n\ell - a - \frac{p_o}{\gamma_w}}{S_s(1-n) + n} \pm \left[\left(\frac{S_s \ell[1-n] + n\ell - a - \frac{p_o}{\gamma_w}}{S_s[1-n] + n}\right)^2 - \frac{4a\ell}{S_s[1-n]+n}\right]^{\frac{1}{2}}\right\} \tag{5.10}$$

Obtaining an expression for the stability depth h_s is still insufficient to determine the stability of the soil, for if the equilibrium depth h_o is less than the stability depth h_s, the soil will be stable. That is, there will be equilibrium between the entrapped air and the infiltrating water, but there will be insufficient air pressure to lift the soil and water. Thus, it appears the criteria for stability may be expressed as

$$h_s > h_o \tag{5.11}$$

or

$$\frac{S_s\ell[1-n]+n\ell-a-\frac{p_o}{\gamma_w}}{S_s[1-n]+n} \pm \left[\left(\frac{S_s\ell[1-n]+n\ell-a-\frac{p_c}{\gamma_w}}{S_s[1-n]+n}\right)^2 + \frac{4a\ell}{S_s[1-n]+n}\right]^{\frac{1}{2}}$$

$$> (\ell - \frac{p_o}{\gamma_w} - h_c - a) + [(\ell - \frac{p_o}{\gamma_w} - h_c - a)^2 + 4\ell(h_c + a)]^{\frac{1}{2}} \qquad (5.12)$$

In this equation ℓ may vary in different situations. n depends primarily on the soil packing and may be constant for a number of soils. S_s is fixed for any given soil. p_o is a constant. γ_w is a constant, and h_c may vary widely from soil to soil depending upon the soil particle size, the soil packing and the orientation of the soil grains. It appears that by fixing n and ℓ, which makes the left side of the inequality constant, a condition of instability might be reached for large values of h_c.

5.1.3 Special cases and examples

An interesting special case arises when $a = 0$. In this case Eq. (5.10) simplifies to

$$h_s = \frac{S_s\ell(1-n) + n\ell - \frac{p_c}{\gamma_w}}{S_s(1-n)+n} + \left[\left\{\frac{S_s\ell(1-n)+n\ell-\frac{p_o}{\gamma_w}}{S_s(1-n)+n}\right\}^2\right]^{\frac{1}{2}} \qquad (5.13)$$

which reduces to

$$h_s = \frac{1}{2}\left\{\frac{\ell[S_s(1-n)+n]-\frac{p_o}{\gamma_w}}{S_s(1-n)+n} + \left|\frac{\ell[S_s(1-n)+n]-\frac{p_o}{\gamma_w}}{S_s(1-n)+n}\right|\right\} \qquad (5.14)$$

For small values of ℓ the first term is dominated by p_o/γ_w, so the term is negative; the second term is numerically the same as the first, but it is always positive. Thus, the two terms will be of equal magnitude but of opposite sign, so they will cancel if ℓ is small enough. For large enough values of ℓ both terms will be positive. The critical value of ℓ, which makes the numerator equal zero, may be easily calculated. Hence, if $S_s = 2.65$, $n = 0.40$, $p_o/\gamma_w = 1033$ cm, it is seen that

$$\ell_{crit} = \frac{p_o/\gamma_w}{S_s(1-n)+n} = \frac{1033}{2.65 \cdot 0.6 + 0.4} = 519.1 \text{ cm} \tag{5.15}$$

The significance of the above result is that less energy expenditure is required to lift the medium in short columns than is required to compress the entrapped air in the column. For columns longer than ℓ_{crit}, Eq. (5.14) reduces to

$$h_s = \frac{\ell[S_s(1-n)+n - p_o/\gamma_w}{S_s(1-n)+n} \tag{5.16}$$

This equation is linear in ℓ and in standard form is

$$h_s = -\frac{p_o/\gamma_w}{S_s(1-n)+n} + \ell \tag{5.17}$$

A comparison of the stability depth with the equilibrium depth is not clear-cut except in the case where capillary forces are absent. The equilibrium depth in this special case is given by Eq. (5.2). The condition for instability is $h_o > h_s$. Equations (5.2) and (5.17) may

be compared to see if there is a column length which could produce instability. The instability condition is

$$\ell - \frac{p_o}{\gamma_w} > \ell - \frac{p_o / \gamma_w}{S_s(1-n) + n} \tag{5.18}$$

It is evident that the only time instability could occur is when

$$S_s(1-n) + n < 1.0$$

The value of S_s, which will produce instability, will be

$$S_s < \frac{1-n}{1-n} = 1.0 \tag{5.19}$$

This result is not new, for Archimedes was aware of it some time ago when he recognized that an object would float if it could displace a volume of water weighing more than its own weight.

Figure 5.2 illustrates the results obtained by evaluating Eqs. (5.9) and (5.10) for various column lengths and capillary characteristics. The numerical values were obtained on the IBM 7090 digital computer.

When water is ponded to some depth a on the surface of a porous medium, the equation describing the equilibrium depth and the stability depth become more difficult to interpret. Several numerical examples will be given to help clarify the relation between h_o, h_s and the characteristics of the media.

As a specific numerical example consider a medium with the following characteristics: $a = 0.01$ cm, $S_s = 3.00$, $n = 0.40$, and $h_c = 75$ cm.

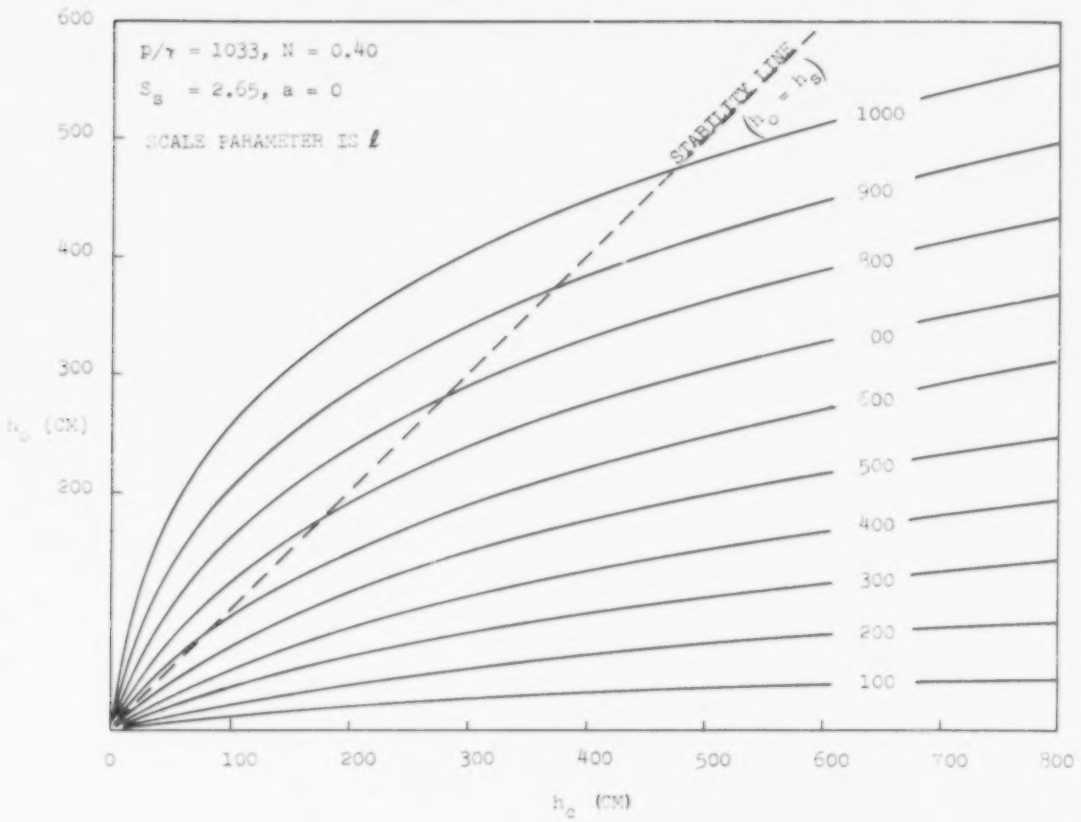

Figure 5.2. Equilibrium Interface Position and Soil Stability.

Let this be packed such that the depth ℓ to an impermeable layer is 8.00 cm and water is ponded to a depth a = 1.0 cm over the surface of the medium. Then from Eq. (5.9)

$$h_b = \frac{1}{2}\left[(8 - 1033 - 79 - 1) - \left[1101^2 - 4 \cdot 8 \cdot 79\right]^{\frac{1}{2}}\right]$$

which becomes

$$h_b = 0.55 \text{ cm}$$

That is, after infiltration has taken place to a depth of 0.55 cm, the infiltrating water will be unable to advance due to the opposing force of the compressed entrapped air, so infiltration will cease. The stability depth must be calculated to determine whether this condition can actually be reached, for it may be possible to reach an unstable condition before the infiltration will cease. From Eq. (5.10)

$$h_s = \frac{1}{2}\left\{\frac{2.00 \cdot 8.00(1.00 - 0.40) + 0.40 \cdot 8.00 - 1.3 - 1033}{2.00(1.00 - 0.40) + 0.40}\right.$$

$$\left. \pm \left[\left(\frac{1018}{1.96}\right)^2 + \frac{4 \cdot 1.3 \cdot 8.00}{1.96}\right]^{\frac{1}{2}}\right\}$$

or

$$h_s = 0.01 \text{ cm}$$

Therefore the medium will break and infiltration will cease very soon after water is applied. The infiltration will stop not because of an equilibrium between the pressure of the entrapped air and the pressure

on the interface, but because of the physical break in the flow path of the water.

It should be noted that the values of h_o and h_s are dependent upon ℓ. For example, if ℓ were 400 cm rather than 8.0 cm and a was 1.0 cm. Eq. (5.9) would yield

$$h_o = \frac{1}{2}\left\{(400 - 1033 - 79 \cdot 1) + [(709)^2 + 4 \cdot 1 \cdot 79 \cdot 400]^{\frac{1}{2}}\right\}$$

which becomes

$$h_o = 40.5 \text{ cm}$$

From Eq. (5.10)

$$h_s = \frac{1}{2}\left\{\frac{2.00 \cdot 400 \cdot 0.60 + 0.40 \cdot 400 - 1.0 - 1033}{2.00 \cdot 0.60 + 0.40} + [(\frac{250}{1.80})^2 + \frac{4 \cdot 1 \cdot 400}{1.80}]^{\frac{1}{2}}\right\}$$

which yields

$$h_s = 1.08 \text{ cm}$$

From Eq. (5.11) this is an unstable condition since $h_o > h_s$. However, an increase in ℓ from 400 cm to 700 cm with other factors remaining constant would result in a value of h_o of 103 cm. The corresponding value of h_s increases sharply to 358 cm. This indicates a stable situation hence no breakage would occur.

A wide variety of other cases are illustrated in Fig. 5.4. Ponding is seen to play a significant role when the capillary head is small. As expected, for large values of capillary head ponding plays a less significant role. Figure 5.4 shows the effect of column length and

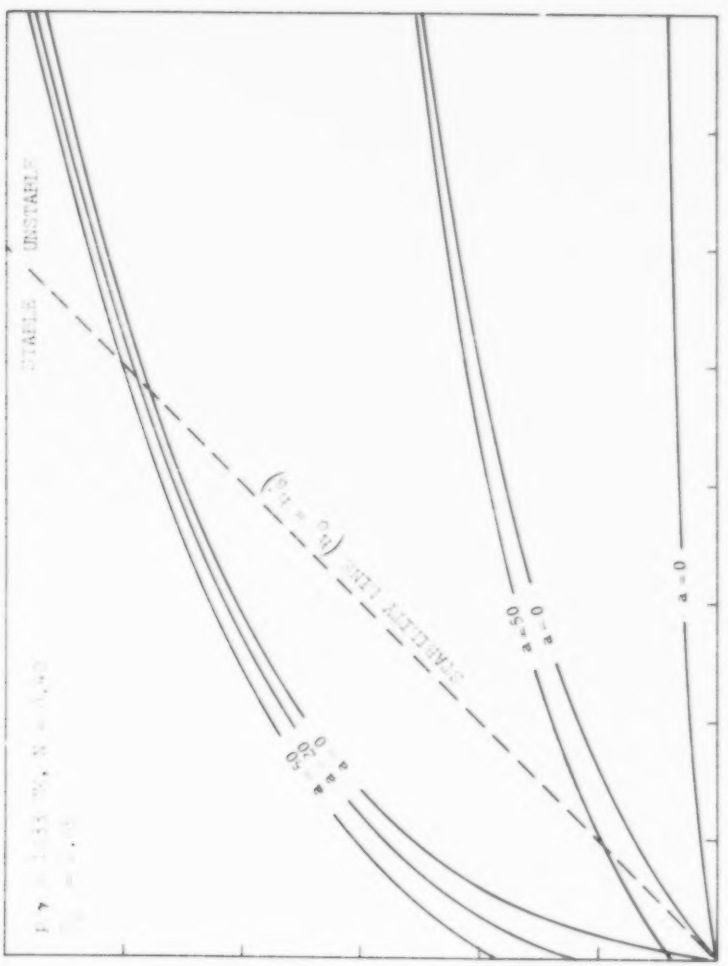

Figure 5.3. Equilibrium Interface Position and Soil Stability.

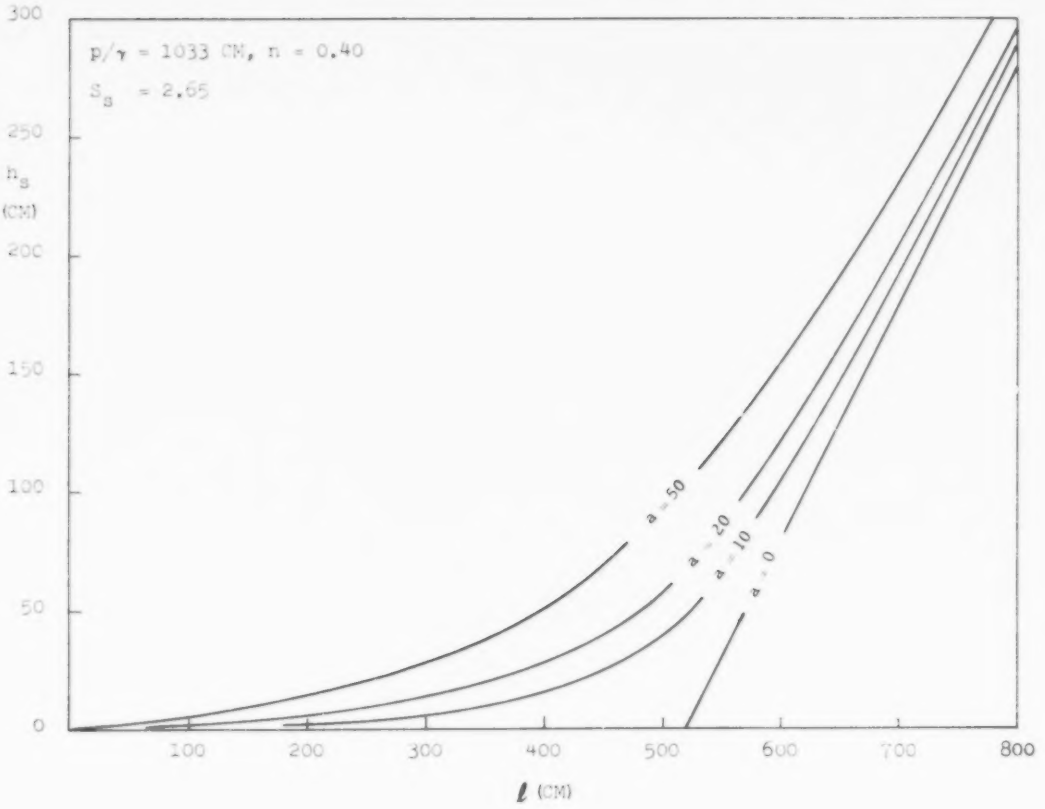

Figure 5.4. Stability Depth.

ponding depth on stability. As the depth of water ponded on the surface is increased, the depth at which a break may occur increases rapidly. Even small depths of ponding shift the location of the stability position. Friction would have a similar effect.

5.2 Experimental Work

5.2.1 Introduction

Experimental tests related to equilibrium of the air-water interface and stability of the porous medium were carried out using columns of various lengths. These columns were in three categories according to length: those about 10 cm long, those about 30 cm long and those about 100 cm long. The 10 cm long columns were placed in ordinary chemical test tubes. The inside diameter of the test tubes was constant for any particular test tube, but the diameters varied from 1.3 cm to 1.4 cm for the various test tubes which were used. The 30 cm columns were in 500 mℓ or 1000 mℓ graduated cylinders of the type ordinarily used in the laboratory for volumetric measurements of liquids. The inside diameters of the graduated cylinders varied from 5.9 cm to 7.0 cm, depending on the particular cylinder used in an experiment. The longest columns were placed in a tube of rectangular cross section, 0.35 cm by 4.44 cm. The length of the sample could be varied by partially filling the tube. The walls of the rectangular column were made of plexiglass.

5.2.2 Mediums used and general conduct of tests

Various porous mediums were used in the tests, such as glass beads, sand, soil and other material. The glass beads are easy to

work with, as they are commercially available in convenient sizes. The individual beads are nearly spherical. Beads of one size may be mixed with accurately weighed portions of beads of other sizes to obtain samples with a specified grain size distribution. The sands were sieved and their grain size distribution was found to approximate closely the geometrical-normal distribution. The soils which were used were silty topsoils obtained from roadside cuts and foundation excavations in the vicinity of Stanford University. Dry Portland cement was used as a special material which would have a very low permeability and would react with the water.

The tests were conducted by ponding water on the surface of the porous medium, then observing the wetting front as it moved into the medium. There was always a disturbance in the upper layers of the medium created by the scouring action of the water as it was poured into the column. This permitted some of the air in the column to escape. Usually there were some pores in the medium which would not become saturated with water very quickly. As a result there was some escape of air through these pores as the wetting front moved ahead. If the medium was fine enough, these pores would become filled with water by the time the wetting front had moved one or two centimeters. In coarser mediums the air would escape continuously until the wetting front reached the bottom of the column.

5.2.3 Tests on 10 cm columns

The results obtained from the 10 cm long columns using media with particle diameters less than about 0.03 cm were reasonably consistent. After the initial escape of air the pores near the surface would fill up with water and the wetting front would continue moving downward under the action of gravity and capillary forces. Then a break would appear in the porous medium at the wetting front and the saturated portion of the medium would be lifted up. The break occurred at a depth of about 0.75 cm below the surface for glass beads, having a diameter of 0.0038 cm: for 0.01 cm diameter glass beads the break occurred at a depth of 1 to 2 cm, depending on how quickly the pores through which the air was escaping filled with water; and for 0.029 cm diameter glass beads the break occurred at a depth of 1.5 to 2.5 cm. The time between the first contact of the water with the medium and the break varied from 5 sec to 30 sec, depending on the amount of air which initially escaped and the permeability of the medium.

Some of the sands which were used were coarser than the glass beads. Those sands having a mean grain diameter of less than about 0.03 cm behaved in the same manner as the glass beads of the same size. Sands having a mean size above about 0.03 cm usually did not break. In these cases the water did not fill up all of the pores, so there was a continuous escape of air from ahead of the wetting front to the atmosphere. Obviously, there was a lower infiltration rate for these samples than there would have been for samples with an open bottom, due to the slightly higher back pressure of air and

the counterflow of air and water. The coarse sands were completely wet, except for scattered air pockets within 1 min after the beginning of a test. As the mean size of a sample decreased, the water was able to fill all pores periodically, blocking the escape of air. The resulting air pressure build-up as the wetting front progressed was sufficient to produce isolated cavities which quickly collapsed as the air would again break through to the surface. These cavities could be better characterized as large isolated bubbles which disturbed the flow locally rather than fully developed breaks which disrupted the flow passages and brought the infiltration rate to zero.

The wetting front advanced slower through the topsoils than it did through the glass beads and the sands because of the lower permeability of the topsoil. The topsoils exhibited a breaking pattern similar to that of the glass beads.

Dry Portland cement and sawdust were used as two special mediums. The Portland cement did not break and the wetting front appeared to reach an equilibrium position within one hour after water was ponded on the surface. The saturated cement reacted with the water to produce a jelly-like mass which may have had too low a permeability to permit the wetting front to move. The sawdust formed a loose mat which allowed the air to escape fairly readily. The sawdust quickly became water-logged and would not float so that no break appeared. It had very little capillarity and was porous enough to permit the air to escape without sufficient pressure build-up to cause a break to occur while infiltration was under way.

The breakage phenomenon is illustrated in Fig. 5.5 which shows the breaks which occurred in several different mediums. The left tube contained a rather coarse Olympia sand, having a geometric mean diameter of about 0.05 cm. A slight break is visible through the tube. The second tube from the left contained Roseville white sand, having a geometric mean diameter of 0.03 cm. The center tube contained soil from a roadcut near Stanford University and illustrates the double break phenomenon. The two tubes on the right contained 0.0080 cm diameter glass beads. One column broke cleanly while a partial break occurred in the other, which permitted the wetting front to move ahead.

5.2.4 Tests on 30 cm columns

Glass beads were the only mediums used in the 30 cm long columns. The same problems which were encountered in the shorter columns were present in these columns. The initial disturbance of the surface permitted air to escape until the wetting front had moved one or two centimeters. Apparently, due to the lack of side support caused by the larger diameter of the columns, the air cavities collapsed more easily than they had in the smaller diameter test tubes. This permitted the wetting front to move ahead in steps. One column containing 0.010 cm diameter particles had the first well-formed cavity appear 2.5 cm below the surface after one minute. This cavity subsequently collapsed and the wetting front again moved ahead. After 10 minutes a second cavity formed 12 cm below the surface. This cavity did not completely interrupt the flow and the wetting front continued moving slowly ahead. After 21 minutes a very small break

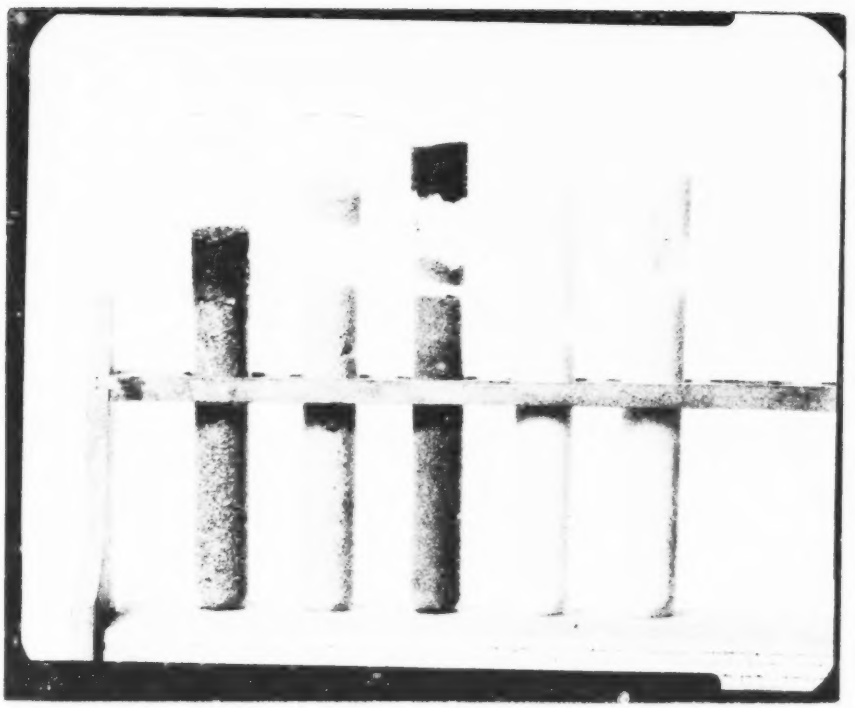

Figure 5.5. Photograph of Column Breakage.

was apparent at a depth of 22 cm. No appreciable inflow occurred after this, and three days later there was no noticeable change in the position of the wetting front. Apparently, an equilibrium situation had been reached in which the compressed air had sufficient pressure to prevent further inflow but insufficient pressure to overcome the weight of the overlying medium and water and the wall friction forces.

Somewhat similar results were obtained using a column of particles with diameter 0.0038 cm. The cavities which formed collapsed after a few minutes permitting air to escape to the surface. A cavity formed at a depth of 0.75 cm after 22 sec, but soon collapsed and a second cavity occurred at a depth of 5.5 cm. This cavity collapsed after 27 minutes.

5.2.5 Discussion of tests on 10 cm and 30 cm columns

No pressure measurements were taken with the 10 cm and 30 cm columns. The infiltration rates were not measured, but a comparison of the lengths of time required for the wetting fronts to reach the bottom of the tubes when there was air resistance and when the air was free to escape through the bottom of the tube gives a qualitative idea of the effect of air resistance. It required only 180 sec for a 10 cm long sample of 0.010 cm diameter medium to saturate when the air was free to escape from the bottom of the tube. Some of the test tubes containing this same medium but with no provision for the escape of air required three weeks for the entire length of column to appear wet. Even then it did not appear saturated ahead of the break, but it appeared the medium had slowly become moistened as moisture was diffused into it.

The behavior of a column after the first break appeared was very difficult to predict and seemed to depend largely on how the break occurred. A clean break which divided the medium into two parts caused infiltration to cease, except for a small amount of water which continued to move down the walls of the tube. This water would gradually wet the medium ahead of the break. The resulting displacement of air would force the broken medium up the tube. In some cases the separation of the cavity was 2 to 3 cm. Dirt on the walls of the tubes promoted the movement of the thin film of water down the tube walls after a break occurred. If the first break which occurred was not a complete break all the way across the tube, but was a cavity over a portion of the cross-section, then water continued to flow through the unbroken section of the porous medium. The partial cavity was more likely to be unstable than a complete clean break, and the air in the cavity would frequently migrate to the surface as a big bubble.

5.2.6 Tests on longer columns

In one test of sand with a geometric mean size of 0.030 cm and a column length of 66.3 cm no breaks or cavities occurred. The air escaped through a few pores to the surface. After the first minute of inflow the net pressure difference between the water ponded on the surface and the pressure in the air ahead of the wetting front became about constant at 15 cm of water. The air escaped to the surface at such a rate that this net pressure was maintained throughout the experiment. Similar results were obtained from a second test of the same sized sand, except the air pressure was slightly higher, indicating

more resistance to the escape of air through a few of the pores in the sand. A test of 0.0080 cm diameter glass beads in a column 67.8 cm long produced no fully developed breaks, but cavities formed and collapsed as the air escaped to the surface. The pores through which the air was escaping to the surface became filled with water after the first few minutes and the air pressure rose steadily. The rate of advance of the wetting front decreased until it appeared to reach an equilibrium position about 25 cm below the surface. A few small isolated bubbles of air escaped to the surface at about two minute intervals. The air pressure reached a maximum of 69.4 cm of water, which was enough to produce equilibrium by halting the inflow, but this pressure was insufficient to produce a break in the medium.

An interesting break was observed during the wetting and draining cycle on a 99.2 cm long column with a glass bead medium. The geometric mean size of the medium was 0.0123 cm and the geometric standard deviation was 0.004 cm. The medium was subjected to alternate wetting and drying cycles in which about 500 ml of water were poured on the surface, then the column was allowed to drain by gravity for 24 hours, when the effluent was again poured on the surface of the medium and the cycle was repeated. This procedure was followed for several days, then the bottom of the column was sealed after the water was ponded on the surface. Bubbles rose to the surface as the water moved into the column. Several hours later a distinct break over about 75% of the column was observed at a depth of 5 cm below the surface of the medium. About 20 cm of water were still ponded on the surface of the medium. Apparently there

was only a small volume of air in the drained column, so that the air pressure rose quickly as the ponded water sealed the surface and infiltration took place.

5.2.7 Summary of experimental tests

In summary the experimental results show the necessity of considering the effects of air ahead of the wetting front. With fine-grained mediums which develop large capillary forces breaks may be expected to occur in short columns. The location of the break is not predicted accurately from theory, as the theory made no allowance for air escape and friction, both of which are present in the tests. For grain diameters of greater than 0.03 cm breaks become less likely, especially as the column size is increased. Instead there is a counter-flow of air and water. The pressure build-up in the air obviously has a retarding effect on the infiltration rate, as will be discussed in the next chapter. For short columns successive breaks may occur especially if the walls of the tube are dirty, or if there is some contact between portions of the medium above the break and below the break. For longer columns an equilibrium situation may be reached in which the air pressure is great enough to halt infiltration before the column becomes saturated. Over a long period of time minor effects which are usually neglected, such as diffusion of water vapor and air, probably slowly allow the medium to become wet even if a break has occurred. In some of the short columns three weeks were required for the medium to appear wet ahead of the break.

During infiltration in the field the breaks could be expected to occur as isolated pockets or cavities of air rather than as one continuous break. This undoubtedly would have an effect on the infiltration rate, as no flow would occur through the air cavities.

CHAPTER 6

INFILTRATION EXPERIMENTS

6.1 Experimental Equipment and Procedure

6.1.1 Laboratory arrangement and temperature control

Infiltration is influenced by several temperature dependent properties of water, such as the viscosity, density and surface tension. Also, the moisture measuring equipment is subject to drift with changes in the temperature. Thus, close temperature control was necessary to avoid introducing undesirable variations into the results from temperature fluctuations. The laboratory room had brick and sandstone walls 14 to 18 inches thick, only one of which was an outside wall, while the other three were interior walls which helped reduce temperature changes. A thermostatically controlled air conditioner and heater was installed to maintain the temperature in a suitable range. The temperature was controlled to $\pm 1^{\circ}$ F, but temperature records show that if only the heater was required, or only the air conditioner, the temperature varied less than $\pm \frac{1}{2}^{\circ}$ F. Relative humidity records were also maintained. The relative humidity changed less than 2% during any test. The recording hygrothermograph showed local areas in the room had temperature fluctuation of up to $+ 3^{\circ}$ F when the early-morning sun was able to shine through the windows, even though the normal air temperature changed less than $+ 1^{\circ}$ F. To alleviate this problem, the windows were sealed with plywood. The lights and all electrical equipment was left running continuously to insure complete thermal equilibrium.

6.1.2 Construction and tests of the plastic tube

The rectangular plastic tube used to hold the porous mediums is shown in Figure 6.1 and will not be described in detail here. The γ-ray attenuation instrument which was used to determine the uniformity of packing of the mediums and the moisture distribution in the column made it necessary to construct the tube very carefully. It was especially important that the thickness of the column be uniform over its entire length so that moisture determination could be obtained at any location, rather then at precalibrated locations. The premium preshrunk plastic was machined to a tolerance of $\pm$ 0.005 inch, and all joints were fastened with machine screws. An inert, silicon base, high-vacuum, stopcock lubricant was used to insure air-tight joints between the various plastic members. This lubricant was also used to coat both sides of the gaskets used at the inlet and the outlet of the column. To avoid problems with air leakage, no holes were drilled through the plastic walls of the tube. After the tube was assembled, it was submerged in several inches of water and subjected to an internal air pressure of 60 psi. There was no leakage.

6.1.3 Description of the porous mediums

The porous mediums used in the infiltration tests consisted of sands and glass beads. The sieve analysis of the Roseville white sand, which was used in some of the tests, is shown in Figure 6.2. The glass beads are shown in Figure 6.3. Glass beads with a diameter of 0.0080 cm were used in some of the tests in which it was desired to have a narrow pore size distribution. The sphericity of the individual

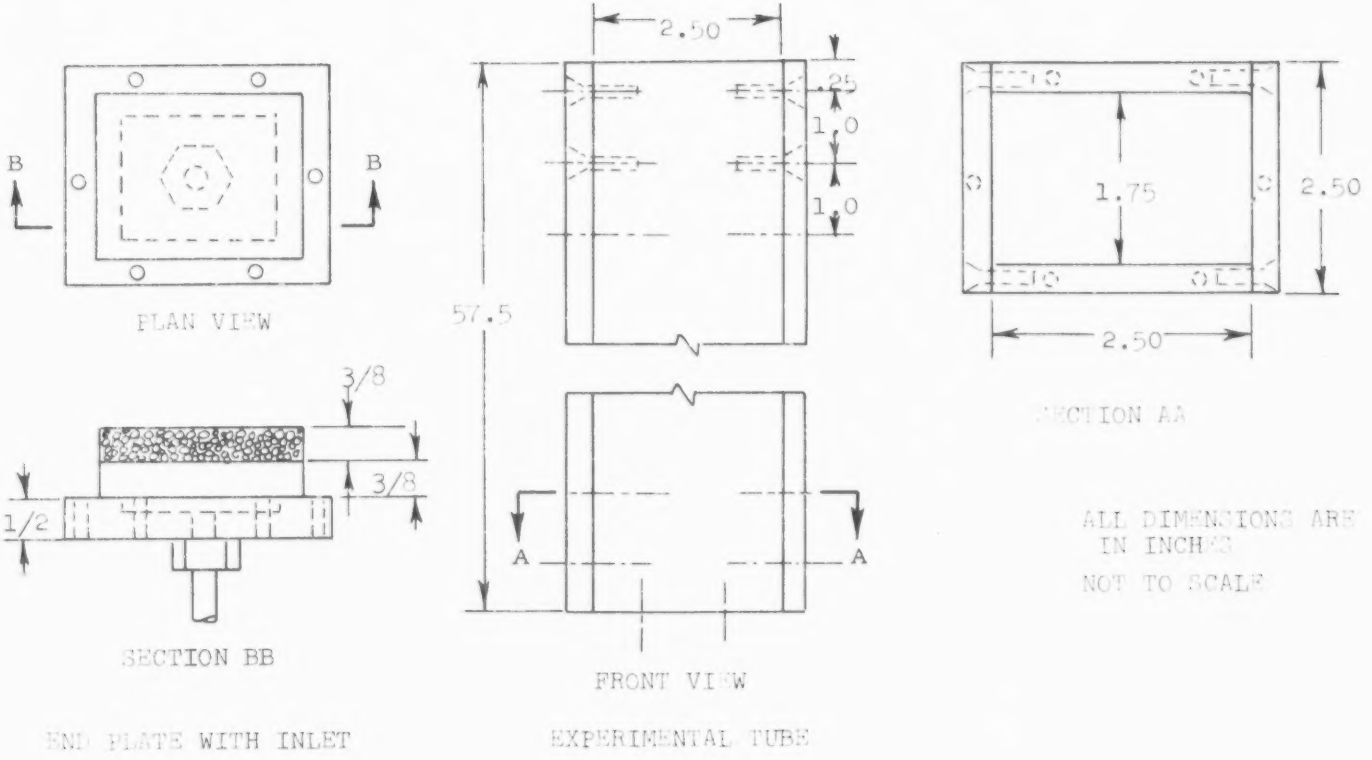

Figure 6.1. Experimental Tube Construction Details.

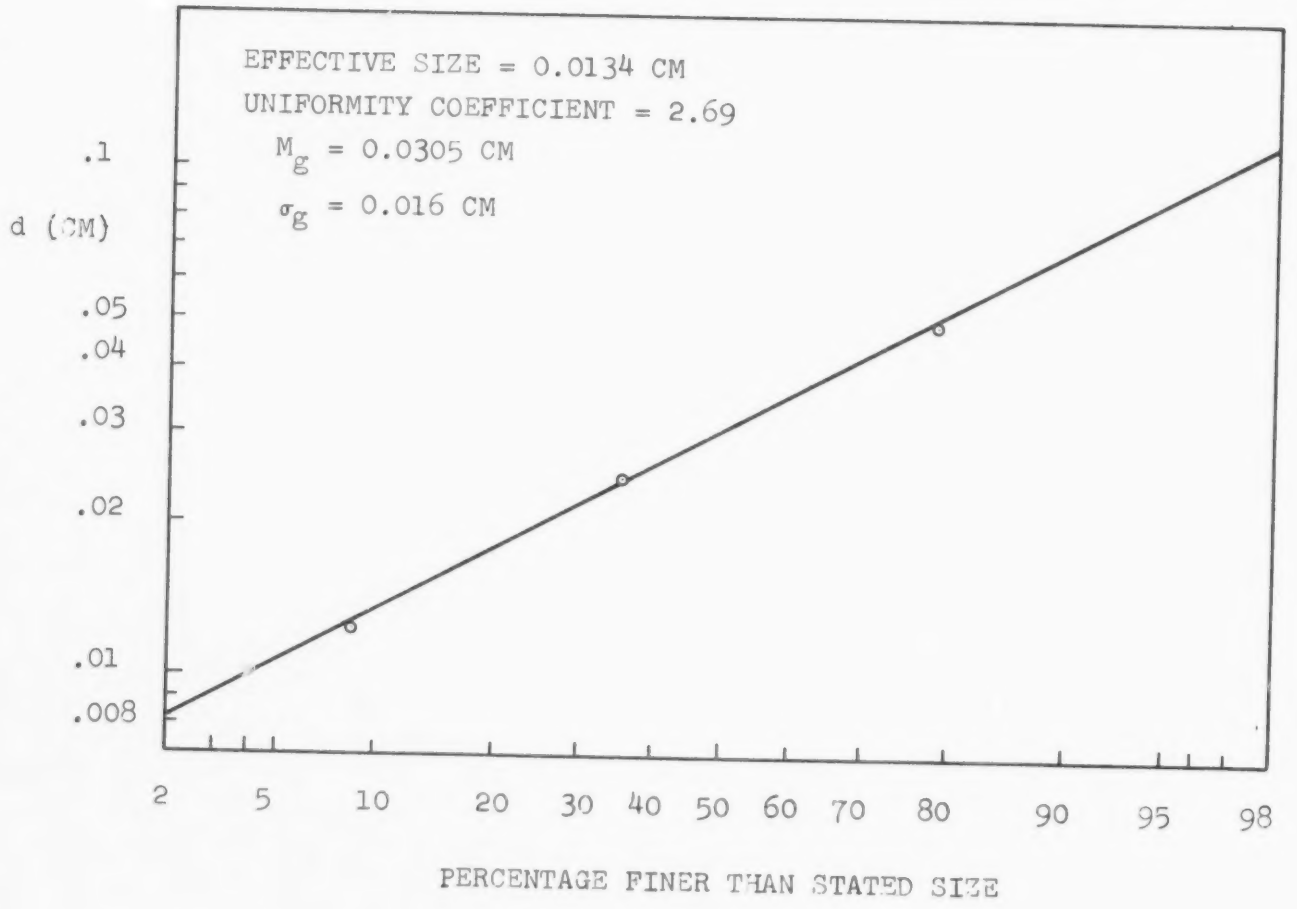

Figure 6.2. Sieve Analysis of Roseville White Sand.

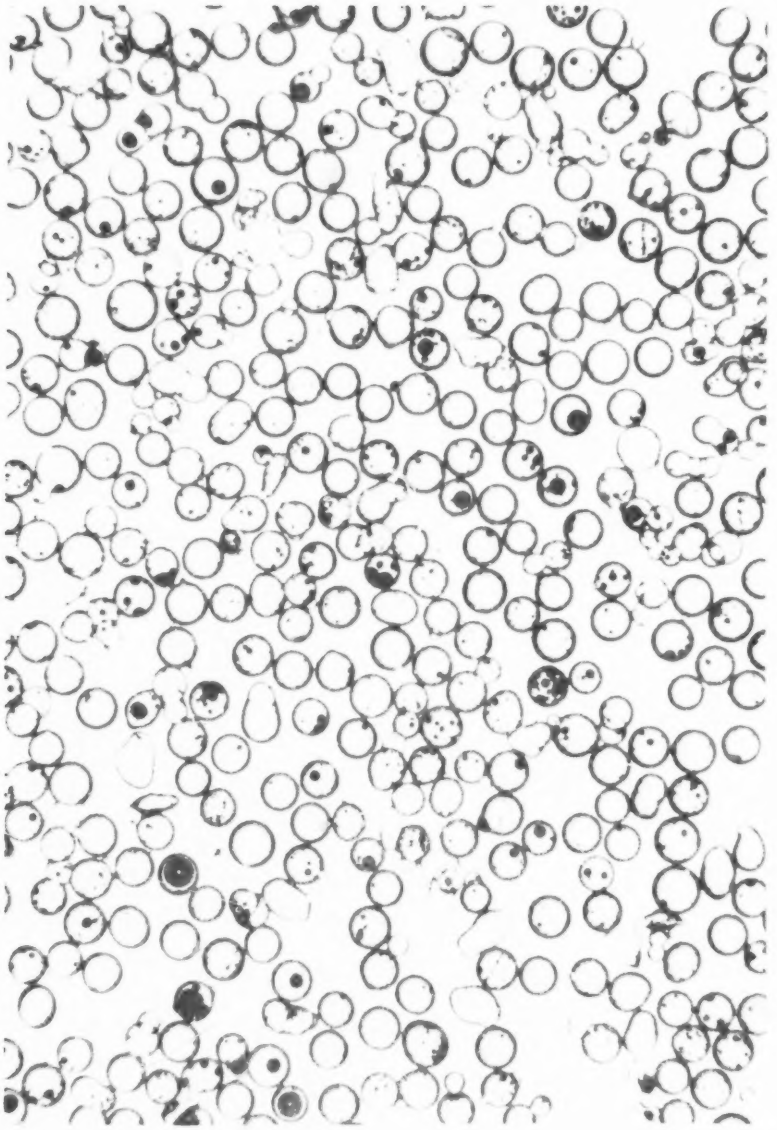

Figure 6.3. Photograph of 0.005 CM Diameter Glass Beads.

beads aided their packing and the uniformity of the column. By weighing out portions of different sized glass beads, a sample was prepared which had a grain size distribution, as shown in Figure 6.4. The geometric mean size was 0.0123 cm and the geometric standard deviation of the sample was 0.054 cm.

6.1.4 Column packing procedure

The column was packed, then by use of the γ-ray measuring instrument the uniformity of the packing could be checked. If the bulk density varied with depth, the column could be repacked until a uniform bulk density was obtained. A variation in the bulk density near the top of the column or near the very bottom of the column was more tolerable than variation in the bulk density in the central portion of the column. Because of the rectangular shape of the column, it was not possible to use one of the mechanized packers, which is suitable for packing round columns uniformly. Instead, a column packing procedure was used which had been found suitable at the Richmond Field Station of the University of California. A sufficient volume of the medium was prepared ahead of time, so there would be no interruption in the pouring schedule until the column was filled. The column was held in such a manner that it could rotate about a vertical axis through an angle of roughly $\pm$ 15°, much like the motion of a swinging door on its hinges. The column holder was held in a vertical position by one person; a second person poured the medium at a uniform rate through a funnel into the column; a third person struck the column with the palm of his hands to keep it rotating back and

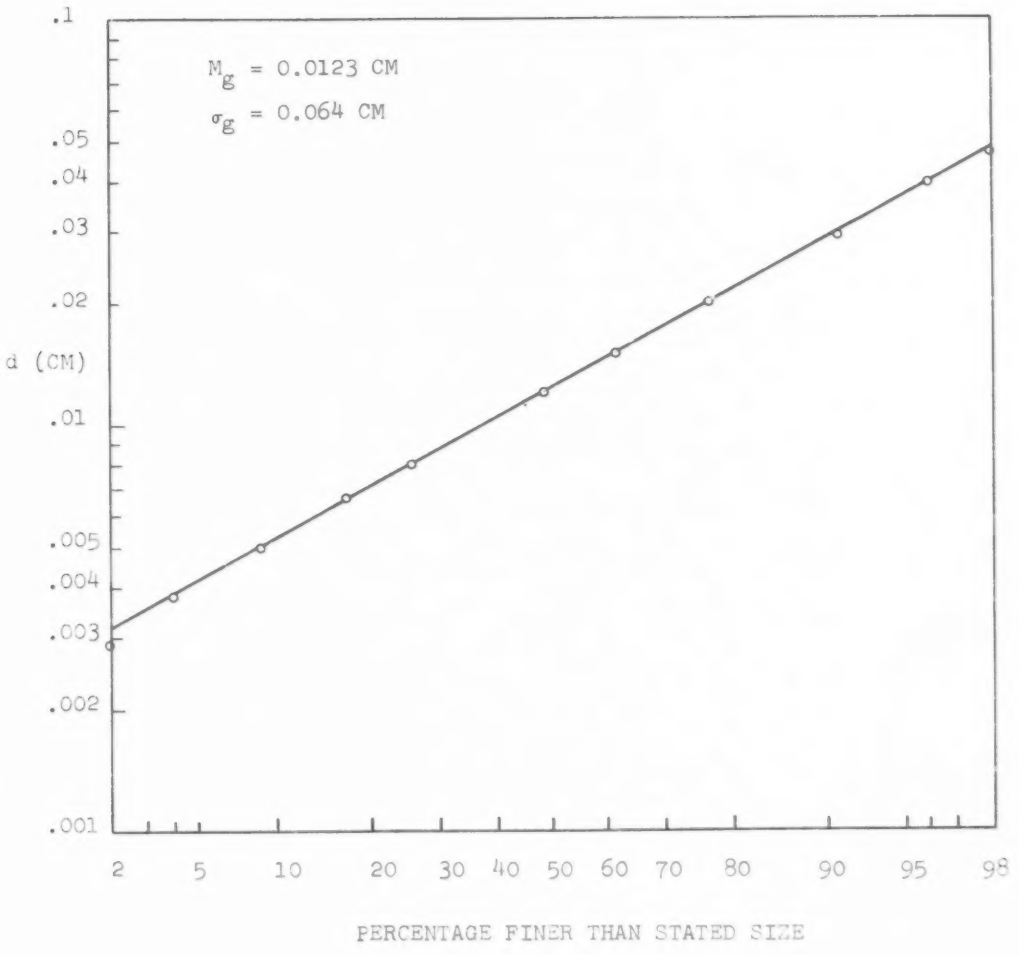

Figure 6.4. Sieve Analysis Glass Beads.

forth through the $\pm$ 15° angle. The column was struck at the level of the surface of the porous medium. The resulting packing was found to be satisfactory when surveyed with the γ-ray instrument in nearly all cases.

6.1.5 Measurements of infiltration and the wetting front

The water was ponded on the surface of the medium. This method of adding the water was decided upon because other methods would not allow the medium to break and separate when there was a large enough air pressure build-up ahead of the wetting front. A steel tape was attached to the outside of the column, so that the water level measurements could be obtained at various times. The progress of the wetting front could be observed visually and its position recorded as a function of time. A water or mercury manometer was attached to the bottom of the column in order to obtain pressure measurements. The water manometer was more sensitive, so it was used whenever the air pressures expected to be within its range.

6.2 Equipment Tests

6.2.1 Attenuation equation

Transient moisture measurements at different elevations in the column were obtained by use of γ-ray attenuation equipment similar to that described by Davidson, Biggar and Nielsen (1963), except that the column was vertical rather than horizontal. The γ-ray attenuation equation

$$I_w = I_o \exp[-(\mu_s \rho_s x_s + \mu_p \rho_p x_p + \mu_w \rho_w x_w)] \qquad (6.1)$$

relates the intensity of the incident radiation to the transmitted radiation in terms of the properties of the column and its contents. The meaning of the terms is:

I_o = intensity of radiation incident to the column,

I_w = intensity of the transmitted radiation through the wet column,

μ_s, μ_p, μ_w = mass attenuation coefficients for the sand, plastic and water, respectively,

ρ_s, ρ_p, ρ_w = mass densities of sand, plastic and water, respectively,

x_s, x_p, x_w = total thickness of sand, plastic or water traversed by the transmitted γ-ray beams.

When the column is dry, Eq. (6.1) becomes

$$I_D = I_o \exp[-(\mu_s \rho_s x_s + \mu_p \rho_p x_p)] \qquad (6.2)$$

where I_D is the radiation intensity transmitted by the dry column. Dividing Eq. (6.1) by Eq. (6.2) results in

$$\frac{I_w}{I_D} = \exp[-\mu_w \rho_w x_w] \qquad (6.3)$$

which means that for moisture measurements it would be sufficient to scan the dry and the wet column.

6.2.2 Moisture and density measuring equipment

The measuring equipment which was used to obtain the data for Eq. (6.3) is shown schematically in Figure 6.5. The voltage stabilizer

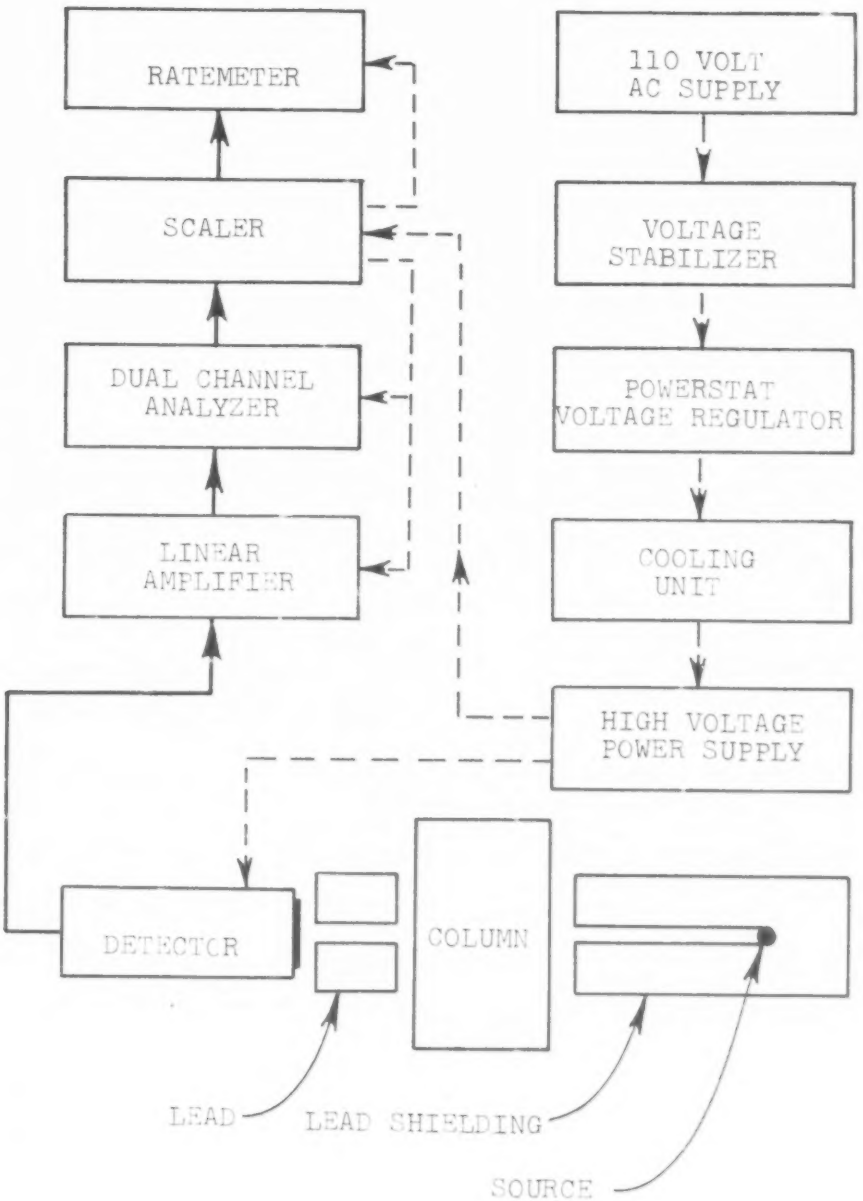

Figure 6.5. Schematic Drawing of the Moisture Measuring Equipment.

and the powerstat voltage regulator provided a constant voltage power supply to the equipment. The γ-rays from the 250 millicurie Cs^{137} source were collimated through a slit 0.030 inch high by 0.75 inch wide. After travelling through the column, they passed through another collimating slit 0.060 inch high and 0.75 inch wide, where they struck the nose of the scintillation detector. The power for the detector was supplied by an adjustable high voltage component. The output of the detector was amplified in the linear amplifier, then the signals were sorted in the pulse height analyzer, with only those having an energy of 0.66 ± 0.15 Mev being accepted. The scaler recorded the pulses which were acceptable during various preset counting periods from 0.1 min to 100 min. A rate meter was connected to the scaler. Various time constants from 0.5 sec to 40 sec could be selected for the rate meter. Time constants of 2.5 sec, 10 sec and 40 sec were used in this study, depending on the rapidity with which the system was changing. Figure 6.6 shows a photograph of the measuring equipment.

6.2.3 Verification of counting accuracy

To determine the suitability of the measuring equipment for moisture measurements, the mass absorption coefficients of several materials were determined and these values were compared to similar values available in the literature. Lead, aluminum and water were selected as the materials with which to check out the accuracy of the equipment. Several rectangular blocks of aluminum were accurately machined, then various combinations of these blocks were placed in the γ-ray beam. Five 4-minute counts of I_o were taken, then

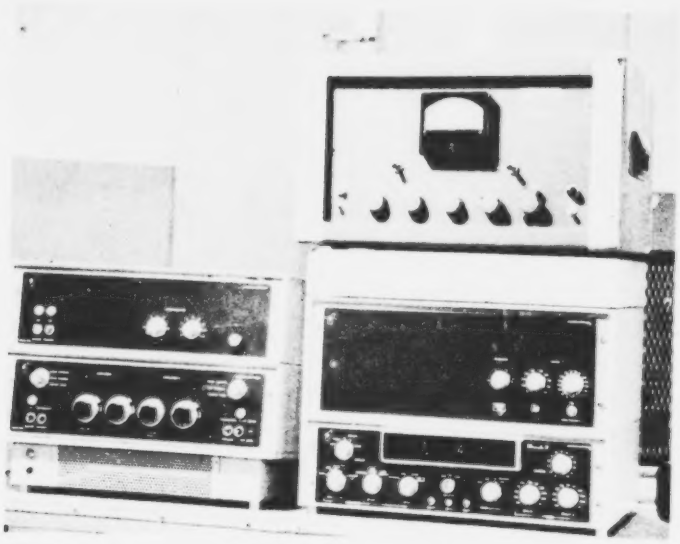

Components

Linear Amplifier	Ratemeter
Pulse Height Analyzer	High Voltage Supply
Cooling Base	Scaler

Figure 6.6. Photograph of the Counting Equipment.

4-minute counts of the transmitted intensity of the γ-ray beam for each thickness of aluminum were recorded. The thickness of each piece of aluminum was determined by a micrometer to $\pm$ 0.001 inch. The resulting plot of relative transmittance versus thickness of aluminum is shown in Figure 6.7. For calculating the mass absorption coefficient, it is convenient to first determine the linear attenuation coefficient σ, which is the product $\mu\rho$, then determine μ from the linear attenuation coefficient. The linear attenuation coefficient of aluminum was $\sigma_A = 0.2007\ cm^{-1}$ and the mass absorption coefficient was $\mu_A = 0.0743\ cm^2/gm$. Evans (1955) lists the value $0.074\ cm^2/gm$ as the mass absorption coefficient of aluminum for 0.66 Mev radiation. A similar procedure was followed to determine the mass absorption coefficient of lead. The linear attenuation coefficient was $1.1982\ cm^{-1}$ and the mass absorption coefficient was $0.1056\ cm^2/gm$. This compares favorably with the values of $0.105\ cm^2/gm$ for the mass absorption coefficient listed by Evans (1955). The plot of relative transmittance versus the thickness of the lead is shown in Figure 6.8.

To determine the mass absorption coefficient of water, several rectangular containers were constructed. These containers were made from accurately machined plastic components. The inside dimensions were measured with an expansible gauge. The accuracy of the measurement was less than the accuracy obtained when measuring the lead and aluminum blocks with a micrometer, but probably was around $\pm$ 0.005 inch. The mass absorption coefficient of water was found to be $0.0839\ cm^2/gm$, as shown in Figure 6.9. Evans (1955) lists a value of $0.085\ cm^2/gm$, while Davidson, Biggar and Nielsen (1963) obtained a value of $0.0815\ cm^2/gm$.

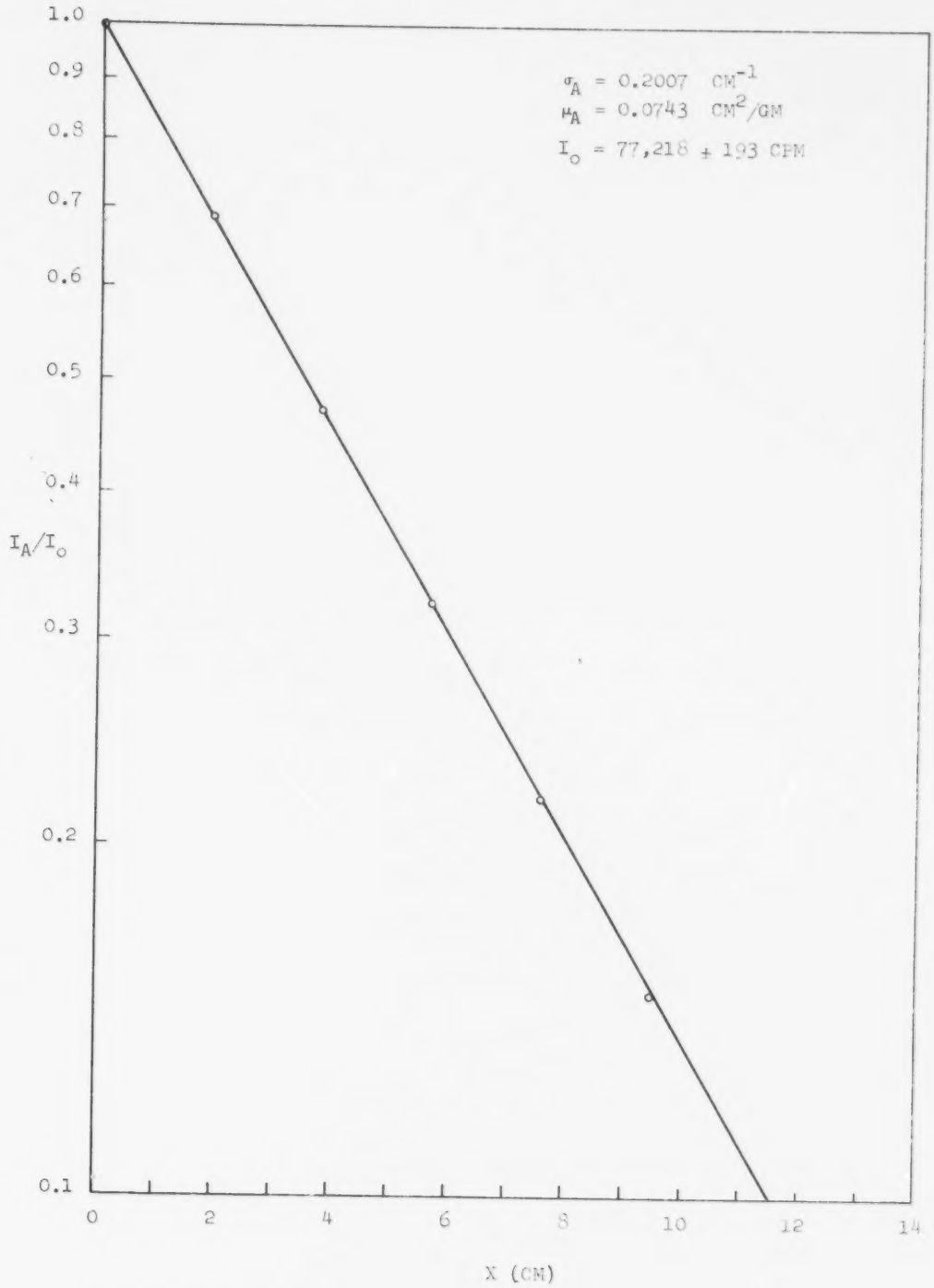

Figure 6.7. Attenuation Coefficient for Aluminum.

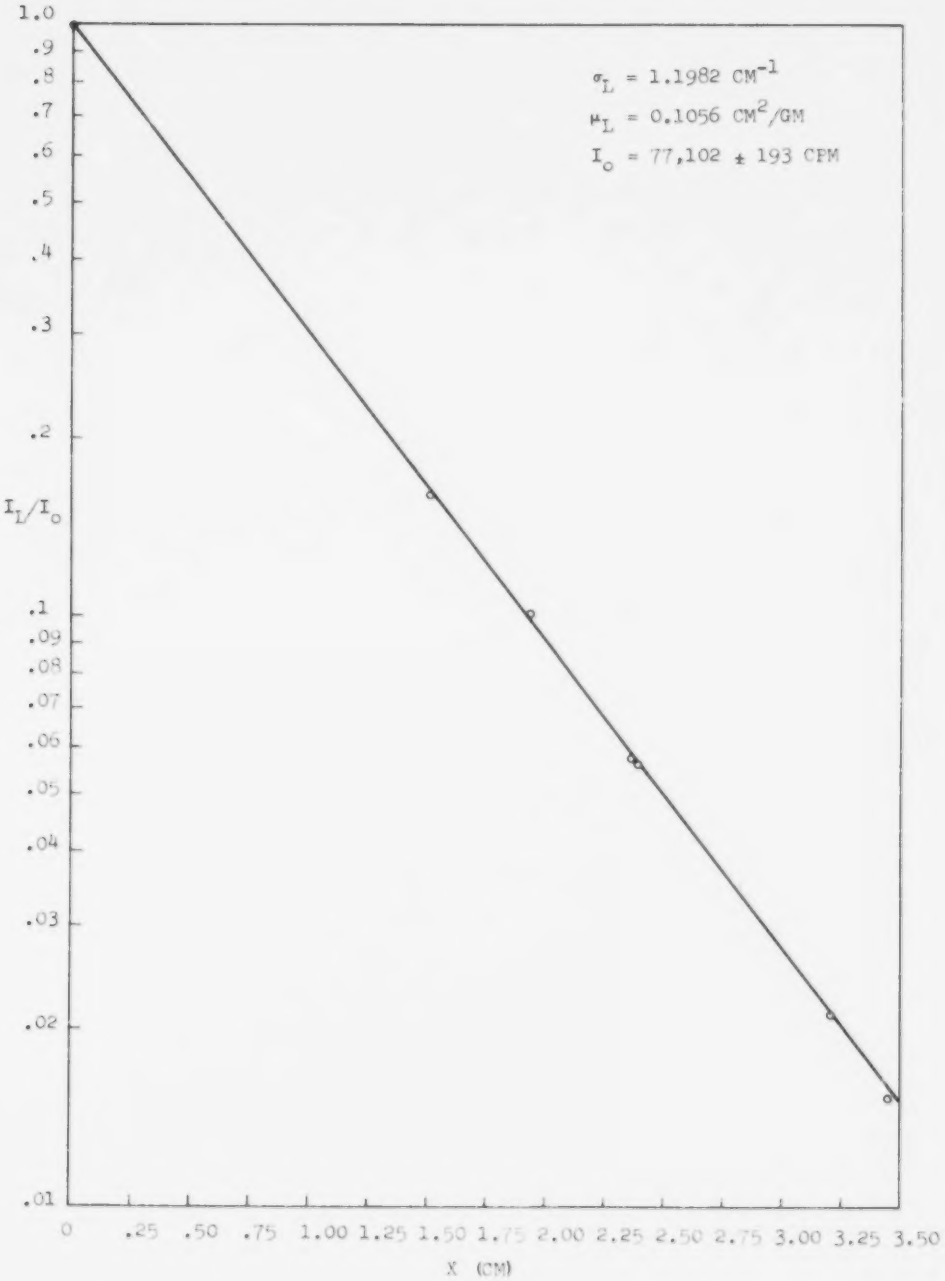

Figure 6.8. Absorption Coefficient for Lead.

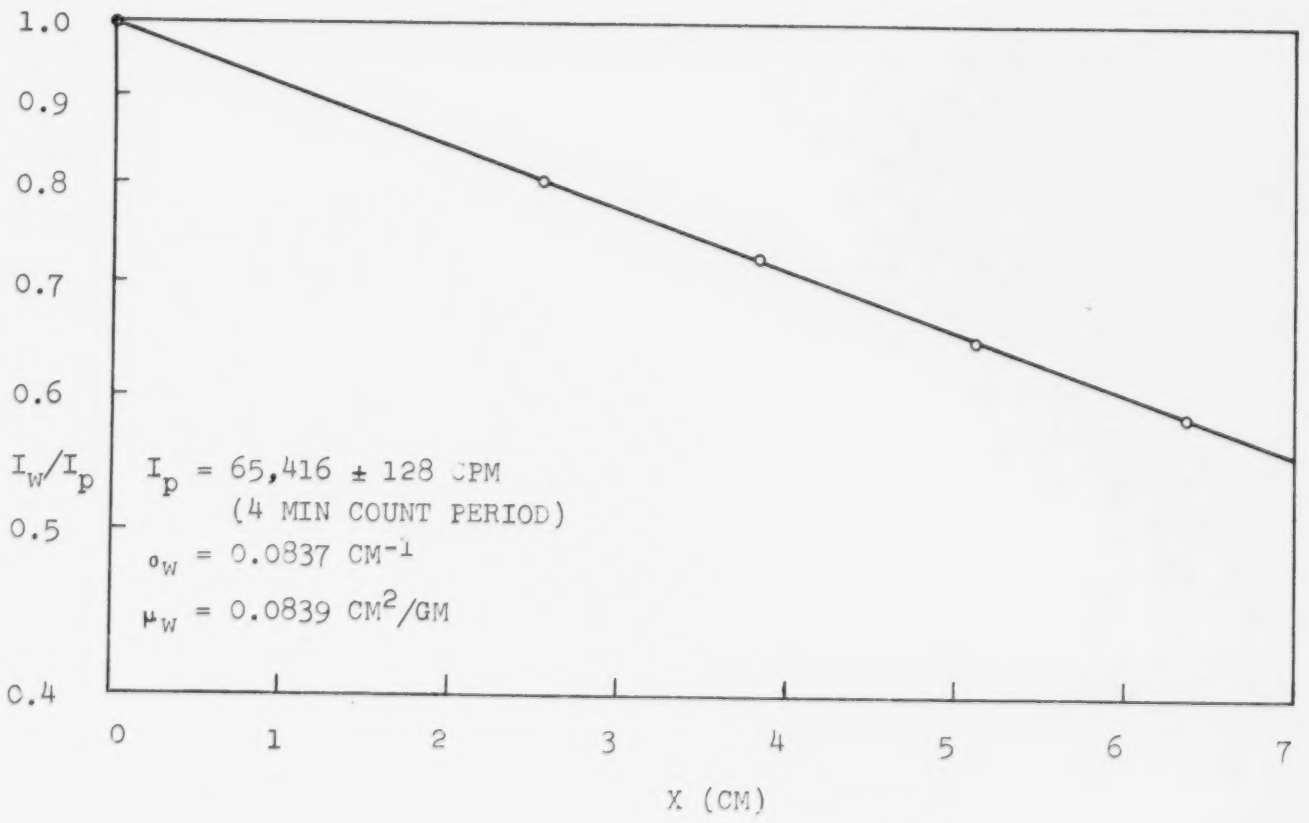

Figure 6.9. Absorption Coeffecient for Water.

6.2.4 Attenuation and absorption coefficients of other materials

For the plastic material the linear attenuation coefficient, which is the product $\mu_p \rho_p$, was found to have an average value of 0.0911 cm^{-1} from five 0.1 minute counts taken for several different thicknesses. The relative transmittance of the plastic as a function of the thickness is shown in Figure 6.10.

The linear attenuation coefficient of Roseville white sand was measured in the plastic tube as 0.1065 cm^{-1} and the mass absorption coefficient calculated from this value was 0.0777 cm^2/gm. Figure 6.11 shows the plot of relative transmittance versus column thickness of the sand.

An average of the results from eight different tests was used to determine the attenuation and absorption coefficients of the glass beads. The linear attenuation coefficient was 0.1147 cm^{-1} and the mass absorption coefficient was 0.0700 cm^2/gm. The attenuation and absorption coefficients which were measured are tabulated in Table 6.1 (see also Fig. 6.12).

Table 6.1

Attenuation and Absorption Coefficients

Material	Linear Attenuation Coefficient, cm^{-1}	Mass Absorption Coefficient, cm^2/gm
Aluminum	0.2007	0.0743
Lead	1.1982	0.1056
Water	0.0011	-
Plastic	0.0837	0.0839
Roseville Sand	0.1065	0.0777
Glass Beads	0.1147	0.0700

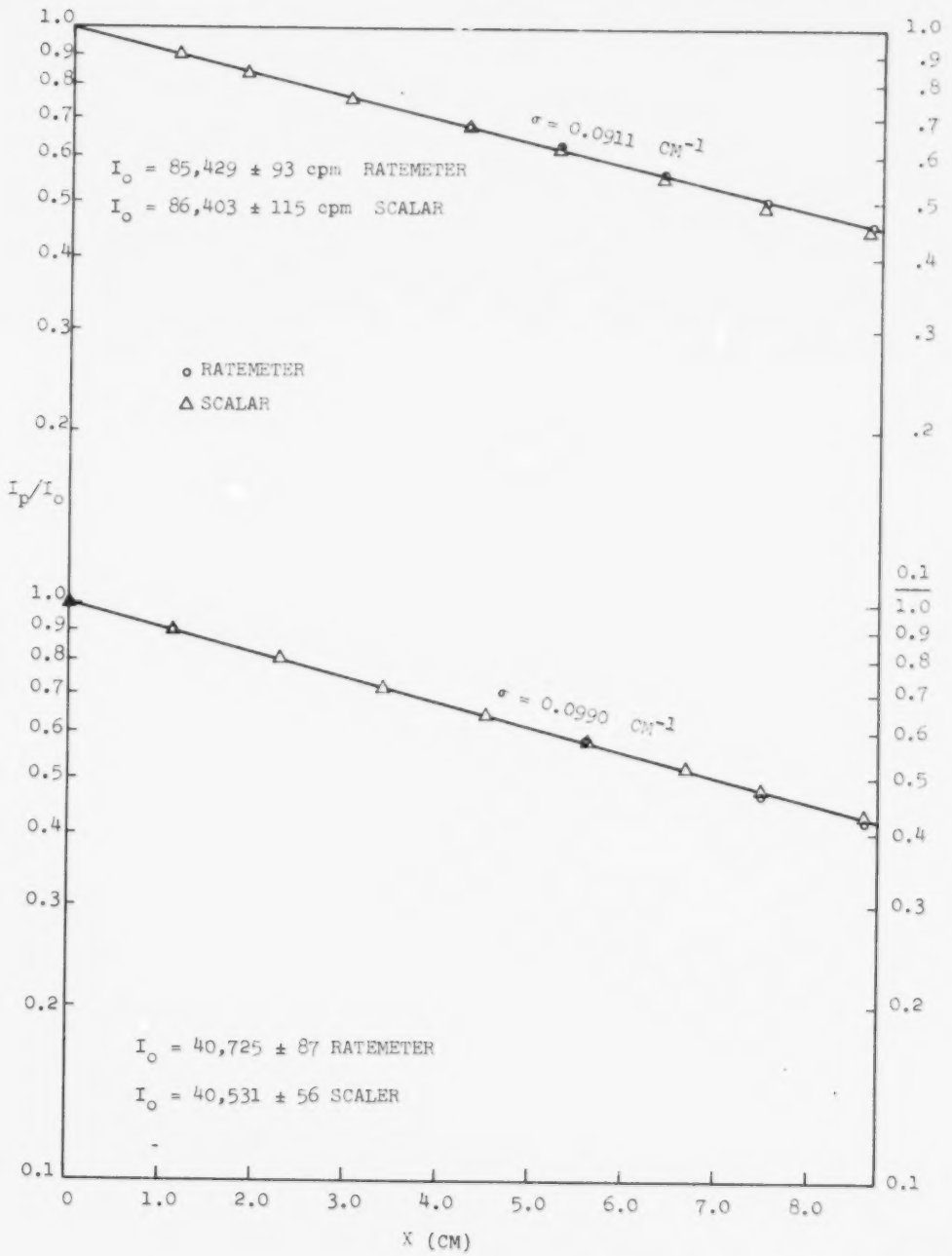
I_o = 85,429 ± 93 cpm RATEMETER
I_o = 86,403 ± 115 cpm SCALAR
σ = 0.0911 CM-1
o RATEMETER
Δ SCALAR
I_p/I_o
σ = 0.0990 CM-1
I_o = 40,725 ± 87 RATEMETER
I_o = 40,531 ± 56 SCALER
X (CM)

Figure 6.10. Linear Attenuation Coefficient for Plastic.

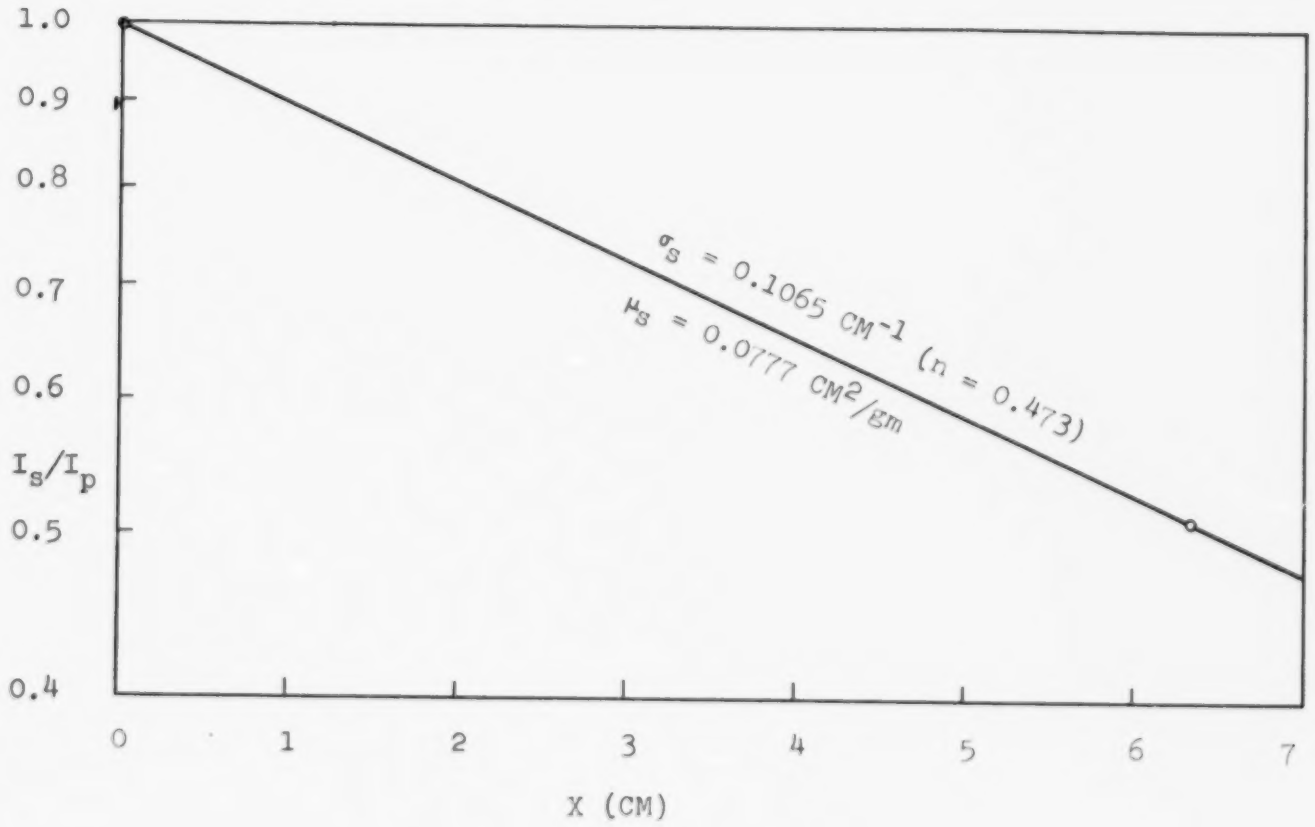

Figure 6.11. Absorption Coefficient for Roseville Sand.

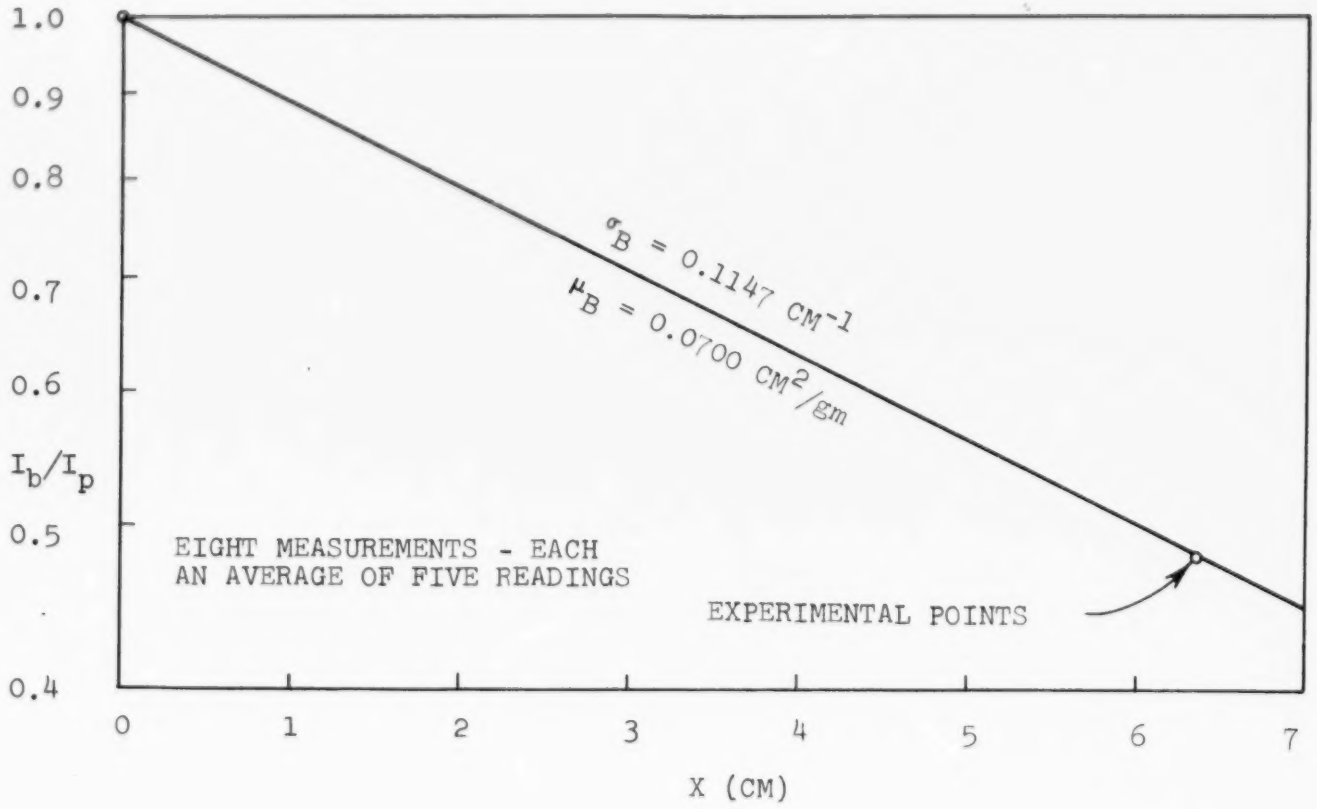

Figure 6.12. Absorption Coefficient for Glass Beads.

6.3 Moisture Distribution During Infiltration

By use of the γ-ray counting apparatus, it was possible to measure the moisture content of the porous medium at various elevations of the column. The lead shielding containing the radioactive source together with the detector and its shielding was mounted on the platform of a hydraulic hoist. This permitted the determination of the moisture content at any position in the vertical column while infiltration was taking place. By use of Eq. (6.3), measurements of the counting rate before infiltration and during infiltration permitted direct determination of the moisture content. To speed the interpretation of the data, two monograms were prepared, as shown in Figures 6.13 and 6.14. The ratio of the counting rates through the wet and the dry columns were used in Figure 6.13 to determine moisture content, while counting rates alone were used in applying Figure 6.14. Both Figures 6.13 and 6.14 are applicable to the 2.500 in. thick container that was used in the experiments.

The Roseville sand, which had a geometric mean diameter of 0.03 cm, did not become completely saturated during infiltration. The moisture content as a function of time at two different locations in the column is shown in Figure 6.15. During this test the air displaced by the wetting front was escaping upward through the sand to the surface, producing a counterflow of the escaping air and the infiltrating water. The coarseness of the sand particles and its grain size distribution appeared to promote its incomplete saturation.

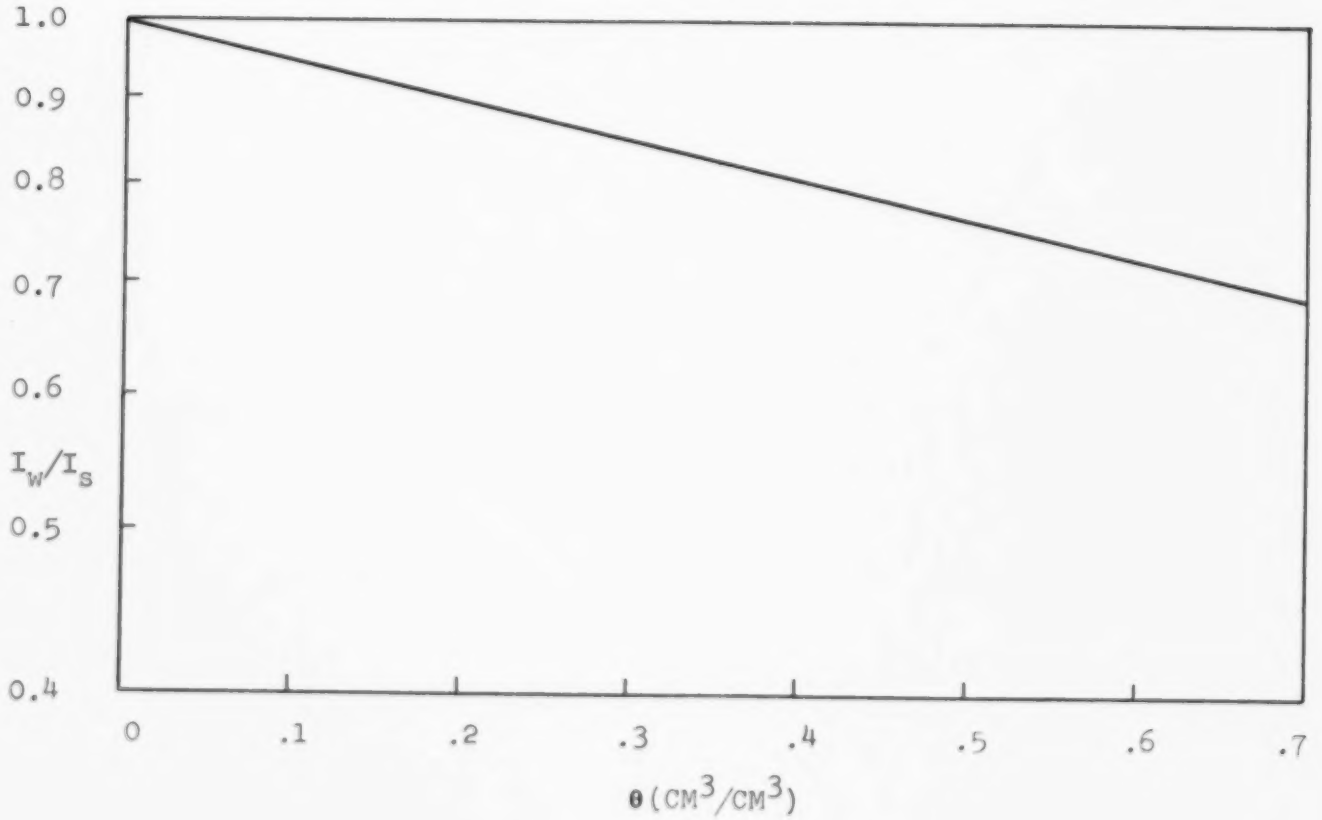

Figure 6.13. Moisture Content for Various Attenuations.

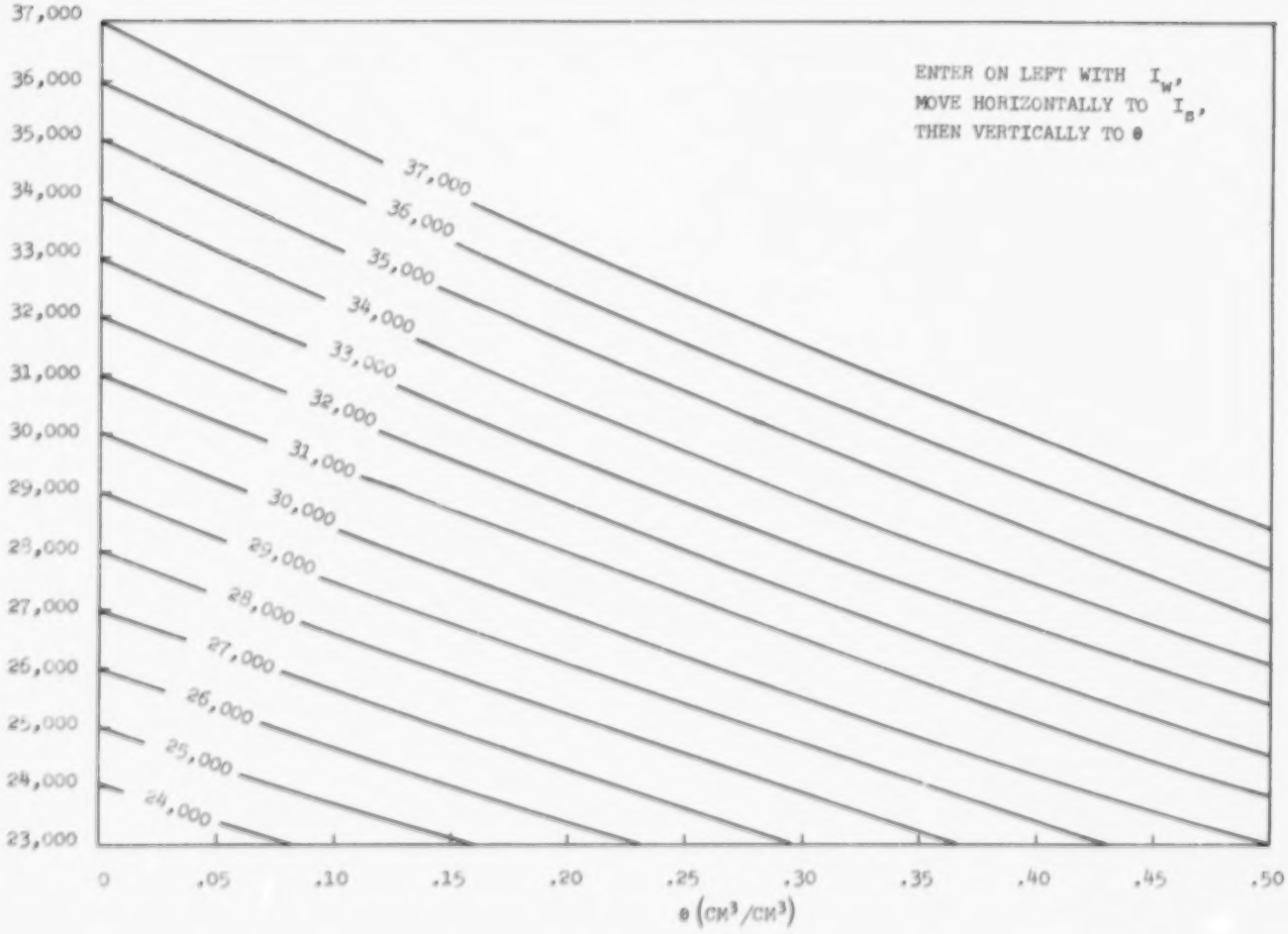

Figure 6.14. Interpolation Diagram for Moisture Content.

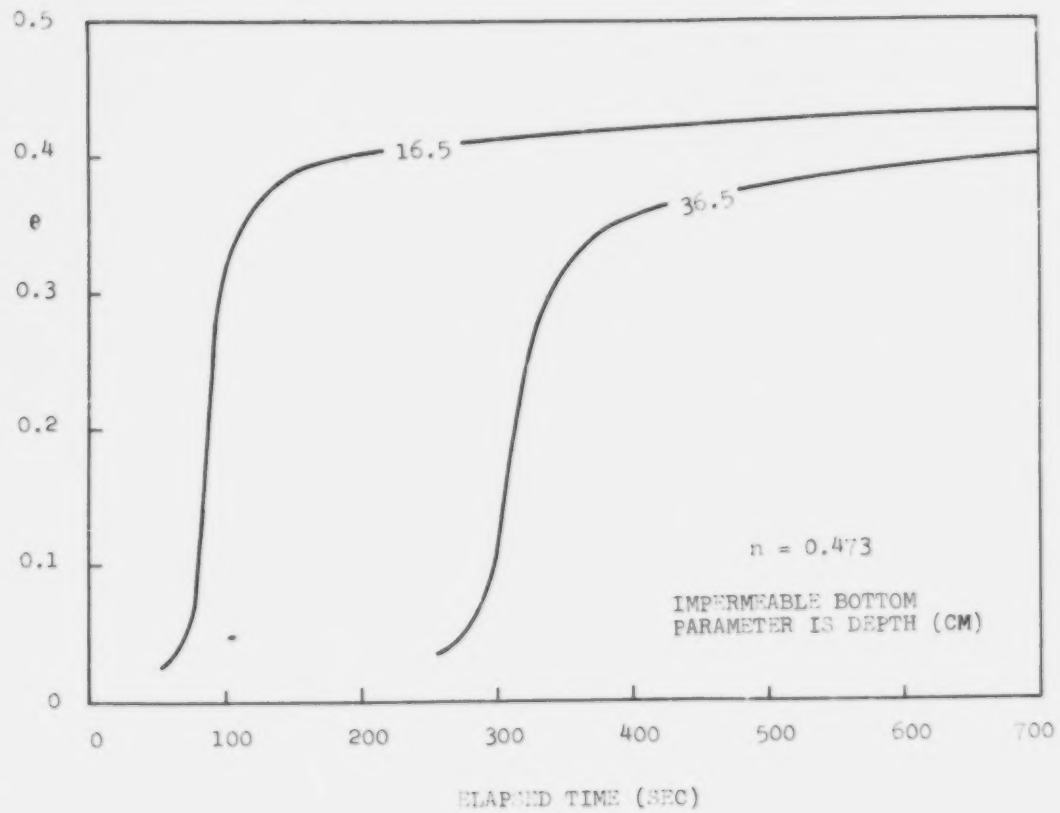

Figure 6.15. Moisture Distribution During Infiltration.

The mediums composed of smaller diameter particles had their pores nearly saturated during infiltration. The displaced air which escaped upwards through the medium moved through only a few pores, usually near the corners of the column. Since this portion of the column was not traversed by the γ-ray beam, the moisture content measurements may not be completely representative of the average conditions in the column. However, the measurement of the total volume of water which had infiltrated into the column was sufficient to calculate the location of the wetting front, assuming all the pore spaces were saturated. A comparison of the calculated location of the wetting front and the observed wetting front shows that for the medium made up of 0.0080 cm diameter particles and the one with particles having a geometric mean diameter of 0.0123 cm the pore space was nearly completely saturated with water. It should be noted that at any instant the degree of saturation varies with position, and the assumption of uniformly complete saturation in the wetting zone is only an approximation.

6.4 Motion of the Wetting Front

6.4.1 Observed and calculated positions of the wetting front

The change in color between the dry and wet portions of the medium was pronounced enough, so that visual observation of the location of the wetting front could readily be made. The wetting front did not move as a plane, but some unevenness was noticed. It appeared that if the wetting front started to move unevenly, with one portion more advanced than the rest, the general shape of the front would not change

much during its movement through the column. Part of the difference between the observed position of the wetting front and its calculated position was probably due to the tendency of visually locating the wetting front by its most advanced position. The observed position of the wetting front as well as the position calculated from the water inflow data is shown in Figures 6.16, 6.17 and 6.18. There was very little air resistance in these three tests as the displaced air was free to escape from the bottom of the column. A graded medium was used in the test upon which Figure 6.17 is based. The sieve analysis of the medium is shown in Figure 6.4. As would be expected, this medium had the greatest difference between the observed and calculated positions of the wetting front. This indicates that some of the pores were by-passed and air was trapped in them. The mediums having a uniform particle diameter had fewer pores by-passed, as is shown in Figures 6.16 and 6.18.

When the air displaced by the wetting front is not free to escape, the particle diameter and the grain size distribution are important in determining how closely the observed wetting front corresponds to the calculated wetting front. Figure 6.19 shows the observed and the calculated wetting fronts for the Roseville sand whose grain size distribution was shown in Figure 6.2. The large size of the pores in this sand evidently resulted in a lot of by-passing of portions of some pores with the result that some air was trapped in the medium. Also, air was flowing through the sand in the direction opposite to the flow of the infiltrating water, so there were continuous air passages as

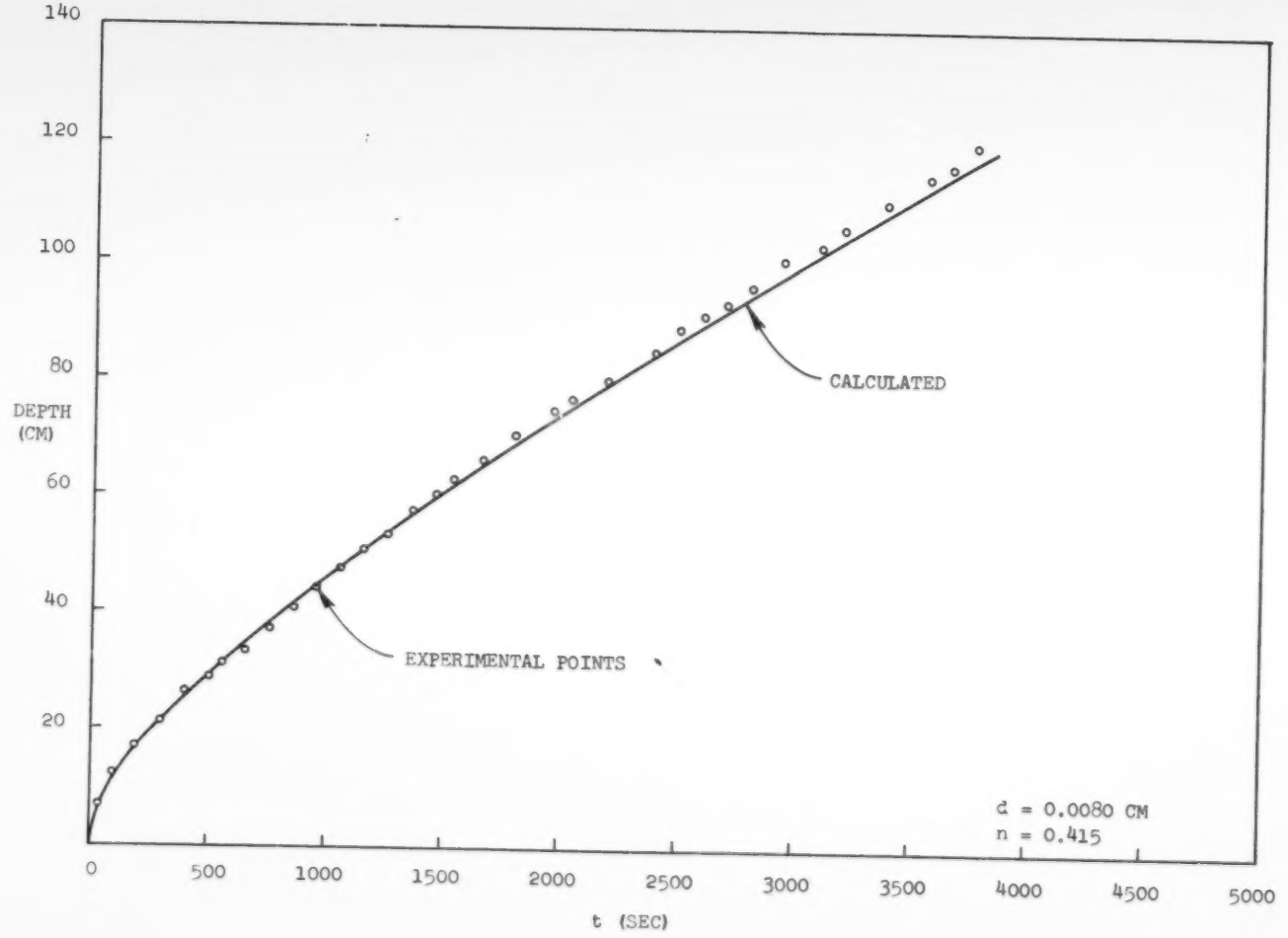

Figure 6.16. Observed and Calculated Position of the Wetting Front.

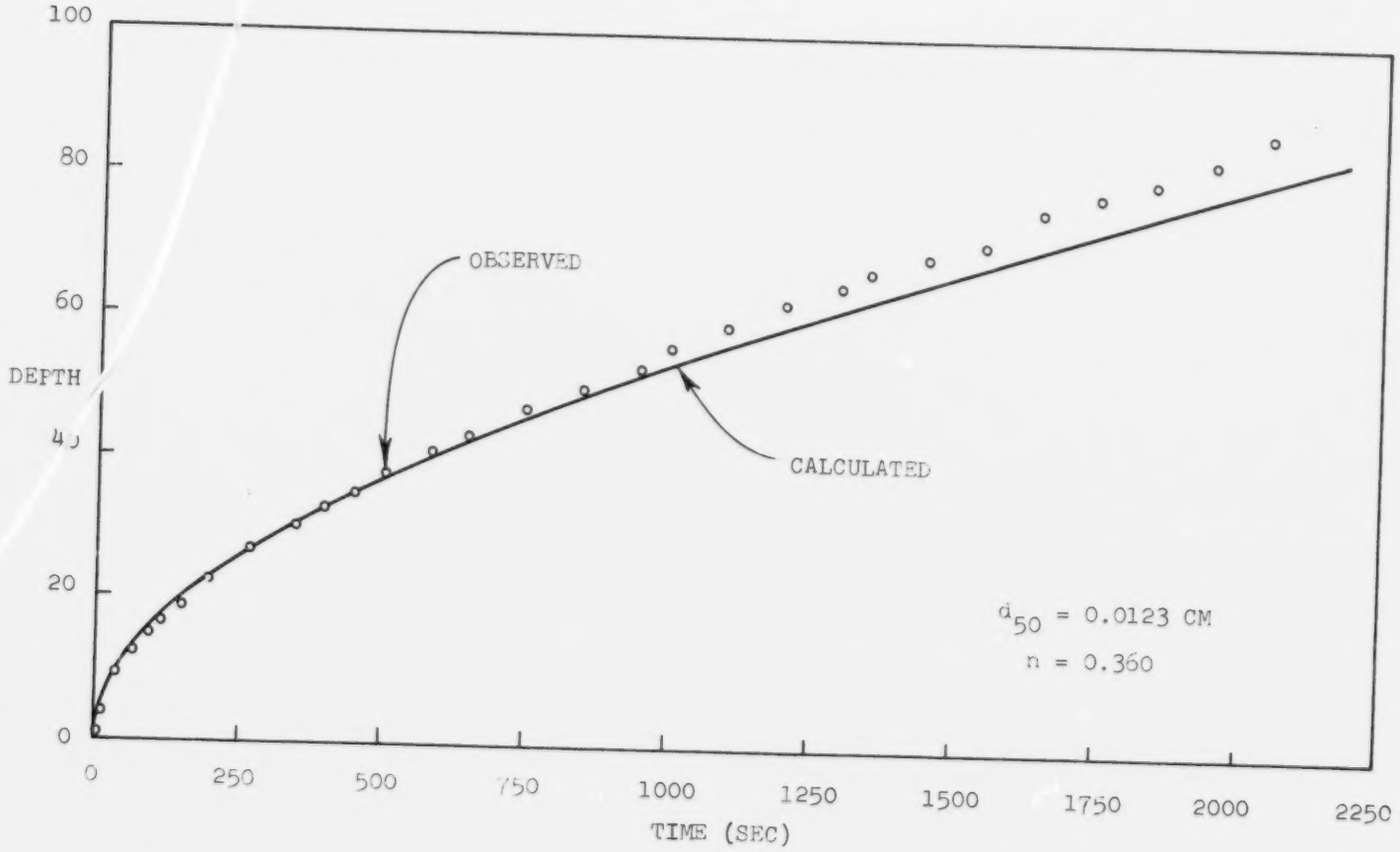

Figure 6.17. Observed and Calculated Position of the Wetting Front No Air Resistance.

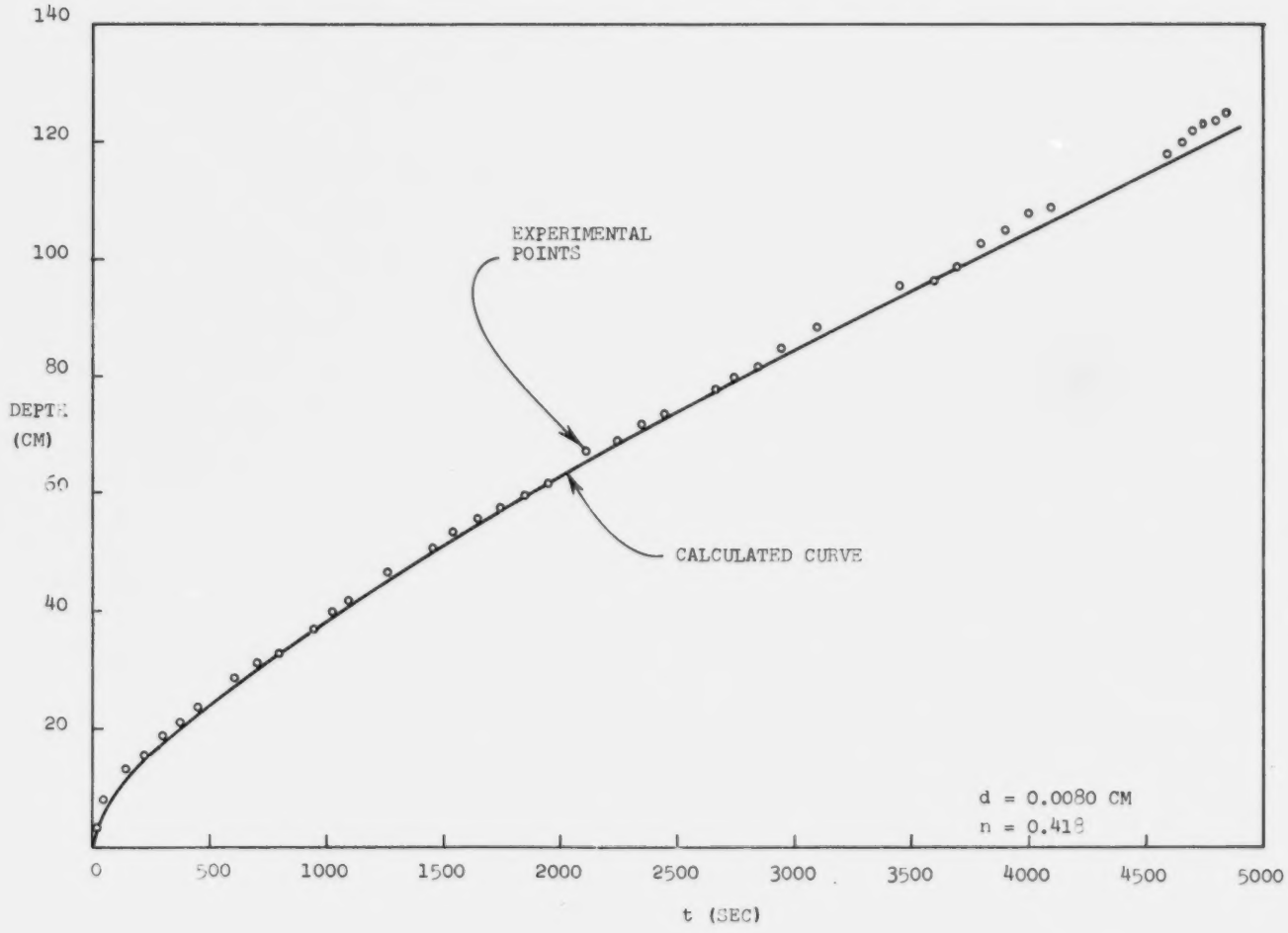

Figure 6.18. Observed and Calculated Position of the Wetting Front.

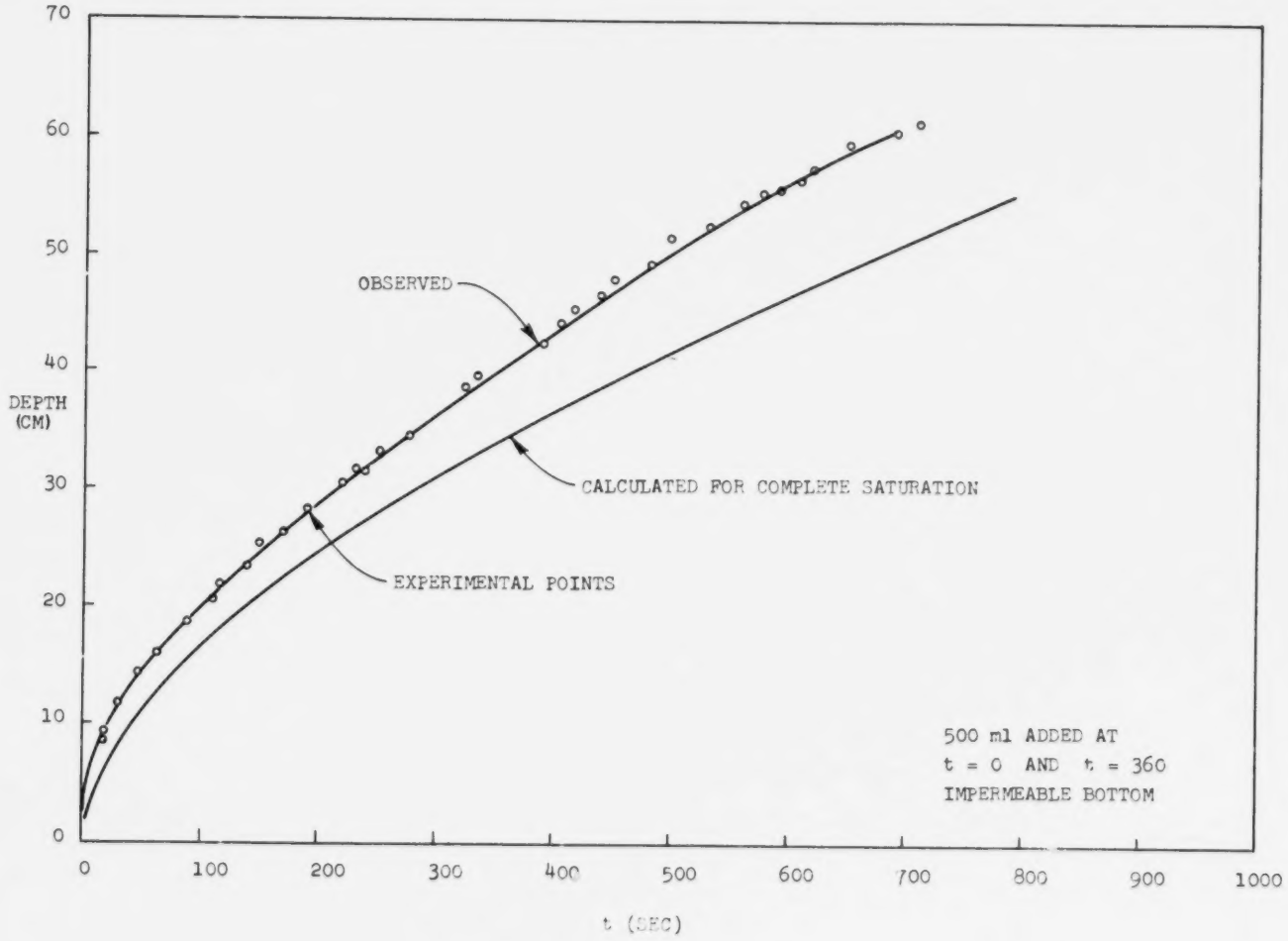

Figure 6.19. Wetting Front Location, Roseville White Sand.

well as the discontinuous passages. Figure 6.20 shows the corresponding result for a medium having a uniform particle diameter of 0.0080 cm. The observed and the calculated positions of the wetting front are almost indistinguishable.

6.4.2 Position of the wetting front compared with theory

The equations which were derived in Chapter 3 are useful in interpreting the results. A dimensionless graph of h^* vs. t^* for various values of h_c^* permits a rapid evaluation of the experimental data. It will be recalled that $h^* = h/\ell$, $h_c^* = h_c/\ell$ and $t^* = Kt/n\ell$. After each test was completed, the permeability of the medium was measured. Figures 6.21 and 6.22 show the comparison of the experimental data and the theoretical curves. In the experiment water was ponded on the surface, so that this results in the experimentally obtained h^* being slightly larger than would be predicted from theory for any given t^* when a^* is taken as zero for convenience. From Figure 6.21 an average value of h_c^* is 0.4 and from Figure 6.22 an average value of h_c^* is 0.6. The column lengths were 95.2 cm and 121.2 cm, respectively, so that the corresponding values of h_c are 38 cm and 72 cm. From Figure 4.6 the values of the expected height of capillary rise vary from 37 cm to 86 cm for the porosity range and particle diameter of the medium used in these columns.

Figures 6.23, 6.24 and 6.25 are for the corresponding situation when the bottom of the column is impermeable. The air resistance slows down the motion of the wetting front, so that the effect of the ponding

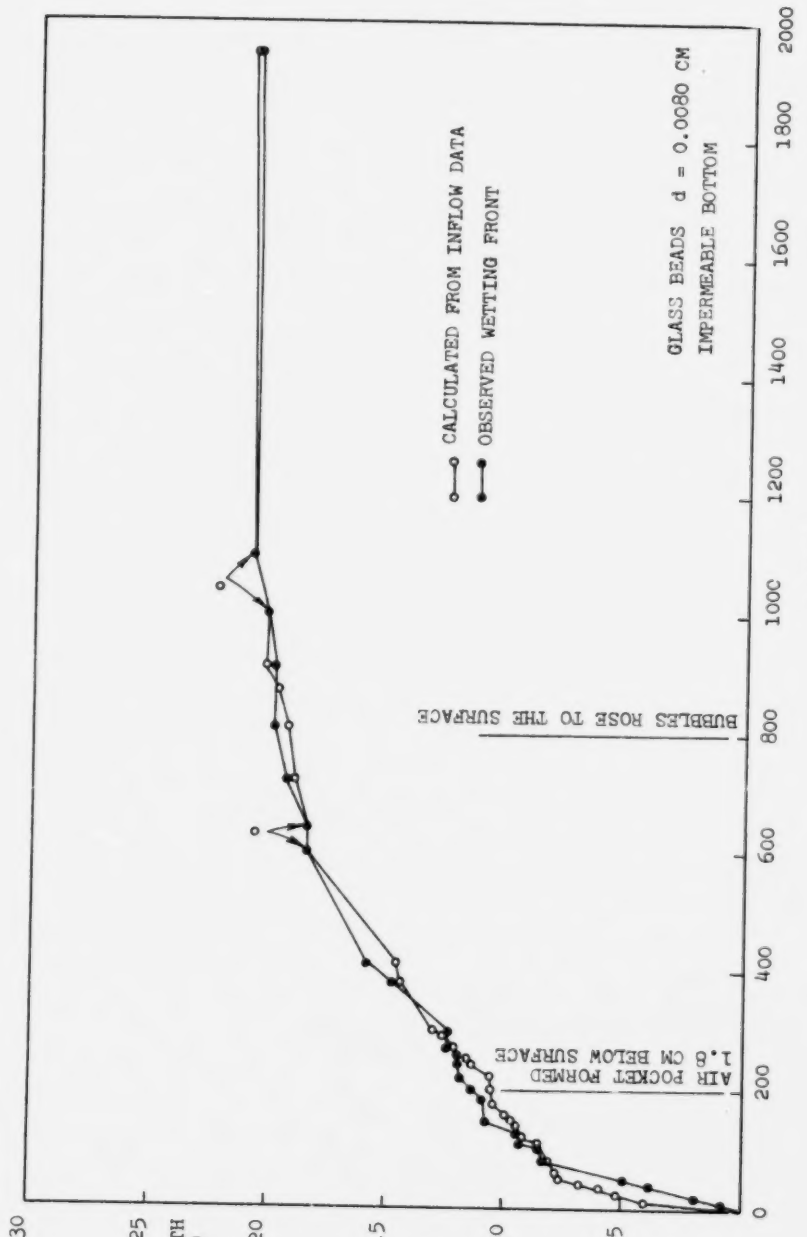

Figure 6.20. Interface Position During Infiltration.

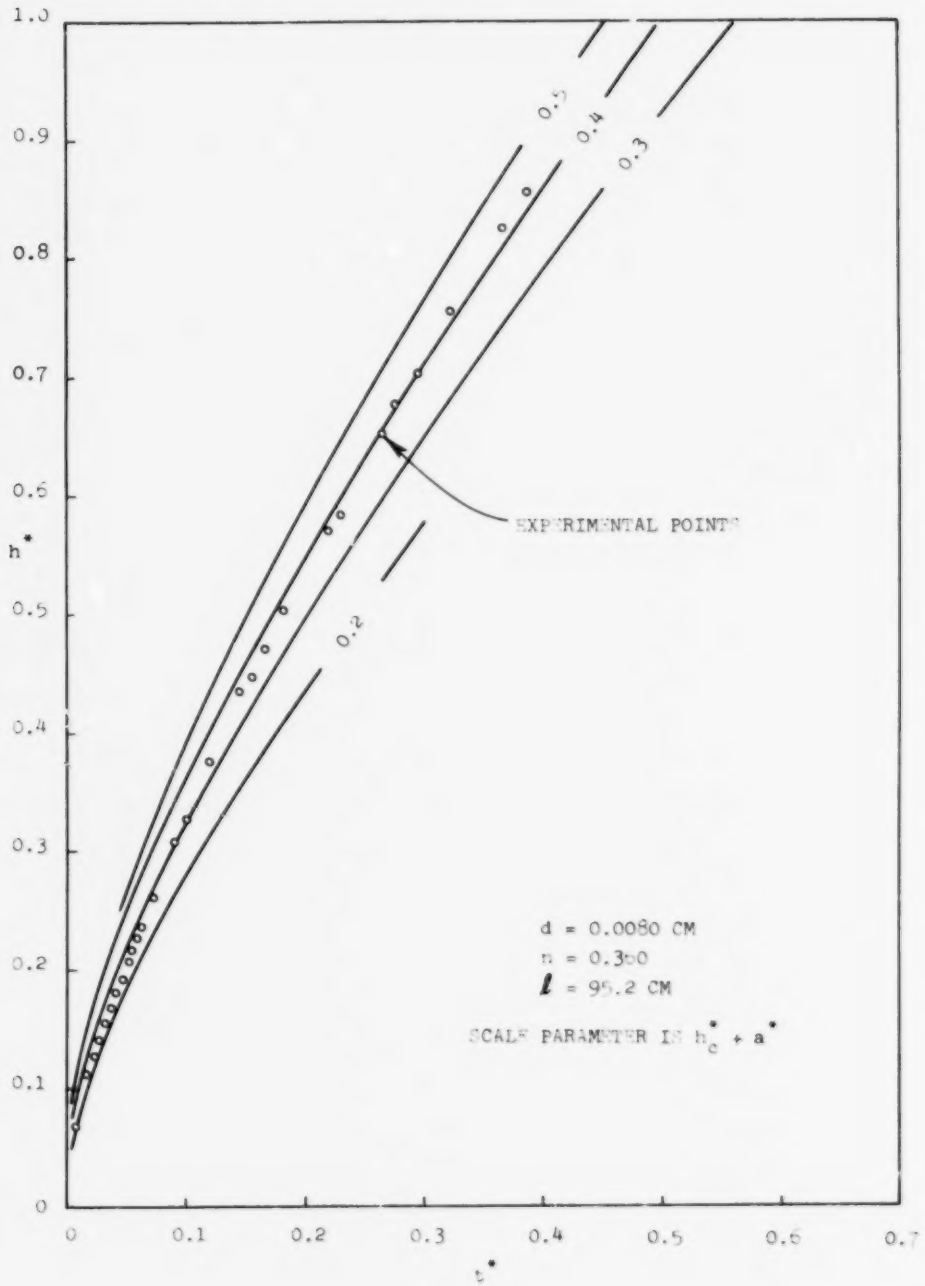

Figure 6.21. Comparison of Theory and Experiment With no Air Resistance.

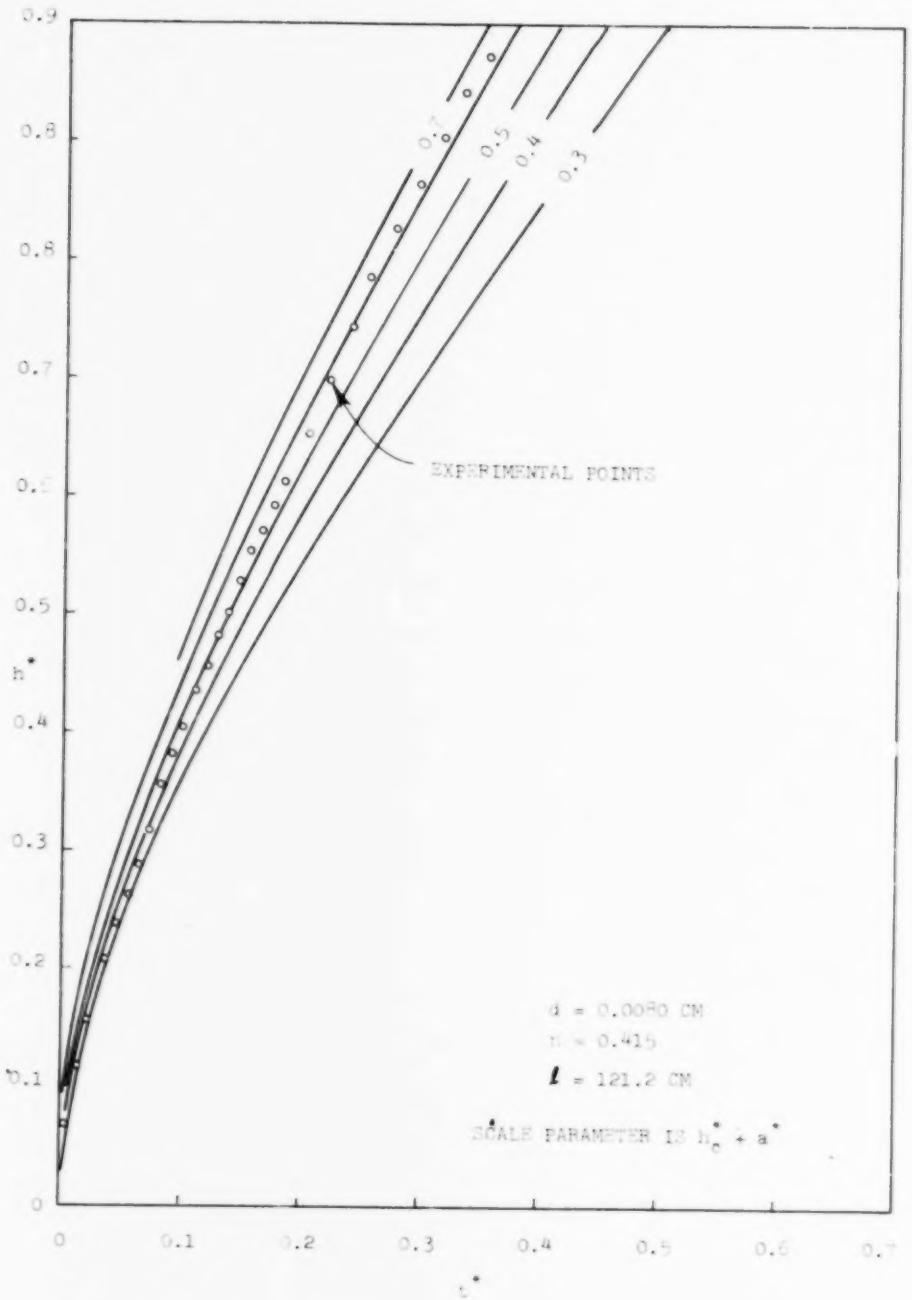

Figure 6.22. Comparison of Theory and Experiment With no Air Resistance.

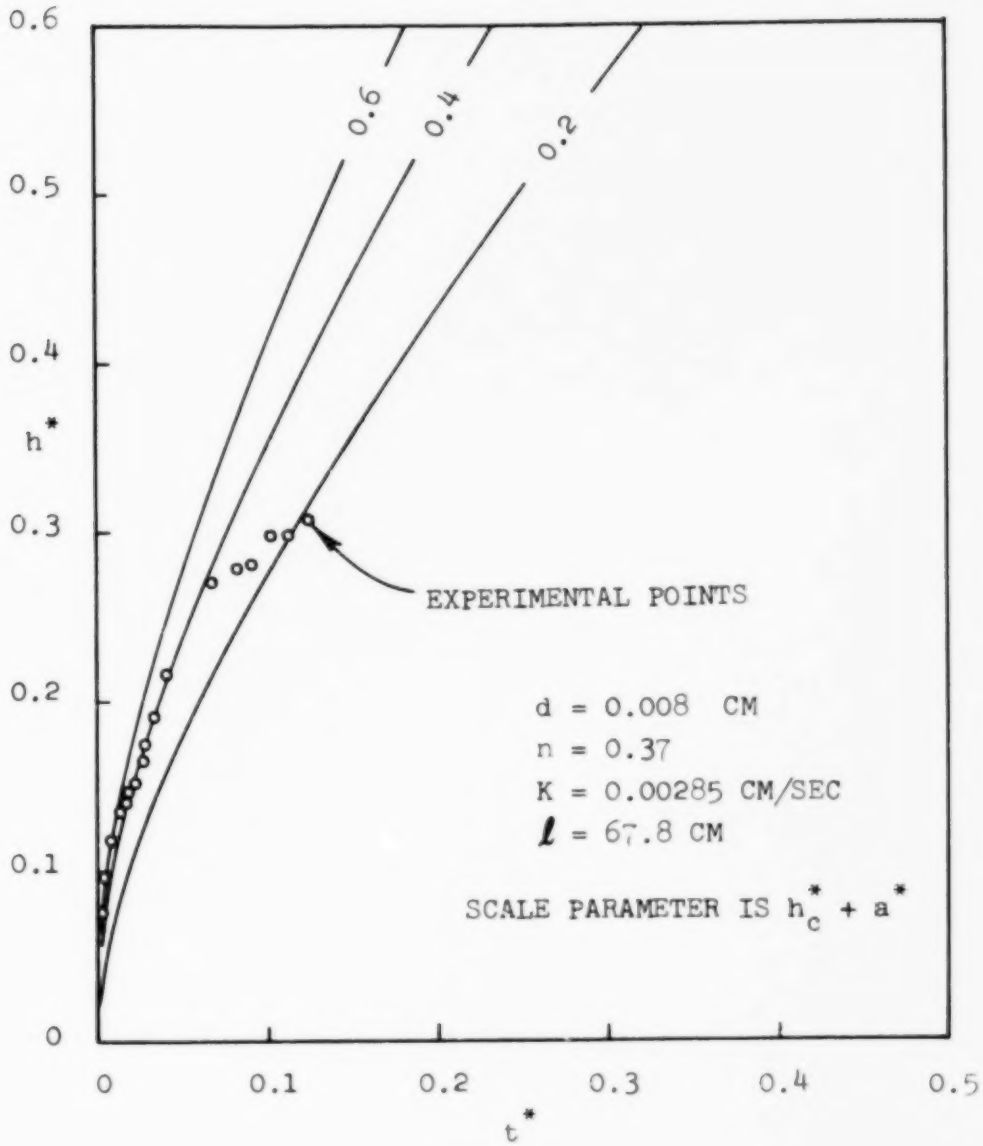

Figure 6.23. Wetting Front as a Function of Time.

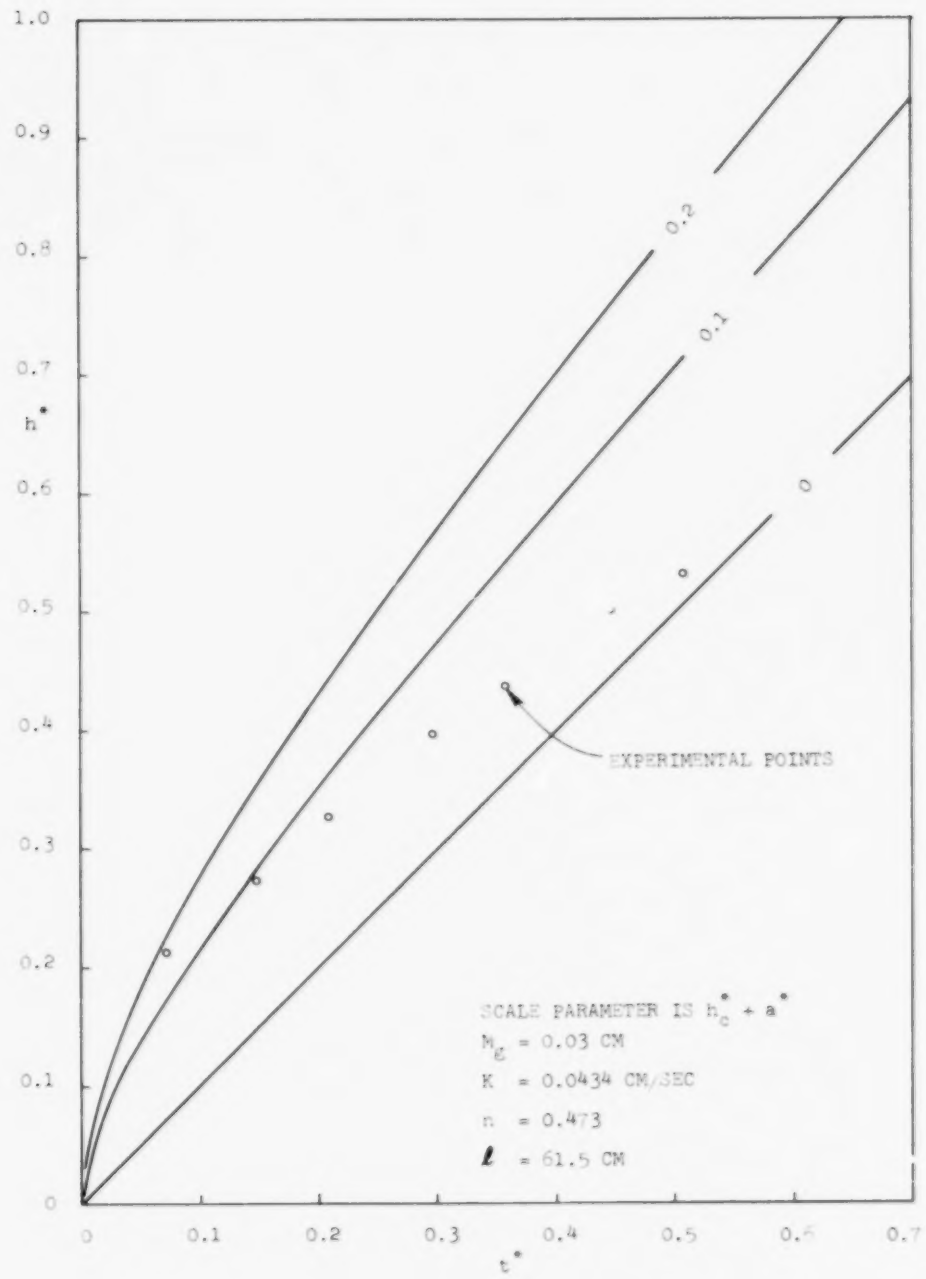

Figure 6.24. Roseville White Sand.

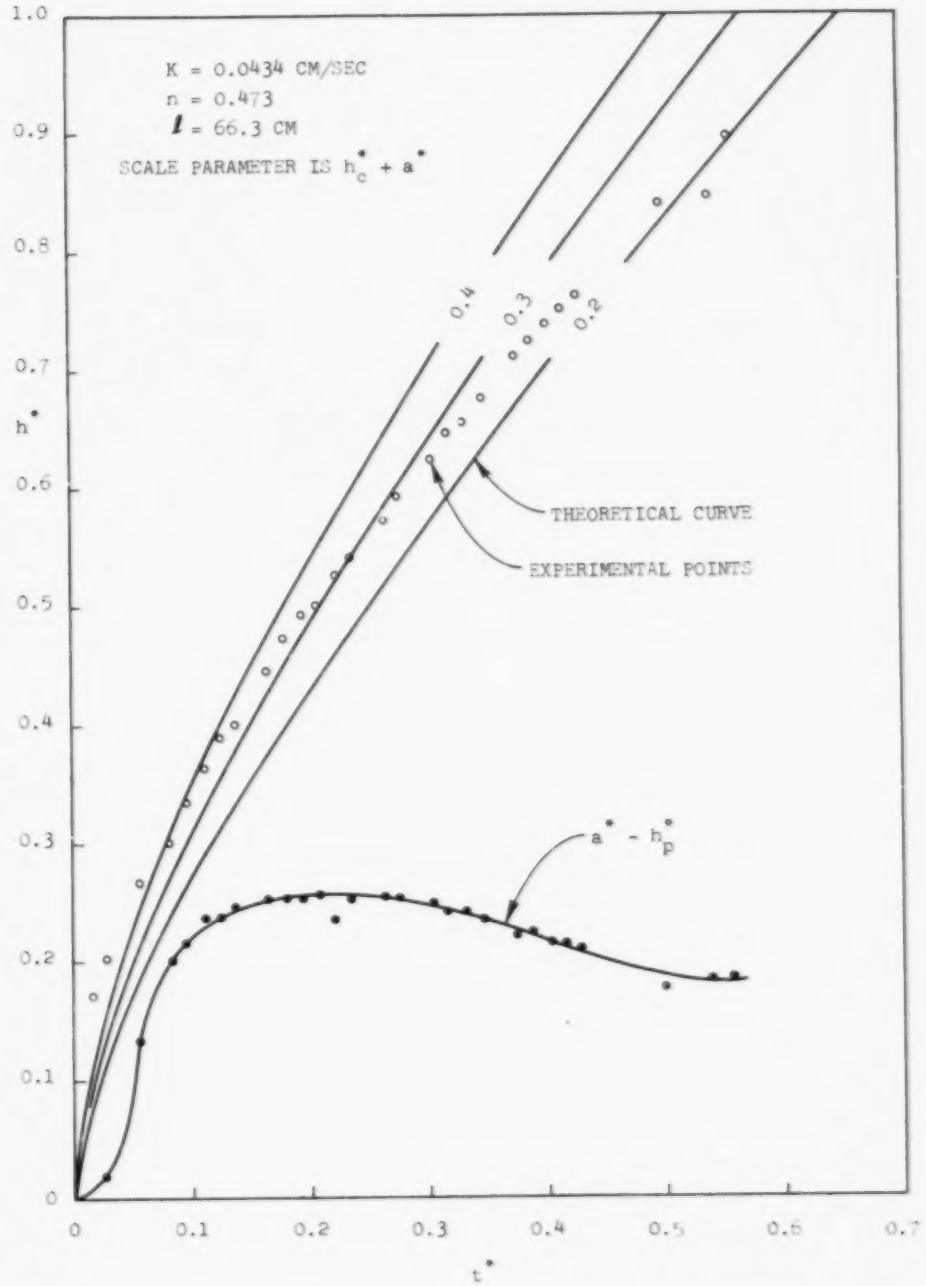

Figure 6.25. Roseville White Sand.

on the surface of the medium is overshadowed. This results in the experimental values of h^* being less than would be predicted from theory when air resistance is neglected. The experimental data all followed the previous trend. However, little additional generalization is possible because of the variability in the air pressure ahead of the wetting front. The rate at which air escaped from the medium was not constant, but varied during each test. Figures 6.24 and 6.25 are both for Roseville sand columns which had very similar characteristics. Yet, the experimental data were considerably different in the two cases. The air escaped upwards through the sand rather readily from the column used to obtain the data for Figure 6.25, so that infiltration was not retarded greatly by the air pressure ahead of the wetting front. The air did not escape as easily from the column used to obtain the data for Figure 6.24, so that the infiltration rate was much less.

From the measurements of the air pressure in columns ahead of the wetting front and the pore volume ahead of the wetting front, it was possible to calculate the total volume of air which had escaped from the column during infiltration. The cumulative air loss is shown in Figure 6.26. The air loss rate is the derivative of the cumulative air loss, so that by numerical differentiation the air loss rate could be calculated. It fluctuated considerably during the early stages of infiltration, then became constant and finally decreased to zero. It appears that a slightly different pore size distribution could result in a much different air loss rate.

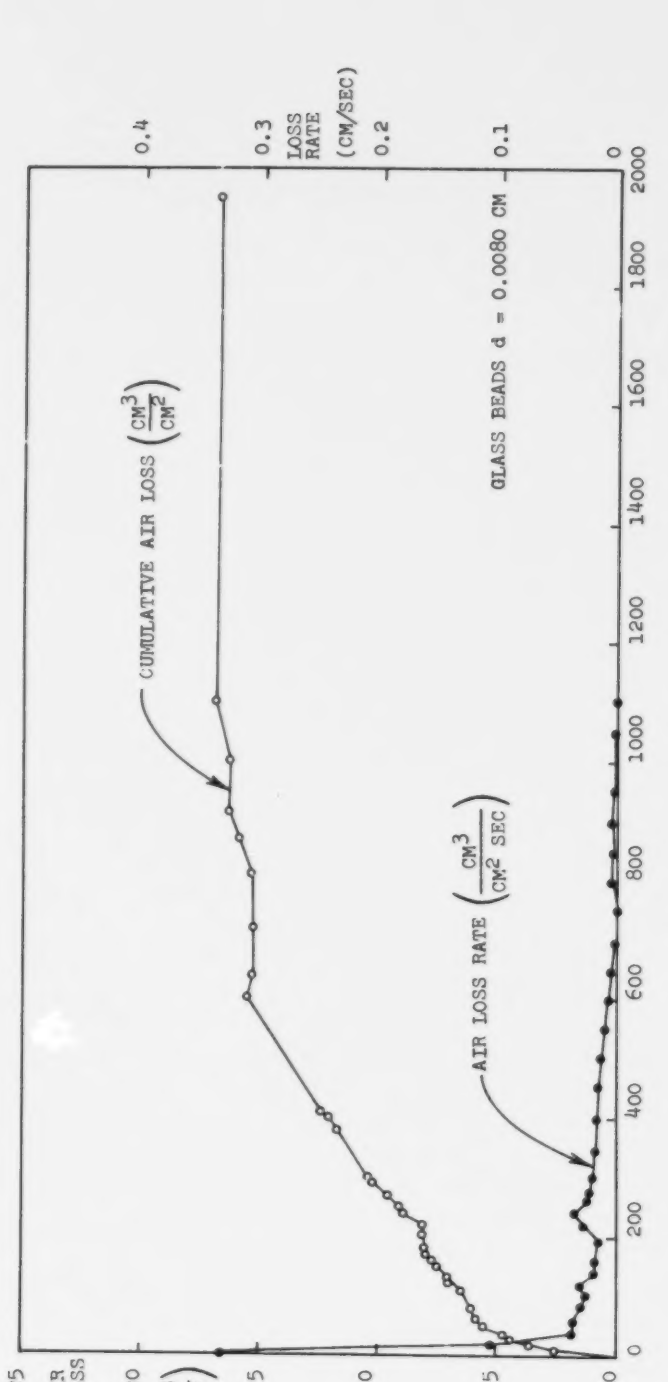

Figure 6.26. Air Escape During Infiltration Impermeable Bottom.

The value of h_c^* is difficult to estimate when there is an air pressure build-up ahead of the wetting front. From Figure 6.25 h_c^* may be about 0.3 , which would mean h_c = 20 cm. This estimate compares favorably with an experimentally determined value of h_c for a similar sand. Between 1956 and 1957 the Stanford Geology Department measured the height of capillary rise in a sand whose grain size distribution is shown in Figure 6.27. The geometric mean sizes of the two sands were nearly the same, although the Roseville sand had a wider grain size distribution than the Geology Department's sand. After one year the water had risen 19.4 cm in this column of sand. The porosity of the column used to measure h_c directly was 0.385 , while the Roseville sand had a porosity of 0.473. For a mean particle diameter of 0.03 cm , Figure 4.6 would give a range of values for the capillary rise between 10 cm and 29 cm.

6.5 Infiltration Rates

6.5.1 Numerical treatment of data

The cumulative inflow into a porous medium could be obtained from the readings taken of the water surface level during the experiment. These data were plotted as a graph of cumulative inflow as a function of time. The infiltration rate is the slope of the tangent to the curve of cumulative inflow, or the derivative of this curve. In order to obtain the derivatives without introducing excessive error, a numerical differentiation technique based on central-differences and a five-point approximation were used [Herriot (1963)]. The ordinates to the cumulative

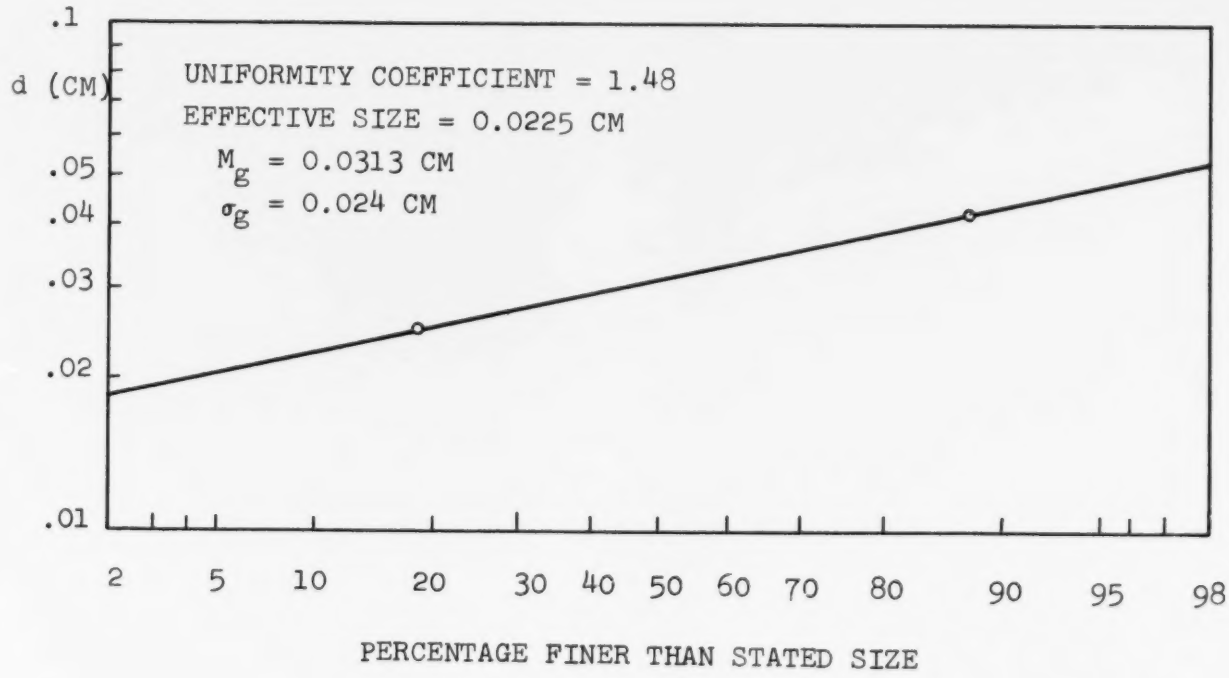

Figure 6.27. Sieve Analysis, Stanford Geology Department Sand.

inflow curves were recorded at regular intervals and these values were used in the formula

$$f'(t_o) = \frac{1}{12\Delta t}\left[- f_{t_o+2\Delta t} + 8f_{t_o+\Delta t} - 8f_{t_o-\Delta t} + f_{t-2\Delta t}\right] \qquad (6.4)$$

where f is the ordinate and Δt is the step width. This formula is satisfactory everywhere except near the beginning or the end of the cumulative inflow curve. The derivative at the end of the cumulative inflow curve is obtained by using the formula

$$f'(t_o-2\Delta t) = \frac{1}{12\Delta t}\left[-3f_{t_o+2\Delta t} + 16f_{t_o+\Delta t} - 36f_{t_o} + 48f_{t_o-\Delta t} - 25f_{t_o-2\Delta t}\right] \qquad (6.5)$$

and at the first position along the curve

$$f'(t_o-\Delta t) = \frac{1}{12\Delta t}\left[f_{t_o+2\Delta t} - 6f_{t_o+\Delta t} + 18f_{t_o} - 10f_{t_o-\Delta t} - 3f_{t_o-2\Delta t}\right] \qquad (6.6)$$

After the derivatives are obtained at the first two positions, the derivatives at the remaining positions may be obtained from Eq. (6.4).

6.5.2 Cumulative inflow and infiltration rates

Figures 6.28, 6.29 and 6.30 show the cumulative inflows and the infiltration rates for three columns which were constructed so that the displaced air could escape through the bottom of the column. The maximum infiltration rates at the beginning of infiltration were 0.0912 cm/sec , 0.1170 cm/sec and 0.2237 cm/sec , respectively.

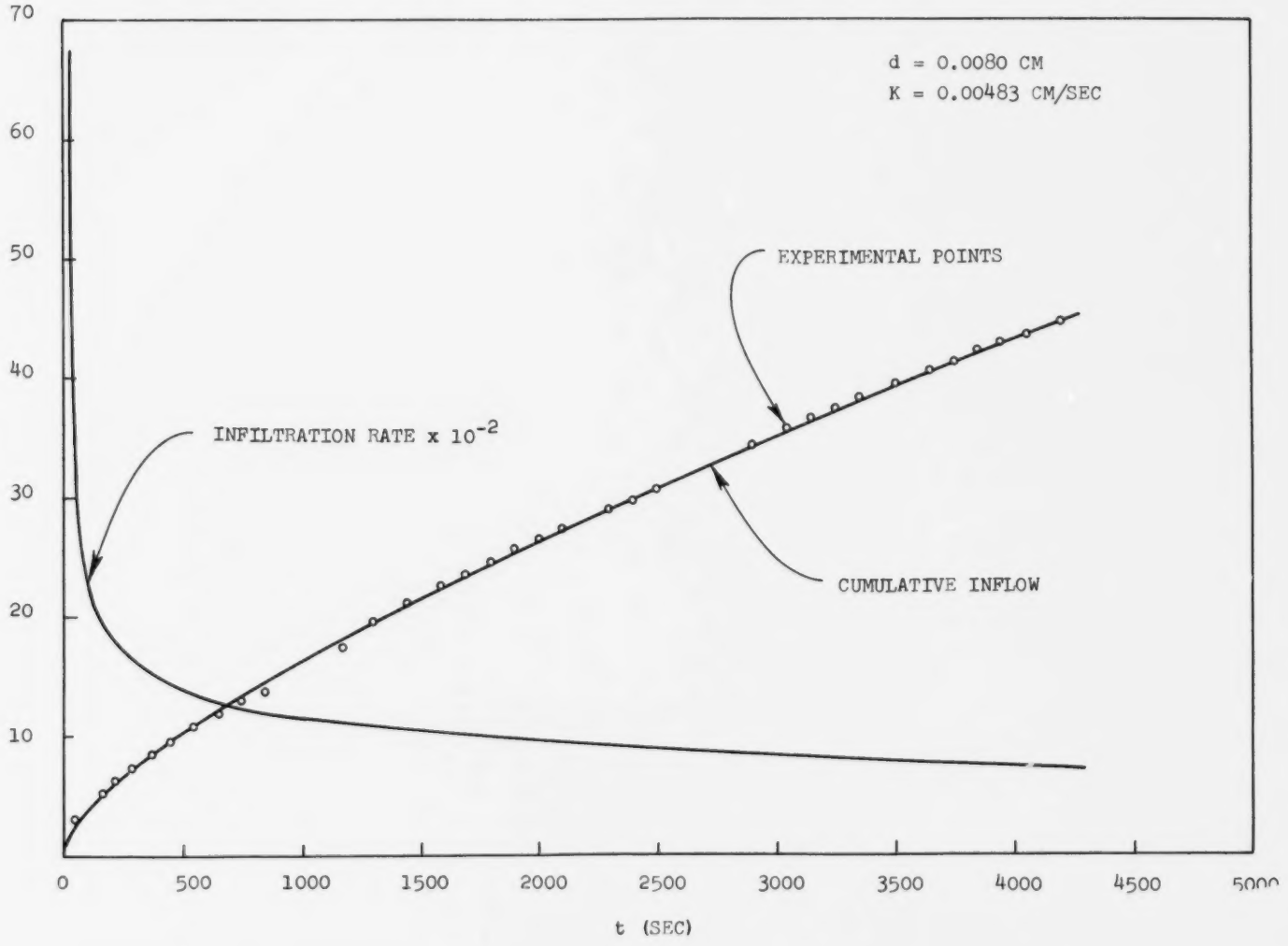

Figure 6.28. Cumulative Inflow and Infiltration Rate No Air Resistance.

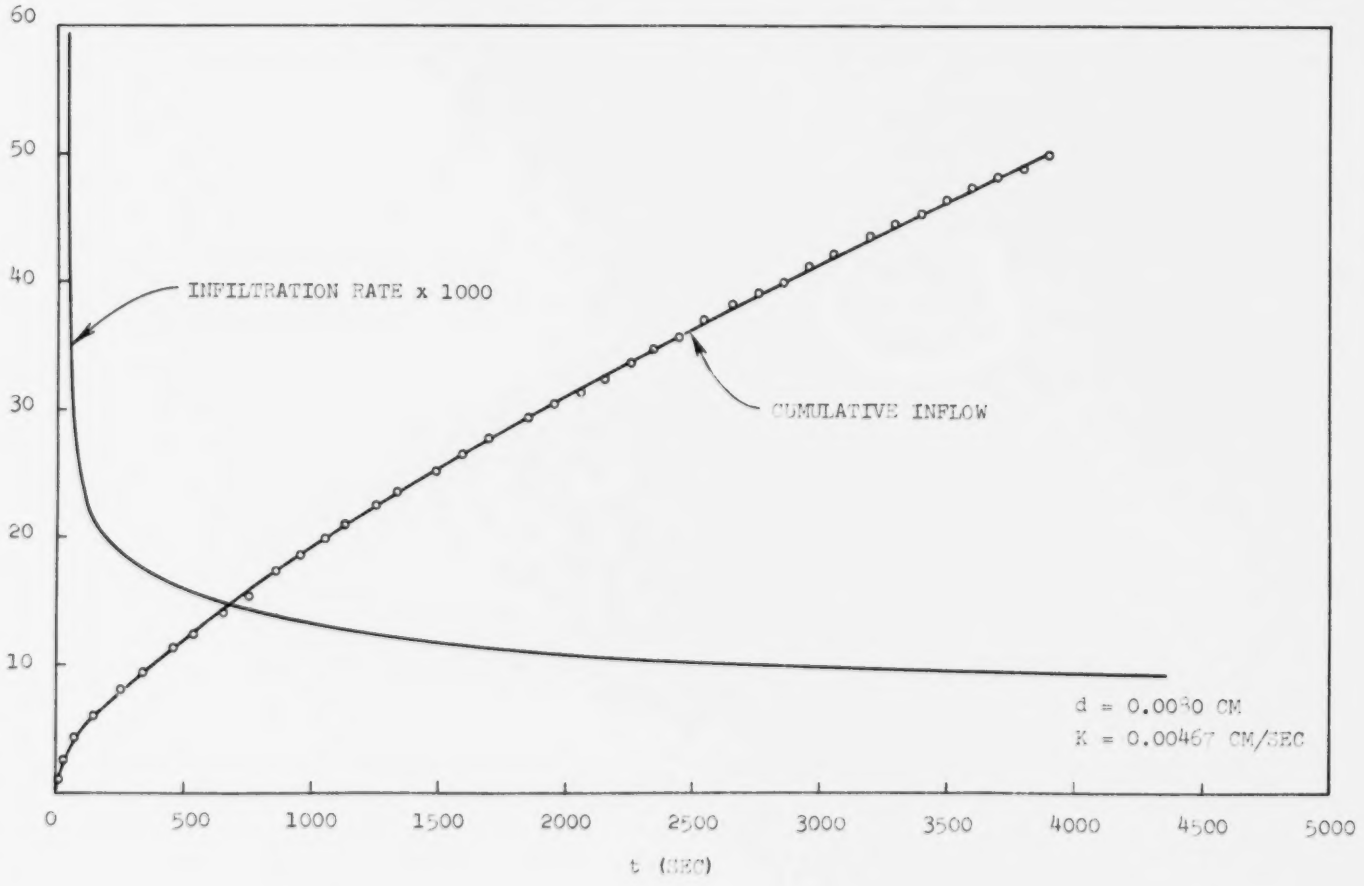

Figure 6.29. Inflow and Infiltration Rate.

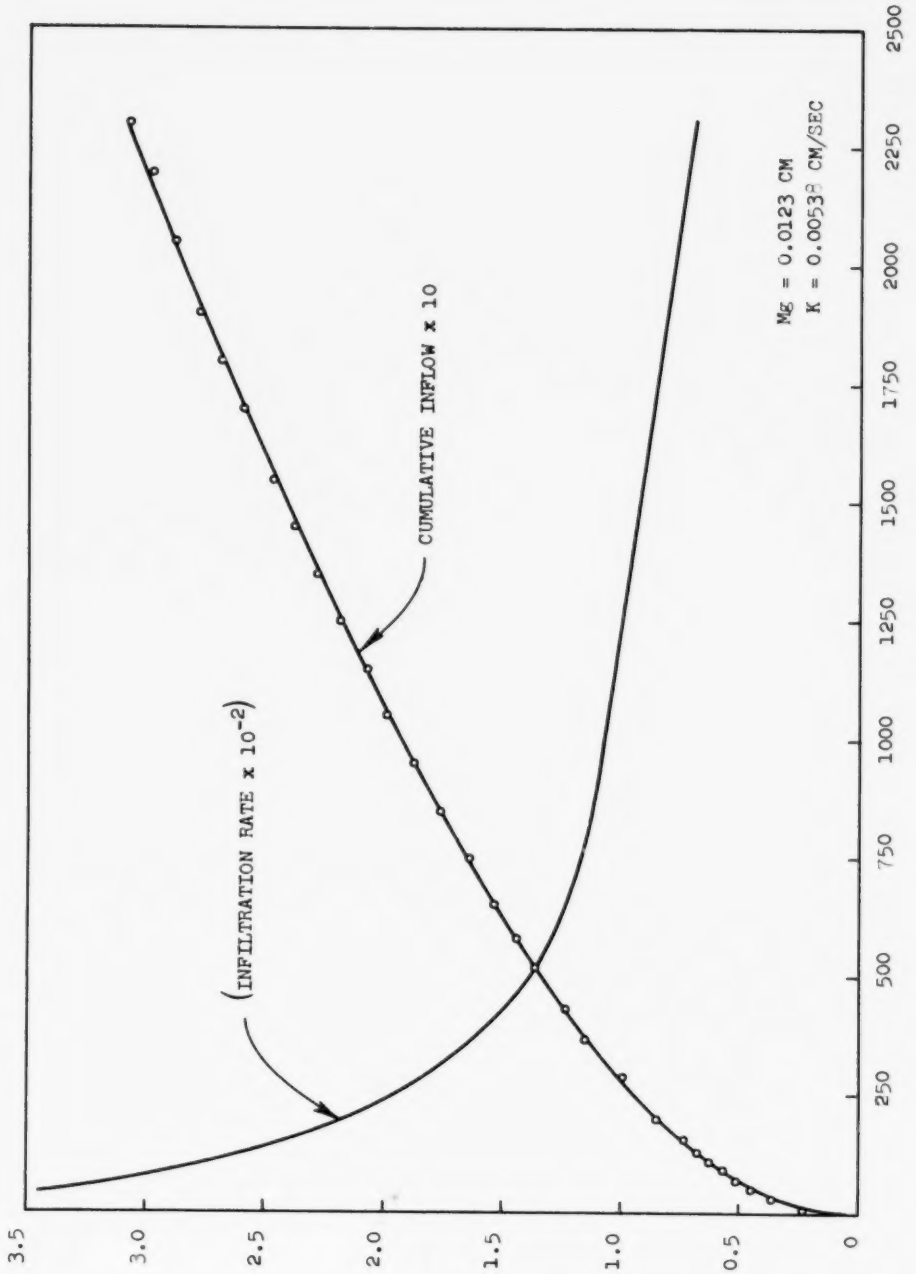

Figure 6.30. Inflow and Infiltration, Graded Beads.

Two columns containing particles of nearly the same size had similar initial infiltration rates, while the third was considerably higher, a reflection of the higher capillary forces which were acting on this fine-grained medium.

Figures 6.31, 6.32 and 6.33 show the cumulative inflow and the infiltration rates for the columns, which were constructed so that air could not escape through their bottoms. The displaced air produced erratic behavior in the infiltration rates, as shown in Figures 6.31 and 6.32 for the Roseville sands. These columns were very similar in their properties, but one column had an infiltration rate after six minutes of 0.026 cm/sec, while the other had an infiltration rate of 0.045 cm/sec. Figure 6.33 shows a case where the infiltration rate approached zero as the air pressure built up ahead of the wetting front. After 35 minutes this column had an infiltration rate close to zero, yet the same type of column which was constructed so that the air was free to escape had an infiltration rate of 0.01 cm/sec after 35 minutes, as shown in Figure 6.29.

6.5.3 Comparison of theory and experiment

In Chapter 3 it was shown that the infiltration rate could be expressed as

$$V = K \frac{h + h_c + a}{h}$$

In dimensionless form this equation becomes

$$\frac{V}{K} = \frac{h^* + h_c^* + a^*}{h^*}$$

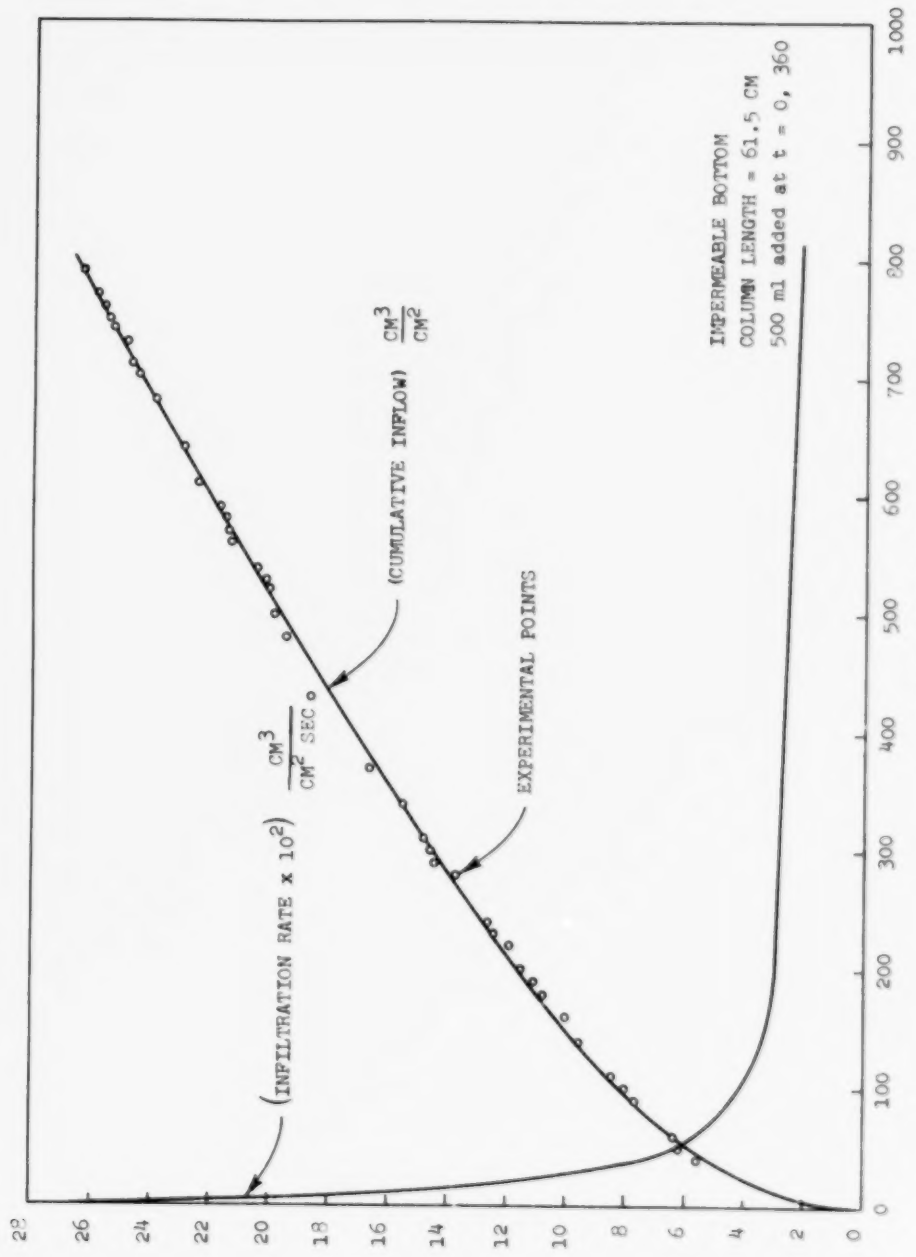

Figure 6.31. Inflow and Infiltration, Roseville Sand.

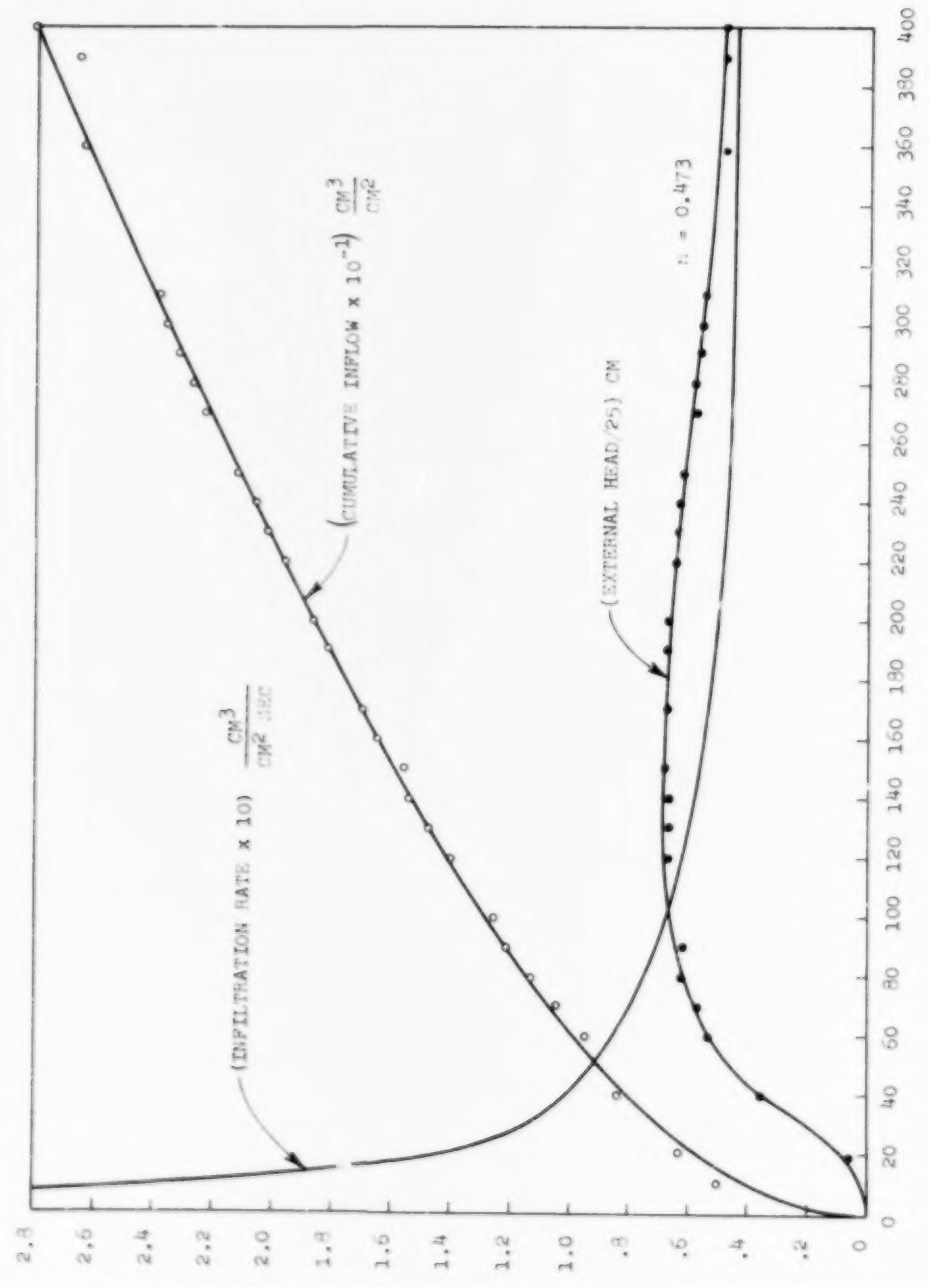

Figure 6.32. Inflow and Infiltration, Roseville Sand.

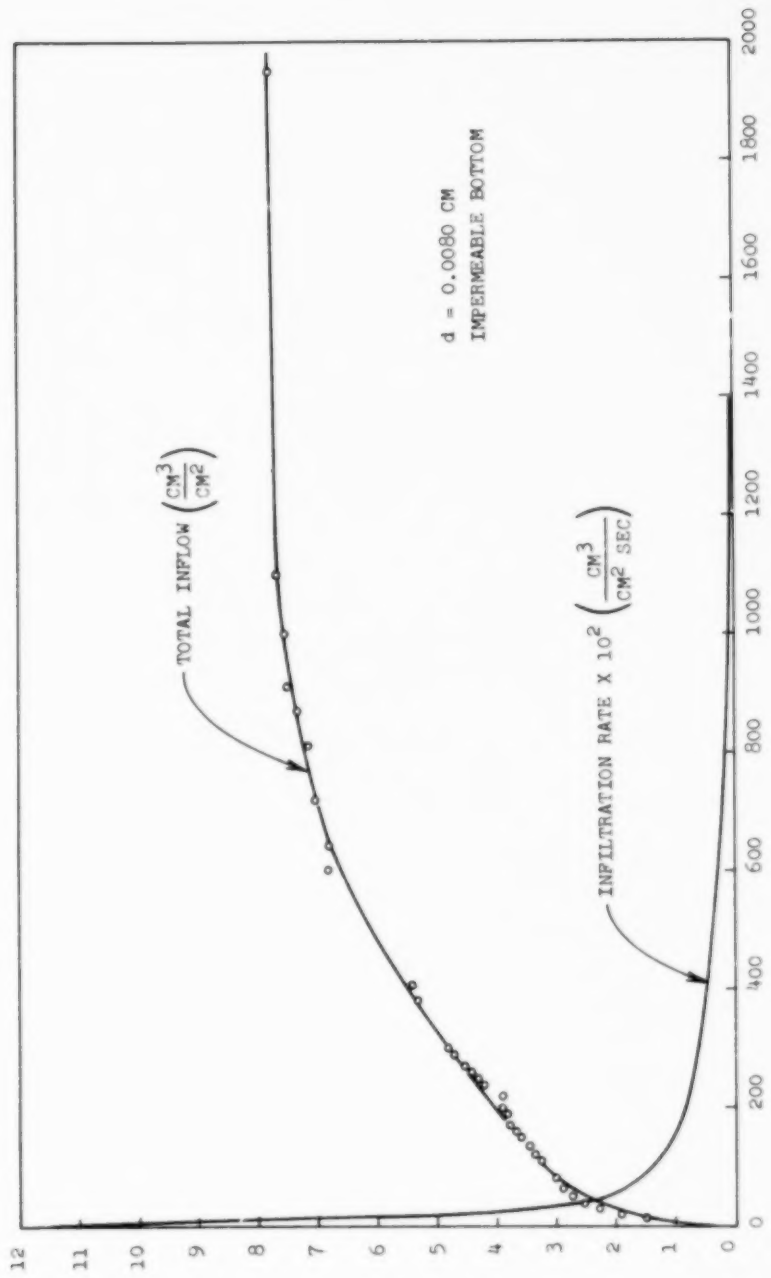

Figure 6.33. Infiltration Rate Glass Beads.

By introducing the equation of continuity $V = n \frac{dh}{dt}$, the distance to the wetting front can be obtained by integration as a function of time in the form

$$h + (h_c + a)\, \ell n\left(\frac{h_c + a}{h + h_c + a}\right) = \frac{Kt}{n}$$

or in the dimensionless form

$$h^* + (h_c^* + a^*)\, \ell n\left(\frac{h_c^* + a^*}{h^* + h_c^* + a^*}\right) = t^*$$

From these equations it is possible to obtain families of solutions, such as a graph of h^* as a function of t^* with $h_c^* + a^*$ as a parameter, and V/K as a function of t^* with $h_c^* + a^*$ as a parameter. These curves are shown in Figures 6.34 and 6.35. In order to compare the experimental data to the theory, it is necessary to measure h as a function of time and V as a function of time. In addition K, n, ℓ and a must be measured. Then the experimental values of h^*, V/K and t^* may be calculated and compared to the theoretical family of curves.

Figures 6.36 and 6.37 show a comparison between the experimental data and the theory for two mediums from which the displaced air was free to escape. Figure 6.38 shows only the experimental data for another test. Most of the scatter of experimental points was caused by using the values of V calculated from the numerical differentiation of the cumulative inflow curve for a particular test, rather than

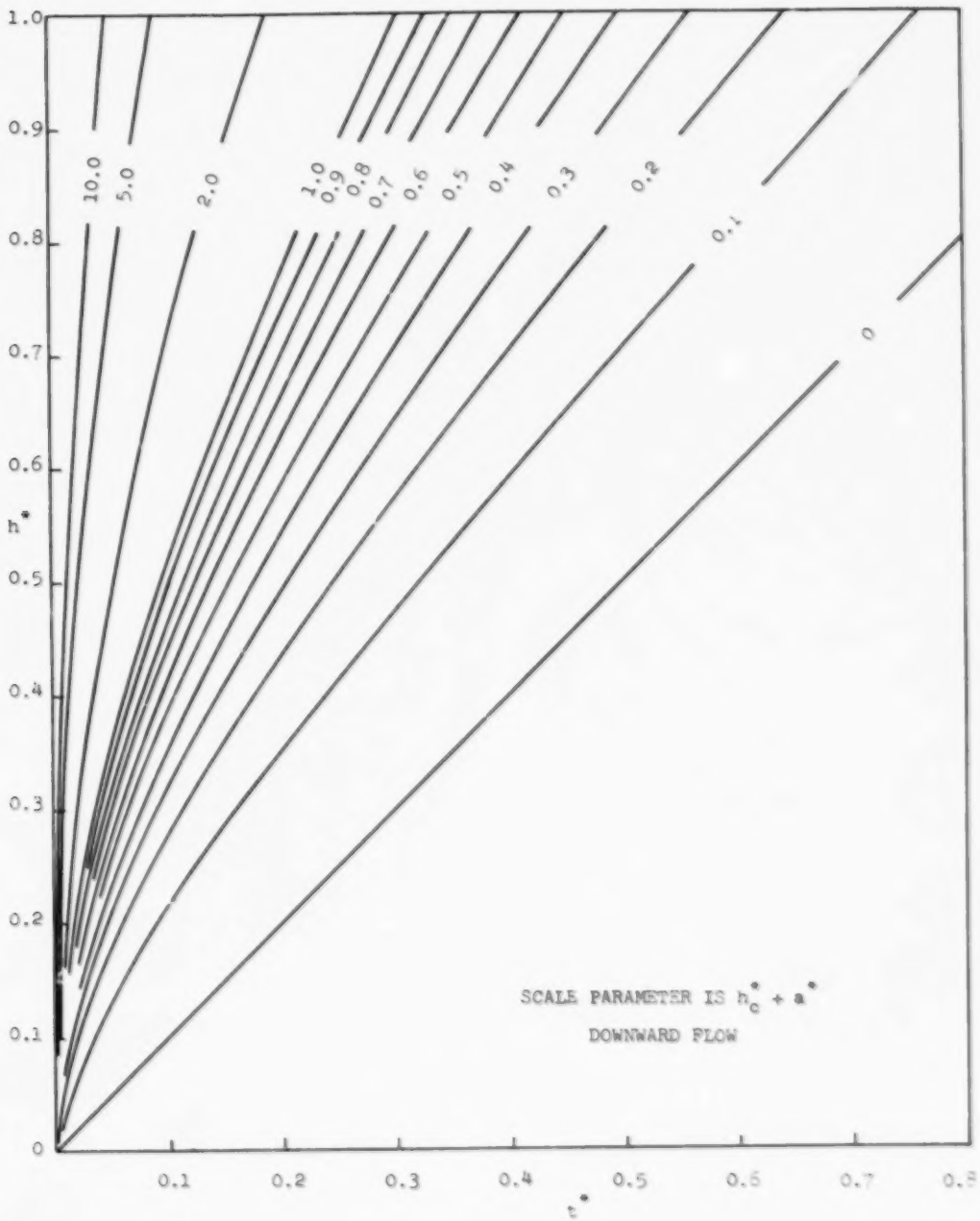

Figure 6.34. Interface Position at Various Times.

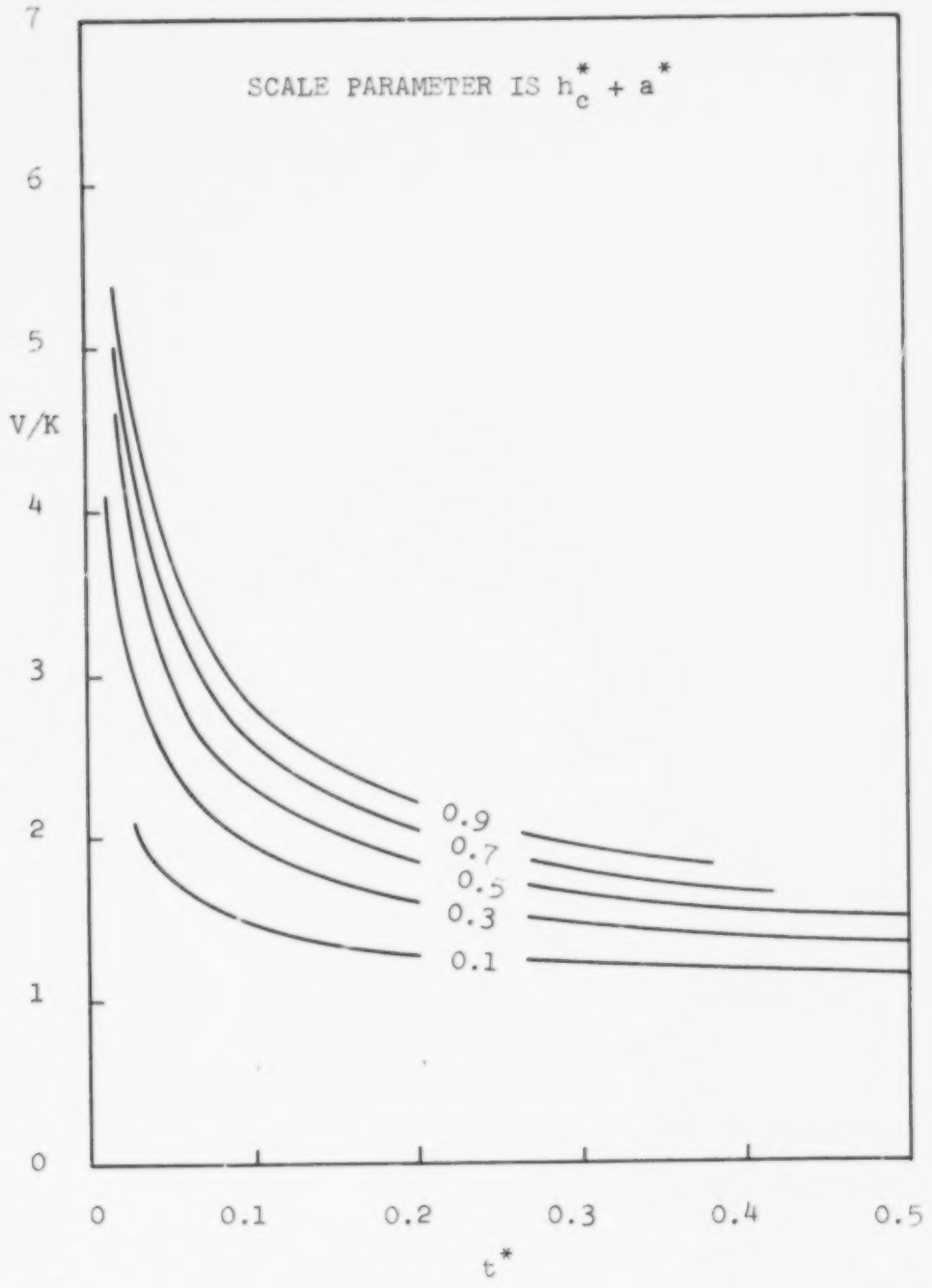

Figure 6.35. Dimensionless Infiltration Curves.

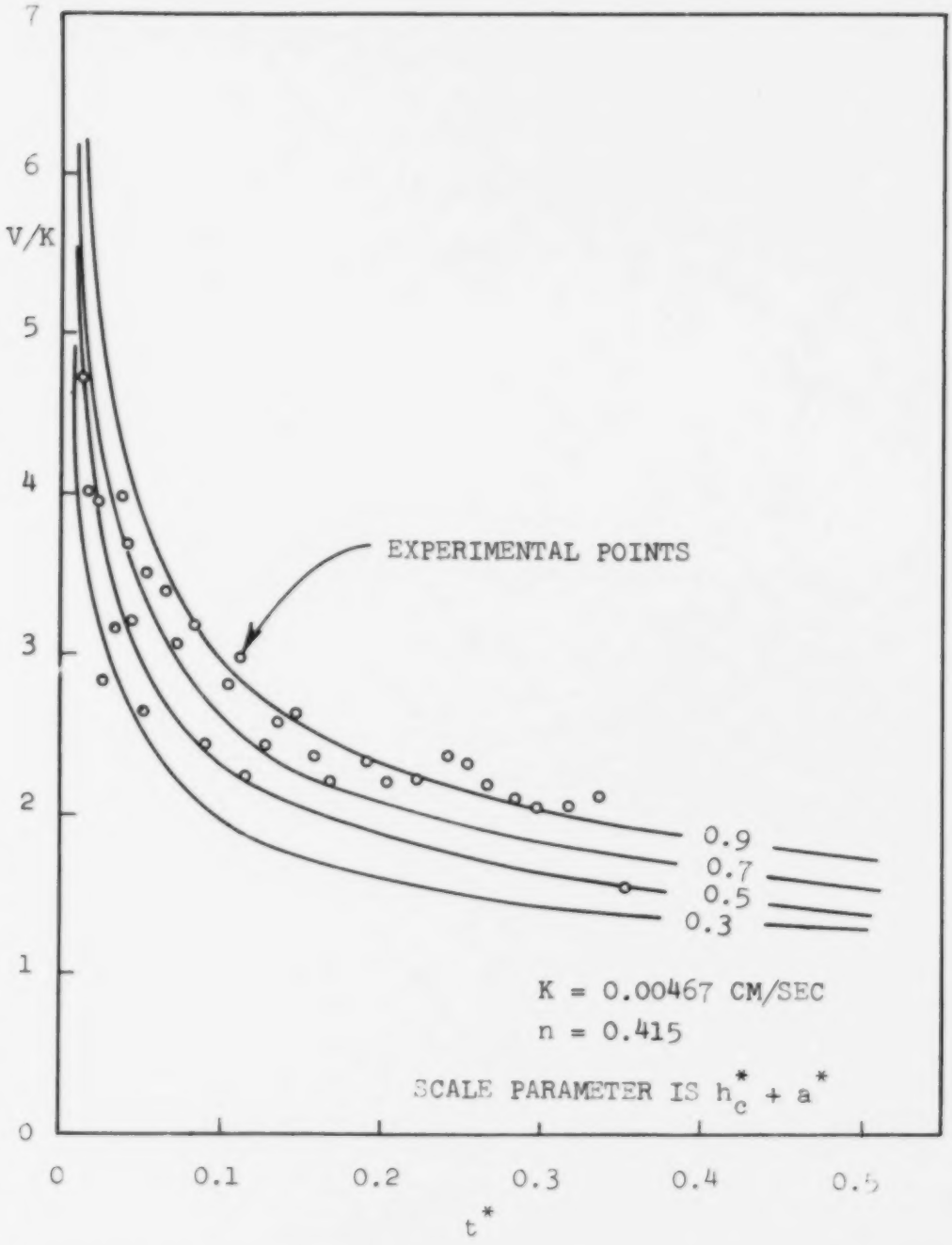

Figure 6.36. Downward Infiltration Without Air Resistance.

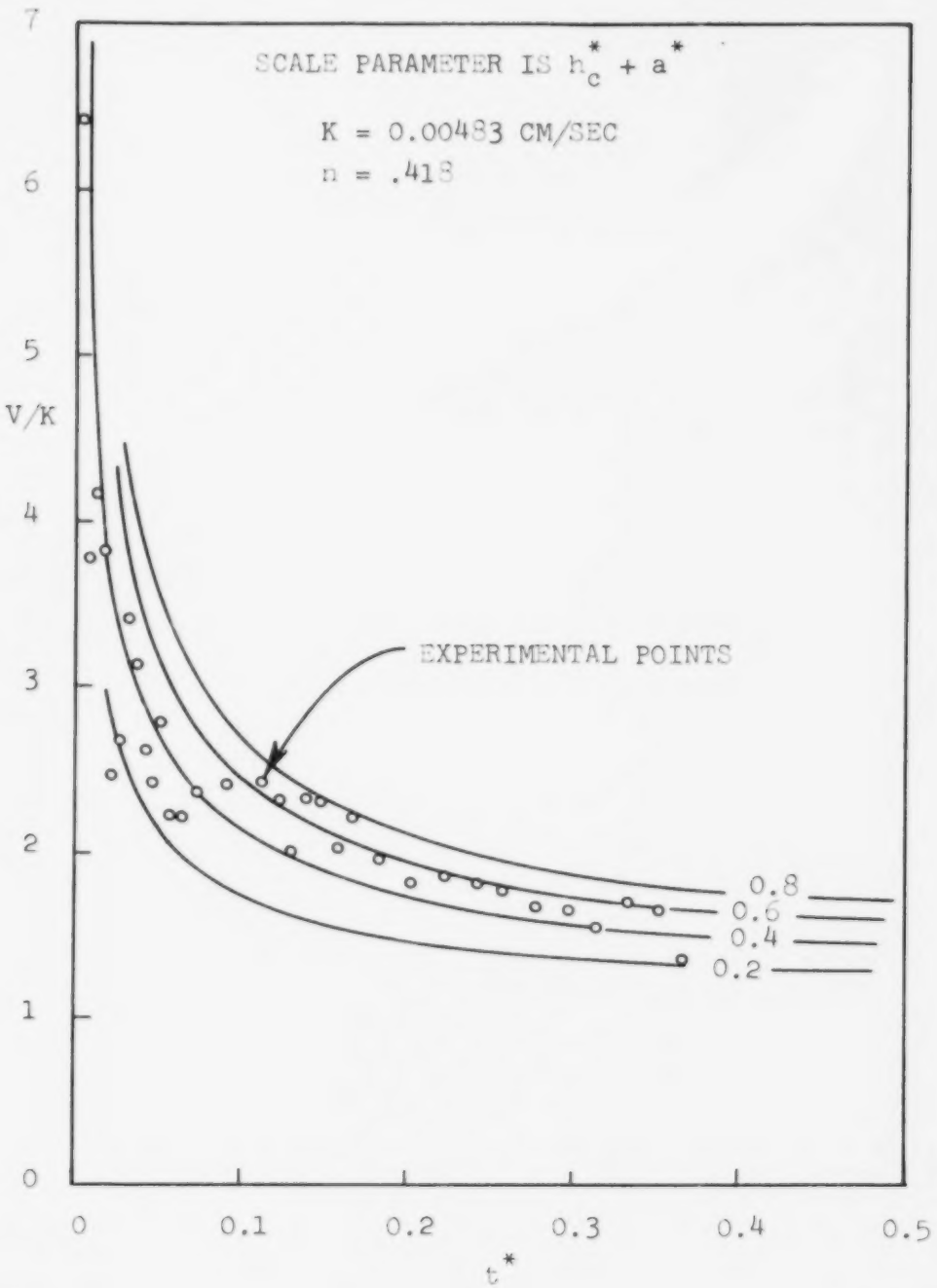

Figure 6.37. Downward Infiltration Without Air Resistance.

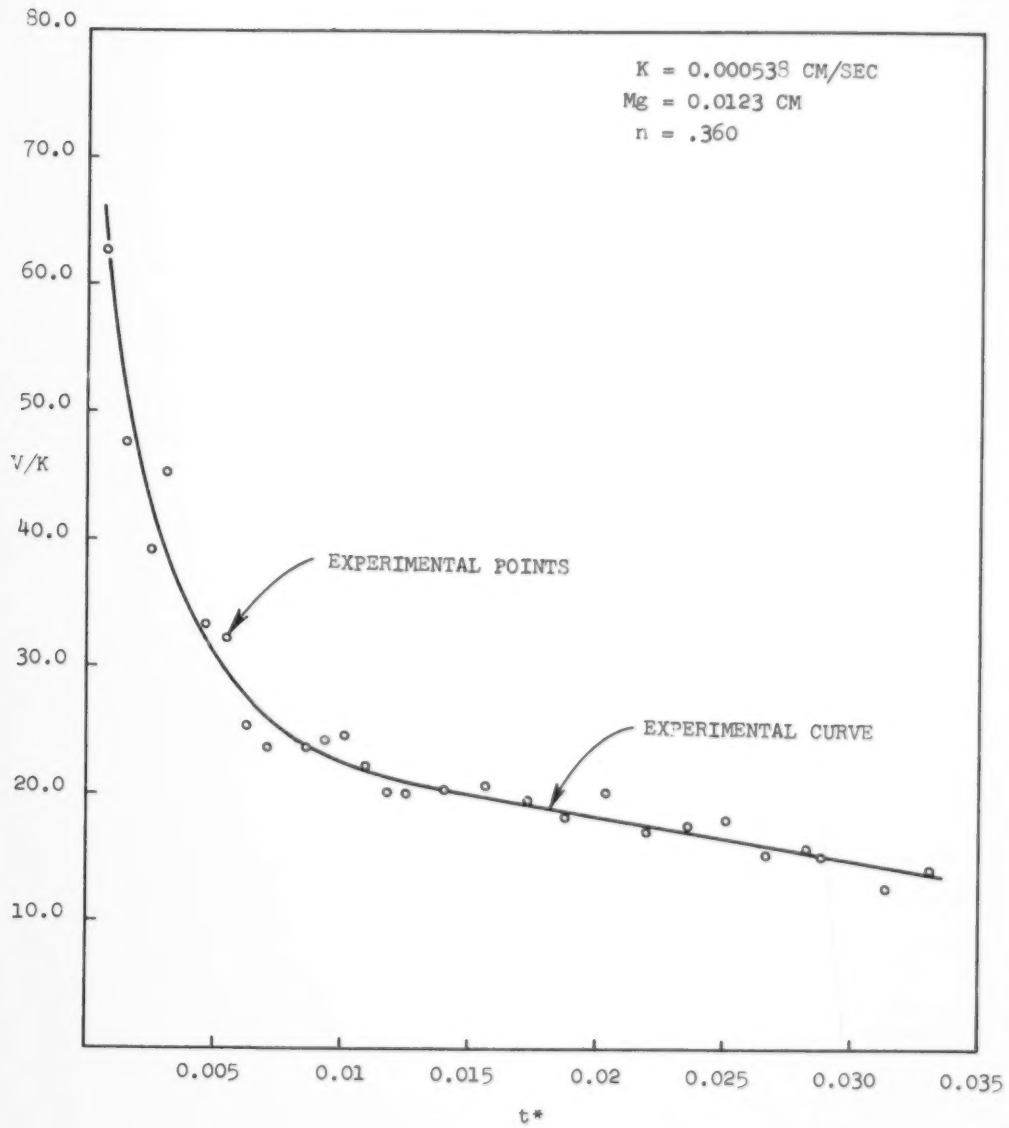

Figure 6.38. Downward Infiltration Without Air Resistance.

smoothed infiltration data. The trend of the experimental data indicates good agreement between theory and experiment.

Figures 6.39, 6.40 and 6.41 show the comparison between the experimental results for columns with impermeable bottoms and the theory based upon the free escape of air. These results show the large effect air resistance can have on the infiltration rate, especially for the mediums composed of the finest particles.

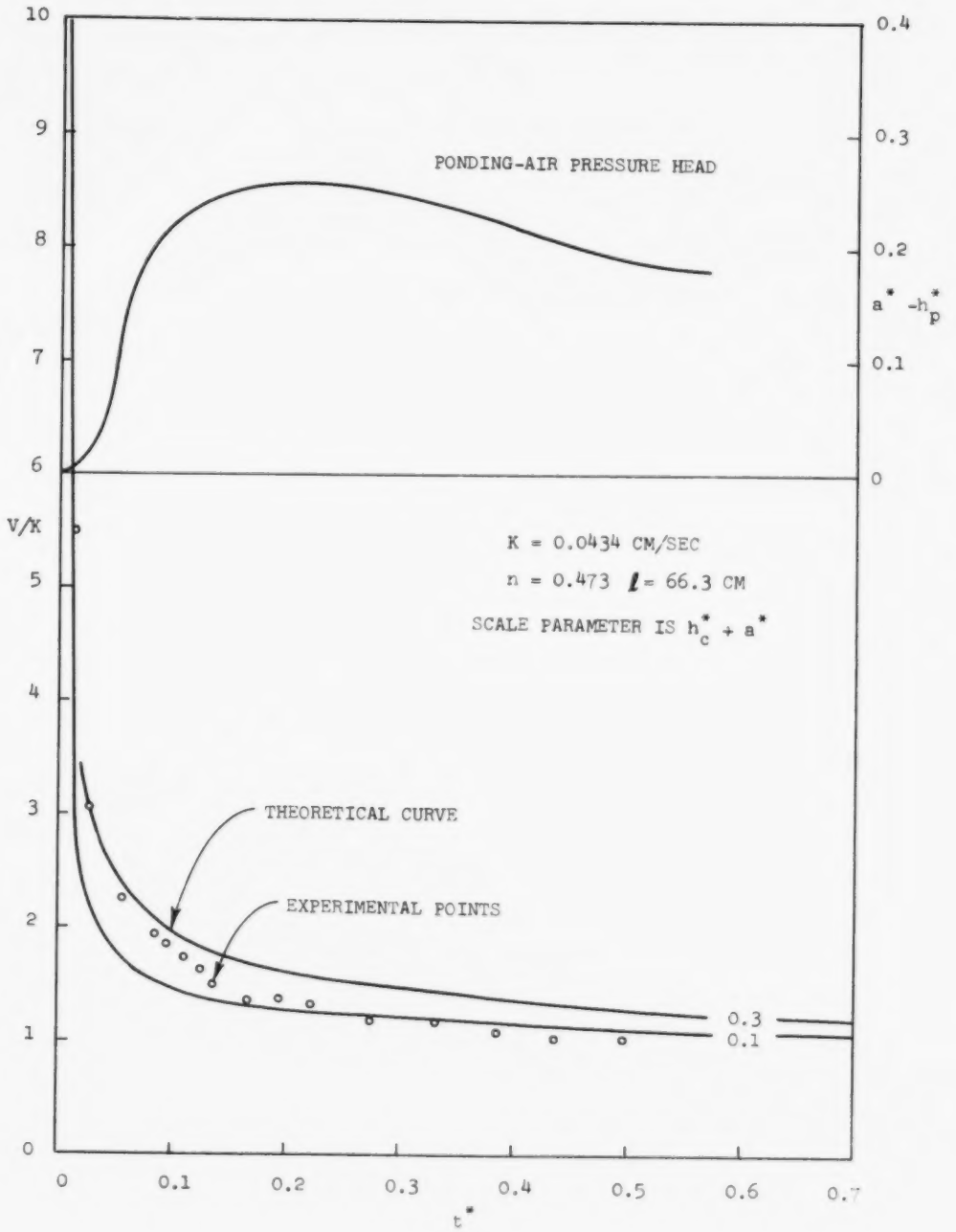

Figure 6.39. Roseville White Sand.

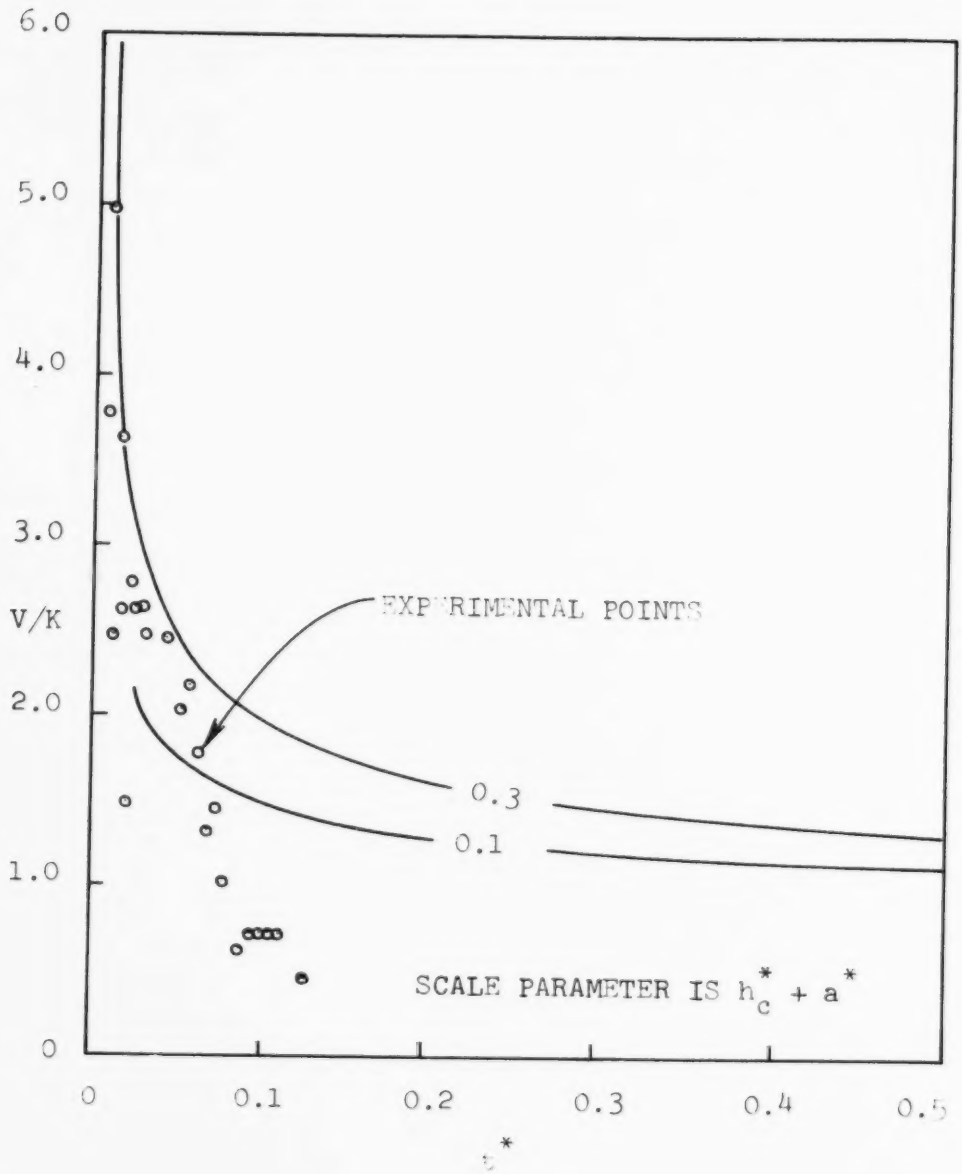

Figure 6.40. Downward Infiltration With Air Resistance.

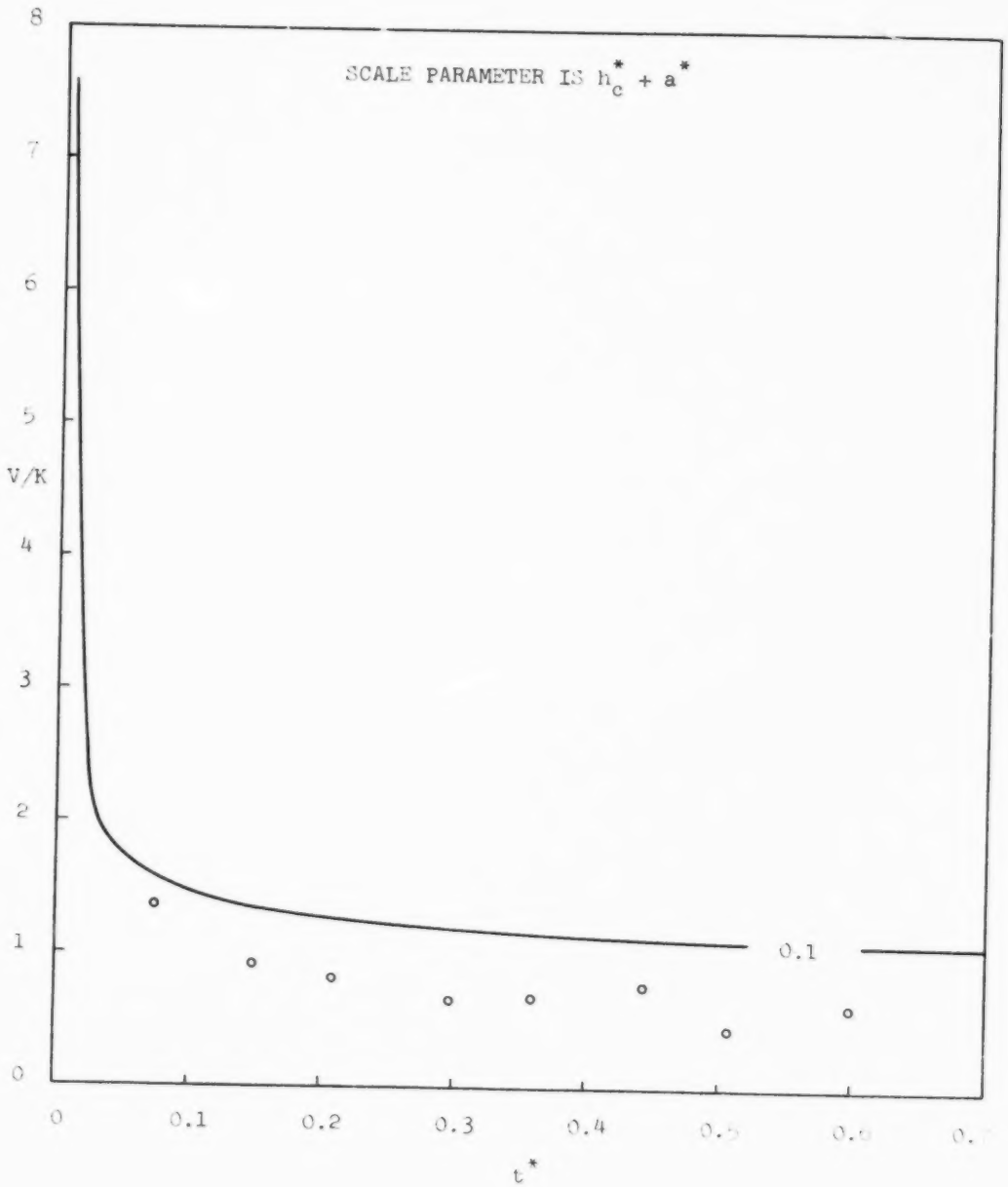

Figure 6.41. Downward Infiltration Without Air Resistance.

CHAPTER 7

SUMMARY AND CONCLUSIONS

In Chapter 2 the equations which describe the motion of water in porous mediums were derived under the assumption that the medium was not saturated. Because of the complexity of these equations it was not possible to predict the effect of air resistance on the infiltration rate. It was necessary to reformulate the equations in Chapter 3 in such a manner that the effects of air resistance could be approximated. The motion of the wetting front and the infiltration rate were predicted on the basis of the more tractable approximate model. The experimental results for the mediums having a small particle diameter show that when there is only a negligible air resistance, the agreement between theory and experiment is good. For coarser mediums and those having a wide grain size distribution, the experimental results did not agree as well with the theory.

The greatest effect of air resistance on infiltration will occur when the displaced air cannot escape through the porous medium, but is trapped ahead of the wetting front. This will produce an air pressure increase if the wetting front continues to move ahead under the action of gravity and capillary forces. This situation was examined in some detail in Chapter 5. It was possible to predict that if none of the air escaped, the wetting front would reach an equilibrium position and infiltration would cease. The experimental

work confirmed that the air pressure build-up could halt infiltration, but this would occur only if the pores of the porous medium were small enough so that the air could not escape upward through the porous medium. The infiltration rates varied widely for similar mediums when there was air resistance and seemed to be influenced largely by slight differences in the pore distribution which would allow the air to escape more readily from one medium than from another.

In Chapter 5 it was also possible to predict that an instability in the porous medium could be produced if there was a great enough pressure build-up in the displaced air. Strong capillary forces were necessary to produce the air pressure build-up. The instability would be manifested by a break in the porous medium. A number of experimental tests on a variety of porous mediums showed that breaks in the medium do occur. Again, it was necessary for the grain size distribution to be such that little air could escape from ahead of the wetting front. Whenever a break occurred across the complete cross section of a column, the infiltration virtually stopped. Some water continued to move by diffusion and as a thin film on the walls of the tube into the medium ahead of the break, but it took weeks for the medium to appear wet where only minutes were sufficient for the entire medium to become wet when the displaced air was free to escape. As the cross-sectional area of the column increased, there was a tendency for the break to be only over a portion of the cross section. This permitted infiltration to continue, but at a reduced rate. Multiple breaks in the column were also produced.

There was some evidence that breakage could occur even when the column was subjected to daily wetting and drying cycles. More investigation of this subject is warranted because of the important practical hydrological implications of this result. If long term studies were carried out over a number of wetting and drying cycles, it may be necessary to modify the design of the plastic container for the porous mediums. The structural design of the container would have to be evaluated carefully to make certain that plastic flow and creep did not occur under the prolonged loads. This would be especially critical if moisture measurements were to be made with a γ-ray attenuation instrument, as it is necessary to know the thickness of the porous medium in determining the moisture content.

Creep and plastic flow must also be considered in the design of the source shielding and collimating slits. Lead is a plastic material which gradually readjusts to fit its state of stress. There was some evidence that the maximum γ-ray counting rate was decreasing with time at a faster rate than would normally be expected for C_s^{137}. This decrease in the counting rate is attributed to a gradual change in the geometry of the collimating slits as the lead shielding gradually readjusts because of its stress conditions.

APPENDIX

A.1 Movement of Air Through Saturated Mediums

A.1.1 Solubility of air in water

In partially saturated porous mediums it has long been known that a continuous flow of air and water could take place simultaneously. Petroleum engineers have studied the flow of gas and petroleum for many years and have shown that Darcy's equation can under certain conditions be applied to each phase to describe its motion. This required that the permeability constant be considered as a function of the saturation.

If one portion of a medium contains water and another portion contains air, then there may be an intermixing of the water and the air by diffusion. This is most easily seen when a porous medium contains two miscible liquids. However, air and water are immiscible so it may be questioned how they could mix by diffusion. Even though air and water are immiscible, water will dissolve a small amount of air and air is known to contain some water vapor.

The amount of air that can be dissolved in water is directly proportional to the pressure on the water. The saturation concentration of air dissolved in water at any pressure is given by Henry's law [Fair and Geyer (1954)] as

$$C_s = k_s \frac{p}{p_o} \qquad \text{(A-1)}$$

where C_s is the saturation concentration of air in water, p/p_o is

the partial pressure of the air, i.e., the dimensionless ratio of the actual pressure to the standard pressure of reference, and k_s is a proportionality constant called the coefficient of absorption. The values of k_s are usually given in the literature at 0°C and 760 mm Hg and are usually constant for the range of partial pressures between 0 and 2. The value of k_s is a function of the water temperature with the solubility decreasing with increasing temperature. Table A.1 shows the effect of temperature on the solubility of air.

T°C	Solubility	
	$\frac{m\ell \text{ air}}{\text{liter water}}$	$\frac{\text{gm air}}{\text{liter water}}$
0	28.8	0.0373
10	22.6	0.0292
20	18.7	0.0242
30	16.1	0.0208

TABLE A.1. Solubility of Air in Water at Various Temperatures Under a Pressure of 1 Atmosphere. The volumes have been reduced to standard temperature.

A.1.2 Steady-state diffusion of air through water

An interesting phenomenon arises when infiltration into an initially dry closed volume of soil is considered. The air pressure in the soil is increased as the wetting front moves downward in the porous medium so that the saturation concentration of the air in the

water near the wetting front steadily increases. However, if the top of the column is maintained at atmospheric pressure and is open to the atmosphere, the saturation concentration at the top of the column will be lower than at the bottom of the column. In this way a concentration gradient of dissolved air in water is established, so diffusion from the region of higher concentration to the region of lower concentration will take place. As expected, the air will be diffusing from the bottom of the column to the top of the column.

To determine the relative significance on infiltration of the diffusion of air through the water, a simple example will be considered. Consider a closed tube of length ℓ filled with a medium which has a capillary rise h_c. If none of the air is assumed to escape by diffusion or by any other process, and if it is assumed that there is a sharp wetting front, it can be shown (Chapter 5) that the maximum depth of infiltration will be

$$h_o = \tfrac{1}{2}\{\ell - \frac{p_o}{\gamma} - h_c) + [(\ell - \frac{p_o}{\gamma} - h_c)^2 + 4h_c\ell]^{\frac{1}{2}}\} \qquad (A\text{-}2)$$

where p_o is the absolute atmospheric pressure. Under these conditions the pressure in the entrapped air is

$$p = p_o + \gamma h_o + \gamma h_c \qquad (A\text{-}3)$$

where p is the absolute pressure of the entrapped air. It is instructive to look at a diagram illustrating the variables involved, as is shown in Figure A.1.

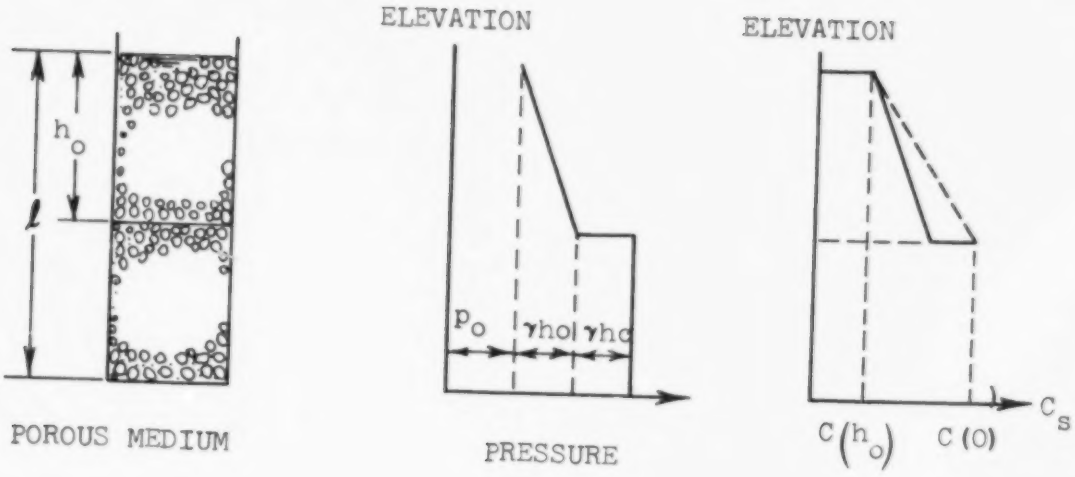

Figure A.1. Water, Pressure and Air Concentration Distributions in a Porous Medium.

A dilemma exists regarding the concentration of air in the water at the interface. On one side of the interface the pressure is $p_o + \gamma h_o + \gamma h_c$, which leads to a saturation concentration of air of $k_s \frac{p_o + \gamma h_o + \gamma h_c}{p_o}$. On the other side of the interface the pressure is $p_o + \gamma h_o$ which leads to a saturation concentration of air of $k_s \frac{p_o + \gamma h_o}{p_o}$. These two saturation concentrations of air are separated by the thickness of the interface which indicates a very large concentration gradient across the interface. Diffusion would reduce this concentration gradient, but this would supersaturate the water immediately above the interface. In turn, air may come out of solution in the supersaturated region. This implies bubbles of air would be found in the water above the

air-water interface. This interesting phenomenon will not be pursued at greater length now; instead, it will be assumed that the saturation concentration of air varies linearly from a maximum of $k_s \frac{p_o + \gamma h_o + \gamma h_c}{p_o}$ at the interface to a minimum of $k_s \frac{p_o}{p_o}$ at the surface of the porous medium.

Under these simplified conditions with the y-axis positive upward and the origin at the interface, the concentration gradient will be

$$\frac{dc}{dy} = \frac{C(h_o) - C(0)}{h_o} = k_s \frac{p_o}{p_o h_o} - k_s \frac{p_o + \gamma h_o + \gamma h_c}{p_o h_o}$$

$$\frac{dc}{dy} = - \frac{k_s \gamma}{p_o} \left(1 + \frac{h_c}{h_o}\right) \qquad \text{(A-4)}$$

Thus if $h_o >> h_c$, the effect of the capillary head is negligible; contrariwise, if $h_c >> h_o$, an extremely large concentration gradient may be established. By Fick's law of diffusion, the rate of movement of dissolved air through the water will be

$$\frac{dm}{dt} = - n k_d \frac{dc}{dy} \qquad \text{(A-5)}$$

where $\frac{dm}{dt}$ is the mass transfer rate in grams/sec-cm^2, k_d is the coefficient of diffusion in cm^2/sec, n is the porosity and expresses the fact that only part of the volume is filled with water and the rest is solid. The diffusion constant for air in water, k_d, is about $1.86 \cdot 10^{-5}$ cm^2/sec. In a porous medium the diffusion constant may be somewhat less than this due to the increased length of passages in the medium compared to the length of the diffusion path in a container of water.

If $\ell = 400$ cm, $n = 0.40$, $h_c = 75$ cm, and $p_o/\gamma = 1033$ cm, then it can be shown that $h_o = 1.1$ cm. At 20° C the concentration gradient would be given by Eq. (A-4) as

$$\frac{dc}{dy} = - \frac{2.42 \cdot 10^{-5} \cdot 980}{1033 \cdot 980} \left(1 + \frac{75}{1.1}\right)$$

$$\frac{dc}{dy} = - 1.62 \cdot 10^{-6} \frac{\text{gm}}{\text{cm}^3 - \text{cm}}$$

The rate of movement of the air through the water is given by Eq. (A-5) as

$$\frac{dm}{dt} = 0.40 \cdot 1.86 \cdot 10^{-5} \cdot 1.62 \cdot 10^{-6} = 1.20 \cdot 10^{-11} \frac{\text{gm}}{\text{cm}^2 - \text{sec}}$$

Converting this to a daily basis gives

$$\frac{dm}{dt} = 1.04 \cdot 10^{-6} \frac{\text{gm}}{\text{cm}^2 - \text{day}}$$

and on a volume basis the loss would be

$$1.04 \cdot 10^{-6} \frac{\text{gm}}{\text{cm}^2 - \text{day}} \cdot \frac{1 \text{ liter}}{1.293 \text{ gm}} \cdot \frac{293}{273} = 8.63 \cdot 10^{-7} \frac{\text{liter}}{\text{cm}^2 - \text{day}}$$

or $8.63 \cdot 10^{-4}$ cm/day. Because of the compressibility of the air, the water would advance less than $8.63 \cdot 10^{-4}$ cm/day.

Over a long period of time the diffusion of air out through the infiltrating water can play only a minor role in the infiltration process. The estimate of the air loss of $8.63 \cdot 10^{-4}$ cm^3/cm^2 - day for the example under consideration may be high due to the assumptions

made in deriving the formulas for the concentration gradient. For example, the actual value of h_o is always greater than indicated by Eq. (A-2) because some bubbles of air escape to the surface in the early stages of infiltration. Also, it was assumed that the transfer rate of air across the interface was sufficiently rapid to keep the water saturated with air, though that may not be the case. Adeney and Becker (1919, 1920) observed that air diffuses through a plane water surface at a maximum rate of about 9 cm^3/cm^2 - day.

The air loss rate which was calculated from the steady state diffusion process in the above example indicates that air can be transferred across the air-water interface at a sufficiently rapid rate to maintain the water in a saturated condition. As a result, the process of air transfer through the water by diffusion may allow infiltration to continue into the closed volume of soil over an extended period of time until the porous medium is completely saturated. For the particular case considered, the infiltration rate due to this effect would be less than $8.63 \cdot 10^{-4}$ cm/day.

A.2 Other Factors Influencing Capillary Phenomena

In previous discussions the height of capillary rise has been viewed as a static condition in which the liquid was at rest. This implies that no water is lost through the air-water interface. However, if evaporation takes place, water must be transported upward to partially or completely replace that which has been lost. This movement results in some head loss which would cause the equilibrium

position to be lower than if the water were completely static. This would be a minor factor except for mediums with very low permeability and a high capillary rise.

It has been shown [Shereshefsky (1956)] that the vapor pressure of a liquid above an interface is dependent on the curvature of the interface, the temperature and certain properties of the liquid. The relation is

$$\ell n \frac{p}{p_o} = \pm \frac{2 \sigma M}{\rho R T r} \qquad \text{(A-6)}$$

where the meaning of the terms is

p_o = vapor pressure measured over a plane liquid surface,

p = vapor pressure measured over a curved liquid surface,

r = the radius of curvature of the liquid surface,

σ = surface tension of the liquid,

M = molecular weight of the liquid,

R = gas constant,

T = absolute temperature,

ρ = liquid density.

The vapor pressure may be increased or decreased by the presence of the curved interface, depending on the type of curvature of the interface. The radius of curvature of a curve at a point (x,y) is

$$r = \frac{ds}{d\varphi}$$

where s is the arc length of the curve measured in the positive

direction and φ is the counterclockwise angle from the positive x-axis to the tangent to the curve at (x,y). In calculus it is shown that

$$r = \frac{[1 + (y')^2]^{3/2}}{y''} \tag{A-7}$$

Equation (A-6) may be expressed in terms of the capillary rise h_c by multiplying the right-hand side by γ/γ and recognizing that for a capillary tube $h_c = \frac{2\sigma}{\gamma r}$. Equation (A-6) then becomes

$$\ell n \frac{p}{p_o} = \pm \frac{h_c \gamma M}{\rho RT} = \pm \frac{h_c g M}{RT} \tag{A-8}$$

To determine the significance of this effect, the capillary rise which will increase the vapor pressure by 1% will be computed. Thus, $\ell n \frac{p_1}{p_o} = ch_{c_1}$, where $c = \frac{gM}{RT}$ and $\ell n \frac{1.01\ p_1}{p_o} = ch_{c_2}$, or $\ell n\ 1.01 = c(h_{c_2} - h_{c_1})$, so that $h_{c_2} = \frac{1}{c} \ell n\ 1.01 + h_{c_1}$. Substitution of the numerical values for water at 20°C into this equation yields

$$\Delta h_c = 5100 \text{ cm}$$

From this result it is obvious that the curvature of the air-water interface will result in only a negligible increase in the vapor pressure of the water, as Δh_c is outside the range of capillary rise found even in fine mediums. From this it can be concluded that water is no more readily available to be lost from a fine medium than a coarse one by vapor transfer. If the vapor pressure would have

increased significantly in the mediums with fine pores, this would have produced significant concentration gradients of water vapor, which would have resulted in vapor transport by diffusion to a region of lower vapor pressure.

This means that vapor transfer will not be accelerated in fine mediums as compared to coarser ones. The most important mechanism promoting vapor transfer is the existence of temperature gradients in porous mediums, for the vapor pressure about doubles for each temperature increase of 12°C. For a saturated atmosphere, such as would be encountered above a water surface, the perfect gas equation of state for water vapor may be written

$$\rho = \frac{p_v}{RT}$$

where p_v is the vapor pressure of the water and ρ is the vapor density. Also the vapor pressure may be approximated by the relation

$$p_v = 1.681 \cdot 10^9 \exp(-\frac{5300}{T}) \qquad \text{(A-9)}$$

where p_v is in dynes/cm^2 and T is in °Kelvin or °Centigrade absolute [Daniels and Alberty (1955)]. This equation was derived from the vapor pressure vs. temperature plot shown in Figure A.2. Since the density of water vapor may be thought of as a concentration, the vapor will tend to move by diffusion from a location of higher density to one of lower density. The condition for vapor transfer in the direction s is then the existence of a negative density gradient $-\frac{\partial \rho}{\partial s}$.

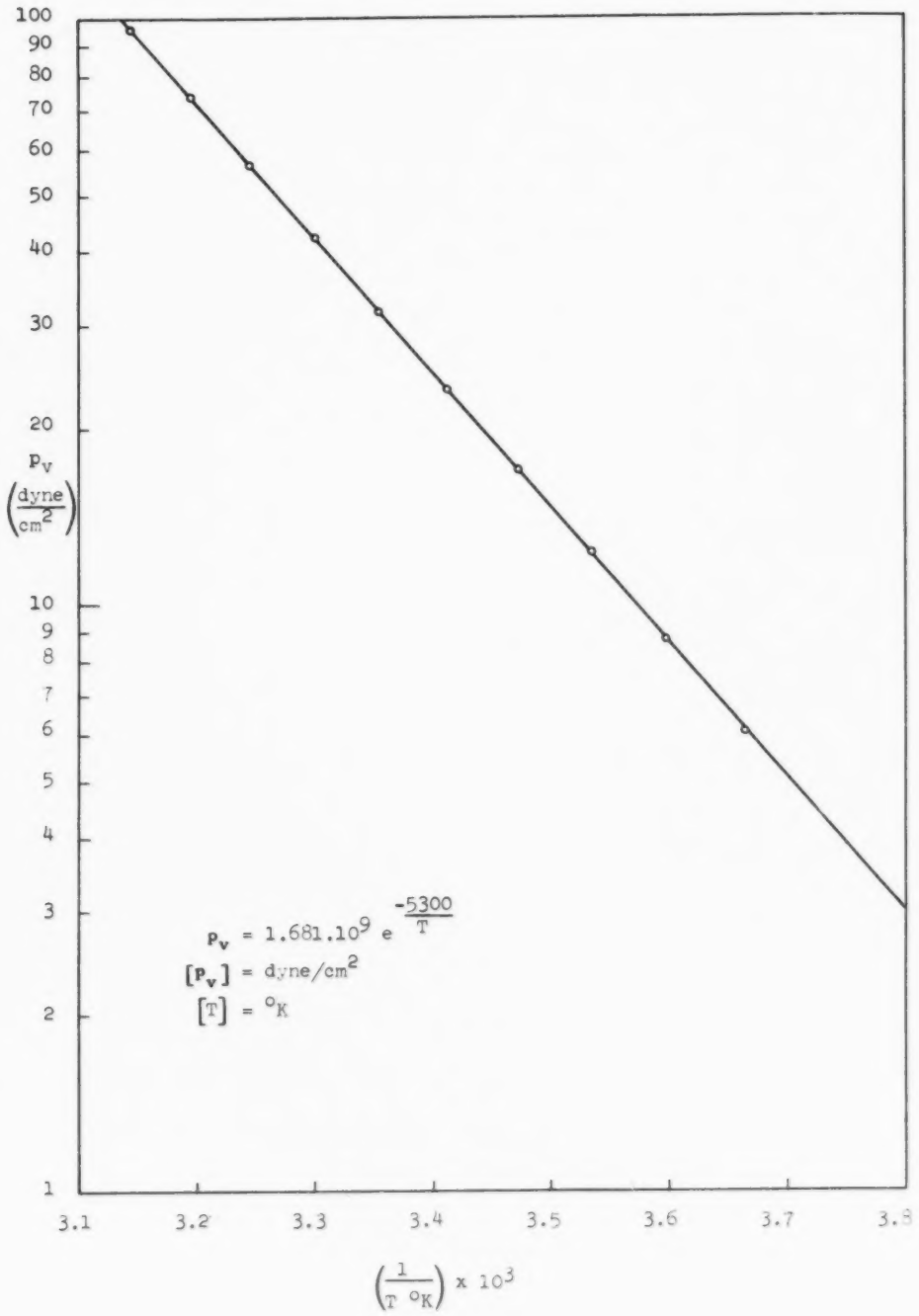

Figure A.2. Vapor Pressure as a Function of Temperature.

The permeation rate of the water vapor will be $P = - D \frac{\partial \rho}{\partial s}$, where P is in grams/cm^2 - sec and D is the coefficient of diffusion in cm^2/sec. For a vapor saturated atmosphere in the medium, the concentration of water vapor expressed by the perfect gas equation $\rho = \frac{p_v}{RT}$ now depends only on temperature because p_v is a function of temperature and R is constant. In general, the temperature will be a function of distance. The functional relationship is of the form $\rho = \rho[T(s)]$ so that $\frac{d\rho}{ds} = \frac{d\rho}{dT} \frac{dT}{ds}$. From the perfect gas equation combined with Eq. (A-9), the concentration gradient is

$$\frac{d\rho}{ds} = \frac{1.681 \cdot 10^9}{R} \left\{ \frac{5300}{T^3} \exp\left(- \frac{5300}{T}\right) - \frac{1}{T^2} \exp\left(- \frac{5300}{T}\right) \right\} \left(\frac{dT}{ds}\right)$$

which becomes

$$\frac{d\rho}{ds} = \frac{1.681 \cdot 10^9}{RT^2} \left[\exp\left(- \frac{5300}{T}\right)\right] \left(\frac{5300}{T} - 1\right) \left(\frac{dT}{ds}\right) \qquad \text{(A-10)}$$

If the positive direction of s is away from the air-water interface, vapor transfer in the direction of s will take place if ρ decreases with increasing s. The right-hand side of Eq. (A-10) will have the same sign as the temperature gradient since $\frac{5300}{T} >> 1$. Thus, vapor transfer will take place from a warmer to a cooler region. Equation (A-10) is also of significance since it shows a temperature gradient is necessary for vapor transfer to take place. If the temperature is constant, $\frac{\partial \rho}{\partial s} = 0$, and no concentration gradient is established through which diffusion of water vapor can take place.

For the case of a saturated atmosphere in a porous medium, water is readily available to be evaporated as the temperature increases.

Hence the atmosphere in the medium remains saturated. However, there are situations where water is not available for evaporation as the temperature increases. In this case the atmosphere of the porous medium does not remain saturated as the temperature increases. The effect is to remove the functional relationship between temperature and vapor pressure expressed in Eq. (A-9). However, the perfect gas equation is still valid and an investigation of it will provide some insight into vapor transfer through dry mediums. In this context "dry mediums" is used to describe those mediums which do not have water available throughout to keep the air saturated. Thus, a column with an air-water interface present some depth below the surface would not be a dry medium if the temperature gradient was negative and vapor was moving in the direction from the interface to the surface, for the atmosphere would remain saturated. If the water vapor was moving in the direction of temperature increase, the column would be considered a dry medium since the atmosphere would not remain saturated in the direction of motion.

The observation that water vapor will move by diffusion from a region of higher concentration to one of lower concentration is valid for a saturated or an unsaturated atmosphere. The perfect gas equation may be written $\rho = \rho(p_v, T)$ and differentiated by the chain rule to obtain the concentration gradient. The chain rule gives

$$\frac{\partial \rho}{\partial s} = \frac{\partial \rho}{\partial p_v} \frac{\partial p_v}{\partial s} + \frac{\partial \rho}{\partial T} \frac{\partial T}{\partial s} \qquad \text{(A-11)}$$

which becomes

$$\frac{\partial \rho}{\partial s} = \frac{1}{RT}\left(\frac{\partial p_v}{\partial s}\right) - \frac{p_v}{RT^2}\left(\frac{\partial T}{\partial s}\right) \qquad \text{(A-12)}$$

when the appropriate differentiations are carried out on the perfect gas equation. To determine the direction of vapor movement, several combinations of cases will be discussed in terms of Eq. (A-12). If $\frac{\partial p_v}{\partial s} > 0$ and $\frac{\partial T}{\partial s} < 0$, then $\frac{\partial \rho}{\partial s} > 0$, which means the flow of vapor would be in the negative s direction. If $\frac{\partial p_v}{\partial s} > 0$ and $\frac{\partial T}{\partial s} > 0$, then an indeterminant form is obtained in which the gradients of p_v and T have to be known to determine the direction of vapor transfer. If $\frac{\partial p_v}{\partial s} < 0$ and $\frac{\partial T}{\partial s} > 0$, the vapor transfer will be in the direction of positive s. If $\frac{\partial p_v}{\partial s} < 0$ and $\frac{\partial T}{\partial s} < 0$, then an indeterminant form for $\frac{\partial \rho}{\partial s}$ is obtained, and it is necessary to know the gradients of p_v and T to determine the direction of vapor transfer. These results are summarized conveniently in Table A.2.

	$\frac{\partial p_v}{\partial s} > 0$	$\frac{\partial p_v}{\partial s} = 0$	$\frac{\partial p_v}{\partial s} < 0$
$\frac{\partial T}{\partial s} > 0$	Indeterminant	+ s	+ s
$\frac{\partial T}{\partial s} = 0$	- s	No Transfer	+ s
$\frac{\partial T}{\partial s} < 0$	- s	- s	Indeterminant

TABLE A.2. Direction of Vapor Transfer for Various Vapor Pressure and Temperature Gradients.

When there is an air-water interface in a column of porous medium, which is maintained at constant temperature, the vapor pressure immediately above the the interface may be expected to be given by Eq. (A-9) and the concentration of water vapor will be called ρ_s . This assumes the water at the interface evaporates rapidly enough to maintain the air in a saturated condition at the interface. This is a reasonable assumption because of the quiescence of the air and the fact that vapor can only be transferred by diffusion. If the column is open to the atmosphere, the open end will be in equilibrium with the atmosphere and will have a concentration of water vapor, ρ_o , lower than ρ_s , unless the atmosphere is saturated with water vapor. That is, $\rho_o < \rho_s$ unless the relative humidity is 100%, in which case $\rho_o = \rho_s$. If the distance between the interface and the end of the column is b , then the diffusion equation and boundary conditions become

$$\frac{\partial \rho}{\partial t} = D \frac{\partial^2 \rho}{\partial s^2} \qquad t \geq 0, \quad 0 \leq s \leq b \qquad \text{(A-13a)}$$

$$\rho(0,t) = \rho_s \ , \qquad t > 0 \qquad \text{(A-13b)}$$

$$\rho(b,t) = \rho_o \ , \qquad t > 0 \qquad \text{(A-13c)}$$

$$\rho(s,0) = f(s) \ , \qquad 0 \leq s \leq b \qquad \text{(A-13d)}$$

This problem can be simplified if the transformation

$$V(s,t) = \rho(s,t) - \rho_o \frac{s}{b} - \rho_s\left(\frac{b-s}{b}\right) \qquad \text{(A-14)}$$

is applied to Eqs. (A-13a-d) to make the boundary conditions homogeneous. The transformed equations may be found by observing that

$$\frac{\partial \rho}{\partial t} = \frac{\partial V}{\partial t}$$

$$\frac{\partial \rho}{\partial s} = \frac{\partial V}{\partial s} + \frac{\rho_o}{b} - \frac{\rho_s}{b}$$

$$\frac{\partial^2 \rho}{\partial s^2} = \frac{\partial^2 V}{\partial s^2}$$

so the partial differential equation of diffusion becomes

$$\frac{\partial V}{\partial t} = D \frac{\partial^2 V}{\partial s^2} \qquad \text{(A-15a)}$$

The boundary conditions become homogeneous

$$V(0,t) = 0 \qquad \text{(A-15b)}$$

$$V(b,t) = 0 \qquad \text{(A-15c)}$$

and the inhomogeneous initial condition becomes

$$V(s,0) = f(s) - \rho_o \frac{s}{b} - \rho_s\left(\frac{b-s}{s}\right) \qquad \text{(A-15d)}$$

Assume $V(s,t)$ has a solution in the form of a product of two functions

$$V(s,t) = S(s)T(t) \qquad \text{(A-16)}$$

where $S(s)$ is a function of s only and $T(t)$ is a function of t only. Substituting this into the diffusion equation yields

$$S(s) \frac{dT(t)}{dt} = D \frac{d^2 S(s)}{ds^2} T(t)$$

which can be simplified to

$$\frac{1}{DT(t)} \frac{dT(t)}{dt} = \frac{1}{S(s)} \frac{d^2S(s)}{ds^2}$$

The left side of the equation is a function of t only, while the right side is a function of s only. This requires that each side be equal to a constant which will be called $-\lambda^2$. Then

$$\frac{dT(t)}{T(t)} = - D \lambda^2 \, dt$$

which leads to

$$T(t) = A \, e^{-\lambda^2 Dt} \tag{A-17}$$

and

$$\frac{d^2S(s)}{ds^2} + \lambda^2 S(s) = 0$$

which leads to

$$S(s) = B \cos(\lambda s) + C \sin(\lambda s)$$

so that Eq. (A-16) becomes

$$V(s,t) = A' \cos(\lambda s) e^{-\lambda^2 Dt} + B' \sin(\lambda s) e^{-\lambda^2 Dt} \tag{A-18}$$

The first boundary condition, Eq. (A-15b), leads to

$$V(0,t) = 0 = A' \, e^{-\lambda^2 Dt}$$

which requires that $A' = 0$. The second boundary condition, Eq. (A-15c), leads to

$$V(b,t) = 0 = B' \sin(\lambda b) e^{-\lambda^2 Dt}$$

This could be satisfied by taking $B' = 0$, but this would produce the trivial result $V(s,t) = 0$, so the other possibility that $\sin(\lambda b) = 0$ is considered. This requires that $\lambda b = n\pi$ where $n = 0,1,2,\cdots$. Equation (A-18) then takes the form of a particular solution

$$V_n(s,t) = B_n' \sin(\frac{n\pi s}{b}) \exp(-\frac{n^2\pi^2 Dt}{b^2})$$

Since Eq. (A-15b) is a linear equation, any linear combination of the particular solutions is also a solution such as

$$V(s,t) = \sum_{n=1}^{\infty} B_n' \sin(\frac{n\pi s}{b}) \exp(-\frac{n^2\pi^2 Dt}{b^2}) \qquad \text{(A-19)}$$

This satisfies the differential equation and the boundary conditions, however the initial condition, Eq. (A-15d), remains to be satisfied. The initial condition requires that

$$V(s,0) = f(s) - \rho_o \frac{s}{b} - \rho_s(\frac{b-s}{b}) = \sum_{n=1}^{\infty} B_n' \sin(\frac{n\pi s}{b})$$

which amounts to a requirement that B_n' be chosen in such a way that the equation is valid. This is accomplished by multiplying both sides by $\sin(\frac{m\pi s}{b})$ and integrating from C to b. This results in

$$\int_o^b [f(s) + (\rho_s - \rho_o)\frac{s}{b} - \rho_s] \sin(\frac{m\pi s}{b}) ds = \int_o^b \sum_{n=1}^{\infty} B_n' \sin(\frac{n\pi s}{b}) \sin(\frac{m\pi s}{d}) ds$$

which in mathematics books discussing Fourier series [Churchill (1941)] is shown to reduce to

$$B_n' = \frac{2}{b} \int_0^b [f(s) + (\rho_s - \rho_o) \frac{s}{b} - \rho_s] \sin(\frac{n\pi s}{b}) ds \qquad \text{(A-20)}$$

The complete solution is then

$$V(s,t) = \frac{2}{b} \sum_{n=1}^{\infty} \left\{ \int_0^b [f(s) + (\rho_s - \rho_o) \frac{s}{b} - \rho_s] \sin(\frac{n\pi s}{b}) ds \right\} \sin(\frac{n\pi s}{b}) \exp(- \frac{n^2 \pi^2 Dt}{b^2}) \qquad \text{(A-21)}$$

If $f(s) = \rho_s - (\rho_s - \rho_o) \frac{s}{b}$, the coefficients B_n' are all 0 so that Eq. (A-21) reduces to $V(s,t) = 0$. The concentration is given by Eq. (A-14) as

$$\rho(s,t) = \rho_s - (\rho_s - \rho_o) \frac{s}{b} \qquad \text{(A-22)}$$

It is seen that this result is independent of time, so that this represents a steady-state flow of vapor through the porous medium. In general, the rate of vapor transfer would be

$$R = - D \left. \frac{\partial \rho}{\partial s} \right|_{s=0} \qquad \text{(A-23)}$$

which becomes in the case of steady flow

$$R = - D \left. \frac{d\rho}{ds} \right|_{s=0} \qquad \text{(A-24)}$$

Evaluation of the transfer rate gives

$$R = D \frac{\rho_s - \rho_o}{b} \qquad \text{(A-25)}$$

This result could have been anticipated since $-\frac{\rho_s - \rho_o}{b}$ expresses the known fact that the vapor concentration gradient under steady flow is constant and Fick's first law of diffusion states that the transfer rate of a diffusing substance is equal to the concentration gradient times the coefficient of diffusion.

Another case of interest is when $f(s) = 0$. Then the Fourier coefficients are

$$B_n' = \frac{2(\rho_s - \rho_o)}{b^2} \int_o^b s \sin(\frac{n\pi s}{b}) ds - \frac{2\rho_s}{b} \int_o^b \sin(\frac{n\pi s}{b}) ds$$

which can be integrated after making the change of variable $z = \frac{n\pi s}{b}$ and noting that $z = 0$ when $s = 0$ and $z = n\pi$ when $s = b$. The resulting equation

$$B_n' = \frac{2(\rho_s - \rho_o)}{n^2\pi^2} \int_o^{n\pi} z \sin z \, dz - \frac{2\rho_s}{n\pi} \int_o^{n\pi} \sin z \, dz$$

can be integrated by parts to obtain

$$B_n' = \frac{2(\rho_s - \rho_o)}{n^2\pi^2} \left\{ - z \cos z \Big]_o^{n\pi} + \sin z \Big]_o^{n\pi} \right\} + \frac{2\rho_s}{n\pi} \cos z \Big]_o^{n\pi}$$

which becomes

$$B_n' = - 2 \left\{ \rho_s - \rho_o(-1)^n \right\}$$

Equation (A-21) becomes

$$V(s,t) = \frac{4}{b} \sum_{n=1}^{\infty} [\rho_o(-1)^n - \rho_s]\sin(\frac{n\pi s}{b})\exp(-\frac{n^2\pi^2 Dt}{b^2})$$

and the concentration of water vapor at any location in the porous medium at any time is given by

$$\rho(s,t) = \rho_s - (\frac{\rho_s-\rho_o}{b})s + \frac{4}{b} \sum_{n=1}^{\infty} [\rho_o(-1)^n-\rho_s]\sin(\frac{n\pi s}{b})\exp(-\frac{n^2\pi^2 Dt}{b^2}) \quad \text{(A-26)}$$

This result is interesting in that the first two terms represent the steady state moisture vapor distribution, while the third term represents the transient moisture vapor distribution. The time effect appears in an exponential which rapidly decreases in magnitude as time increases, so that after a long time the term

$$\frac{4}{b} \sum_{n=1}^{\infty} [\rho_o(-1)^n- \rho_s]\sin(\frac{n\pi s}{b})\exp(-\frac{n^2\pi^2 Dt}{b^2}) \to 0$$

and only the steady state portion of Eq. (A-26) remains.

Other cases could be considered, but the two examples discussed already have illustrated some of the more interesting aspects of the vapor transfer by diffusion. The qualitative aspects of the results could have been anticipated in some cases, such as the result that the transfer rate will approach steady state in time no matter what initial vapor distribution was encountered.

In the experimental work with infiltration, the vapor transfer effects were minimized by the close temperature control of the room

in which the equipment was located. The tests were also short enough, so that the loss of air by diffusion through the infiltrating water would be negligible.

A.3 Gamma Radiation Intensities

The gamma radiation intensity varied during the course of these experiments, although it was essentially constant during any particular test. Part of the difference in the radiation intensity was probably due to small changes in the geometry of the collimating slits, and part of the change was due to changes in the equipment adjustments. Typical counting rates and the fractional change encountered in moving from one position to another is shown in Table A.3.

I_1	I_2	Comment	$\frac{I_1}{I_2}$
84,000	72,000	Air to plastic counting rate	1.17
72,000	36,000	Plastic to dry soil	2.00
36,000	28,000	Dry soil to wet soil	1.28
28,000	36,000	Wet soil to dry soil	0.78
36,000	72,000	Dry soil to plastic	0.50

TABLE A.3. Typical Gamma Radiation Counting Rates

BIBLIOGRAPHY

1. Adeney, W. E. and H. G. Becker, The Determination of the Rate of Solution of Atmospheric Nitrogen and Oxygen by Water, Philos. Mag., vol. 38 (1919) and vol. 39 (1920).

2. Ashcroft, G., D. D. Marsh, D. D. Evans and L. Boersons, Numerical Method for Solving the Diffusion Equation: I. Horizontal Flow in Semi-Infinite Media, Soil Science Society of America Proceedings, vol. 26 (1962).

3. Brooks, R. H. and A. T. Corey, Hydraulic Properties of Porous Media, No. 3, Hydrology Papers, Colorado State University, March 1964.

4. Bruce, R. R., Transient Methods for Measuring the Moisture Diffusivity of Porous Media, Ph.D. Dissertation, University of Illinois, 1956.

5. Churchill, R. V., Fourier Series and Boundary Value Problems, McGraw-Hill, 1941.

6. Daniels, F. and R. A. Alberty, Physical Chemistry, Wiley, 1955.

7. Davidson, J. M., J. W. Biggar and D. R. Nielsen, Gamma-Radiation Intensity for Measuring Bulk Density and Transient Water Flow in Porous Materials, Journal of Geophysical Research, vol. 68 (1963).

8. De Weist, R. J. M., Unsteady-State Phenomena in Flow Through Porous Media, Ph.D. Dissertation, Stanford University, 1959.

9. El Nimr, A., Hydrodynamics of Seepage from Channels and Reservoirs, Ph.D. Dissertation, Stanford University, 1962.

10. Fair, G. M. and J. Geyer, Water Supply and Waste Water Treatment, Wiley, 1954.

11. Fair, G. M. and L. P. Hatch, Fundamental Factors Governing the Streamline Flow of Water Through Sand, Journal of the American Water Works Association, vol. 25 (1933).

12. Hanks, R. J. and S. A. Bowers, Numerical Solution of the Moisture Flow Equation for Infiltration in Layered Soils, Soil Science Society of America Proceedings, vol. 26 (1962).

13. Herriot, J. G., Methods of Mathematical Analysis and Computation, Wiley, 1963.

14. Hubbert, M. K., The Theory of Ground-Water Motion, Journal of Geology, vol. 48 (1940).

15. Klinkenberg, L. J., The Permeability of Porous Media to Liquids and Gases, Drilling and Production Practice (1941), Journal of the American Petroleum Institute (1942).

16. Klute, A., A Numerical Method for Solving the Flow Equation for Water in Unsaturated Materials, Soil Science, vol. 73 (1952).

17. Lamb, H., Hydrodynamics, Dover, 1946.

18. Mavis, F. T. and T. P. Tsui, Percolation and Capillary Movement of Water Through Sand Prisms, Bulletin 18, University Iowa Studies in Engineering, Iowa City, 1939.

19. Nielsen, D. R., J. W. Biggar and J. M. Davidson, Experimental Consideration of Diffusion Analysis in Unsaturated Flow Problems, Soil Science Society of America Proceedings, vol. 26 (1962).

20. Philip, J. R., The Theory of Infiltration: 1. The Infiltration Equation and its Solution, Soil Science, vol. 83 (1957).

21. Polubarinova-Kochina, P. Y., Theory of Ground Water Movement, Princeton University Press, 1962.

22. Schwartz, M., S. Green and W. A. Rutledge, Vector Analysis, Harper (New York), 1960.

23. Scott, V. H. and A. T. Corey, Pressure Distribution During Steady Flow in Unsaturated Sands, Soil Science Society of America Proceedings, vol. 25 (1961).

24. Shereshefsky, J. L. and M. Folman, Liquid-Vapor Equilibrium in Microscopic Capillaries, Journal of Physical Chemistry, vol. 59 (1955).

25. Taylor, A. E., Calculus with Analytic Geometry, Prentice-Hall, 1959.

26. Todd, D. K., Ground Water Hydrology, Wiley, 1960.

27. Wang, F. C., An Approach to the Solution of Unsteady Unsaturated Flow Problems in Soils, Ph.D. Dissertation, Stanford University, 1963.

28. Wilson, L. G., The Effect of Air Flow Ahead of Wetting Front on Infiltration, Ph.D. Dissertation, University of California, Davis, 1962.

29. Wyckoff, R. D. and H. G. Botset, The Flow of Gas-Liquid Mixtures Through Unconsolidated Materials, Physics, vol. 7 (1936).